DISS. ETH NO. 18500

SMART CONDUCTING POLYMER ACTUATORS: STRAIN RESPONSE OF POLYPYRROLE TO REDOX AGENTS IN SOLUTION

A dissertation submitted to

ETH ZURICH

for the degree of
Doctor of Sciences

presented by

CLAUDIA KÜTTEL

M.Sc./Dipl. El. Ing. ETH Zurich

April 30, 1984
citizen of Basel (BS)

accepted on the recommendation of

Prof. Dr. Andreas Stemmer, examiner
Prof. Dr. Andreas Hierlemann, co-examiner
Dr. Xun Wei, co-examiner

2009

Acknowledgements

First and foremost, I would like to thank Prof. Dr. Andreas Stemmer, head of the Nanotechnology Group at ETH Zurich, for giving me the opportunity and support to perform my PhD work in his group, as well as for the combination of constructive guidelines and the freedom to shape the contents of my thesis.

I want to express my gratitude to Prof. Dr. Andreas Hierlemann from the Bio Engineering Laboratory at ETH Zurich, and Dr. Xun Wei from the Nanotechnology Group at ETH Zurich for co-examination of this thesis.

I also thank Dr. Stefan Blunier, Niels Quack, and Simon Steiner from the Institute of Mechanical Systems at ETH Zurich, Dr. Udo Lang from Kistler, Silvan Schmid and Etienne Schwyter from the Group of Micro and Nanosystems at ETH Zurich, Chauncey Graetzel from Optotune, Dr. Salvador Pané i Vidal and Kaiyu Shou from the Institute of Robotics and Intelligent Systems at ETH Zurich for the helpful discussions and technical support.

Nanos, I very much appreciate the time I spent with all of you. Many thanks therefore go to all the members and students of the Nanotechnology Group: Dr. Xun Wei, Dr. Dominik Ziegler, Raoul Enning, Reto Fiolka, Ralph Friedlos, Siegfried Graf, Antje Rey, Miho Sakai, Livia Seemann, Maha Maglinao, Lukas Schlagenhauf, Dr. Manuel Aschwanden, Dr. Markus Beck, Dr. Yury Belyaev, Dr. Javad Farahani, Altan Gürsel, Dr. Nicola Naujoks, and Dr. Andreas Vonderheit.

Finally, I want to thank my entire family for their love, encouragement and support for every step I have taken.

Table of Contents

Abstract

Most actuators today still make use of batteries or other electrical power sources. For certain medical applications, however, batteries are not the first choice, for instance due to their size and weight, as well as inactivities due to recharging. For this reason, actuator materials which can be powered directly by chemical energy available in the environment have been researched. Mainly, hydrogels have been demonstrated to be actuated by changes in chemical energy. The polymer gels mostly feature high strains, but lack mechanical strength and are therefore not suited for all applications where chemical actuation can be an advantage.
Besides other electroactive polymers (EAPs), conducting polymers have attracted great attention as candidates for artificial muscles. In particular, polypyrrole (PPy) achieves strong mechanical properties with moderate strains and can be actuated with lower voltage compared to other commonly used actuator materials. Currently, the direction of ion exchange, whereby the strain of actuators arises, is routinely controlled by applying an external potential to change the redox state of PPy. For future applications, ways of driving artificial muscle actuators other than by an externally applied potential might become important.
In this work we have therefore – to the best of our knowledge – for the first time examined the principle of chemically actuating PPy with redox agents in solution. Due to the low actuation voltages needed, PPy actuators can work in the potential region of most chemical agents. In particular, hexacyanoferrate and L-ascorbic acid, also known as vitamin C, are employed to analyse the strain response of PPy. The redox agents establish a certain potential at the polymer electrode, which results in a corresponding strain change. For comparison, we first analysed the actuators in a system driven by external signals from a potentiostat. The actuation results achieved with the redox agents are in accordance with the strain generated by external voltages via the potentiostat. By adding different relative concentrations of the hexacyanoferrate couple to the electrolyte, we achieve a repeatable linear transition in strain with moderate to low hysteresis. Strain changes are induced by redox pairs as well as redox moieties in solution. The possible pathways of redox-induced actuation were analysed and we concluded that the most probable pathway is the reaction at the PPy film surface with subsequent ion exchange. Influences of pH, electrolyte concentration as well as temperature were found to not affect the actuator strain as much as the redox agents. The configuration we chose to visualise the actuator strains was a bending beam of polyimide/gold/PPy inside a liquid flow cell. This setup is ideally suited for measurements which include a fluid flow, since no problems arise due to leakage. To demonstrate the possible polarities of strain vs. potential, we used an anion-exchanging film – PPy(ClO_4) – as well as a cation-exchanging film – PPy(DBS). Their shrinking and swelling behaviour is inverse. To

improve the strain rates of chemical actuation we showed that it is possible to employ the PPy actuators in a fuel cell setup, in our case as the anode. The electrical connection to the cathode side leads to a strain change within seconds.
Our results indicate that conducting polymer actuators are well suited to sense their environment while directly using this energy to exhibit actuation.

Zusammenfassung

Die meisten Aktoren werden heutzutage noch immer mit Batterien oder anderen elektrischen Energiequellen betrieben. Für einige medizinische Anwendungen sind Batterien jedoch nicht optimal geeignet, sei es wegen der Grösse und des Gewichts oder wegen aufladungsbedingten Totzeiten. Deswegen wurden Aktormaterialien erforscht, die direkt mit chemischer Energie aus der Umgebung angetrieben werden können. Eine solche chemische Aktuation wurde hauptsächlich mit Hydrogelen gezeigt. Diese Hydrogele verfügen meistens über eine grosse Ausdehnung, haben aber generell eine geringe mechanische Festigkeit und sind deswegen nicht für alle Anwendungen geeignet, wo chemische Aktuierung Vorteile bieten kann.
Ein grosses Interesse besteht darin leitfähige Polymere wie auch andere dielektrische Elastomer Aktoren (DEA) für die Realisierung von künstlichen- oder biomimetischen Muskeln einzusetzen. Polypyrrol (PPy) beispielsweise weist eine hohe mechanische Festigkeit mit moderaten Deformationen auf und braucht für den Antrieb geringere elektrische Spannungen als viele andere Aktormaterialien. Die Richtung des Ionenaustausches, der die Grundlage der Deformation bildet, wird generell durch das Anlegen einer elektrischen Spannung gesteuert. Andere Arten der Ansteuerung von PPy könnten für zukünftige Anwendungen von Bedeutung sein.
In dieser Arbeit haben wir deswegen nach bestem Wissen zum ersten Mal das Prinzip des chemischen Antriebs von Polypyrrol mittels Redoxsystemen untersucht. Die niedrigen Aktuationsspannungen ermöglichen die Verwendung von PPy im Potential-Bereich der meisten Chemikalien. Wir haben Hexacyanoferrat(II/III) und Ascorbinsäure, auch bekannt als Vitamin C, verwendet, um eine Deformation in PPy hervorzurufen. Die Redoxsysteme etablieren dabei an der Polymer Elektrode ein gewisses Potential, welches in einer entsprechenden Deformation resultiert. Für Vergleichszwecke haben wir zuerst analysiert wie sich die Aktoren verhalten, wenn sie via Potentiostat angesteuert werden. Die Resultate sind vergleichbar mit denjenigen der chemischen Stimuli. Verschiedene Konzentrationsverhältnisse des Hexazyanoferrat Paares ergaben entsprechende, unterschiedlich starke Ausdehnungen bzw. Kontraktionen mit hoher Wiederholbarkeit und einer geringen Hysterese. Deformationen wurden neben Redoxpaaren auch mit einzelnen Reduktions- und Oxidationsmitteln erreicht. Die möglichen Reaktionswege der chemischen Ansteuerung wurden untersucht und die Reaktion an der Polymer Oberfläche mit anschliessendem Ionenaustausch als wahrscheinlichster Reaktionsweg ausgemacht. pH, Elektrolytkonzentration, sowie Temperatur haben keine vergleichbaren Einflüsse auf die Deformation des Aktors. Um die Ausdehnung und Kontraktion des Aktors zu messen haben wir uns für einen Polyimid/Gold/PPy Biegebalkenaufbau in einer Durchflusszelle entschieden. Diese Konfiguration ist für Messungen mit Flüssigkeitsströmungen ideal geeignet, da undichte Stellen vermieden werden können.

Die Umkehrung der Deformationspolarität wurde anhand eines kationenaustauschenden Polymers, PPy(DBS), gezeigt. Dieser Film kontrahiert beim Anlegen einer positiven Spannung, im Gegensatz zu PPy(ClO_4). Um die Deformationsrate zu erhöhen haben wir den PPy Aktor als Anode in einer Brennstoffzelle eingesetzt. Ein Kurzschluss mit der Kathodenseite ermöglicht die Aktuierung innerhalb einer Sekunde.
Unsere Resultate weisen darauf hin, dass Aktoren aus leitfähigen Polymeren gut dafür geeignet sind, die chemische Energie in ihrer Umgebung direkt als Antrieb zu nutzen.

List of figures

List of tables

Abbreviations

ACN	Acetonitrile
Ag/AgCl	Silver/Silver chloride reference electrode
Au	Gold
$BMIMPF_6$	1-n-butyl-3-methylimidazolium hexafluorophosphate
CE	Counter electrode
CNT	Carbon Nanotube
CV	Cyclic Voltammetry/Cyclic Voltammogram
EAP	Electroactive polymer actuator
IPMC	Ionic Polymer Metal Composite
$LiClO_4$	Lithium perchlorate
$NaBF_6$	Sodium tetrafluoroborate
$NaCF_3SO_3$	Sodium trifluoromethanesulfonate
$NaClO_4$	Sodium perchlorate
NaDBS	Sodium dodecylbenzenesulfonate
$NaPF_6$	Sodium hexafluorophosphate
PANI	Polyaniline
PDMS	Poly (dimethyl siloxane)
PPy	Polypyrrole
Pt	Platinum
PVDF	Polyvinylindene fluoride
RE	Reference electrode
$TBAPF_6$	Tetra-n-butylammonium hexafluorophosphate
WE	Working electrode

1 Introduction

Most actuators today are driven by an external power source like a battery or even a voltage generator. This is understandable from the viewpoint that various actuation devices need high voltages to be actuated and consume a lot of energy. When actuation mechanisms ought to be operated in or near the human body or other biological systems, the use of power devices can pose problems [1]. Batteries today still belong to the most spacious and heavy parts in an electrical assembly. Toxicity of materials can not be fully excluded and special attention to sealing is required. Additionally, device inactivities due to battery recharge and the need for frequent replacement can be very troublesome. A longer service-life is in contrast to miniaturised batteries, which normally hold less energy. Although ongoing research is addressing these issues by scaling down and using more bio-compatible fuels or heat gradients directly from the human body [2], virtually all commercial devices in the near future will be implemented with custom batteries. High voltages and electrical wiring are even less suited to drive devices near or inside the human body. Instead of using a battery or any other external power source, an actuator could be directly powered by its environment, converting chemical energy into mechanical energy. Just as in natural systems, an actuator could be driven by gradients and changes in chemical concentration. Chemical fuels can deliver higher energy densities than batteries, which makes it even more attractive to use the same fuel and fuel delivery systems as employed by natural muscles [3]. Several teams have therefore worked on routes to directly utilise chemical energy to power actuators.

Polymeric hydrogels, researched for more than 50 years, are the most investigated state-changing material which can be chemically powered. They have been shown to directly respond to changes in pH, temperature, light or reagent concentration [4, 5]. Large volume changes can be achieved in those systems with however slow responses and rather low strengths and elastic moduli. This makes them well suited for applications where large strains are required, yet due to their low strengths polymer gels are usually employed in devices where they are shielded from the environment [6]. Actuator systems which catalyse the reaction of a fuel were also reported for the autonomous movement of micro- and nanostructures. Small plates with a Pt area [7], Pt-Au rods [8], and Ni-Au rods [9] have been demonstrated to move autonomously (i.e. translational or rotational) in aqueous hydrogen peroxyde solutions.

Microparticles were shown to move in CH_3CN by the decomposition of H_2O_2 with the help of a synthetic manganese catalyst immobilised onto the particles [10]. Mano and Heller functionalised a carbon fiber, with glucose oxidase on one end and bilirubin oxidase on the other end, which moved on the surface of a glucose-containing solution [11]. They explained the effect with the transport of ions at the interface accompanying the flow of current through the fiber. All of these actuators do only exhibit translational or rotational movements. The liquids used were in most cases organic solutions, which limits the applications of these actuator types.

Von Howard et al. demonstrated two types of chemically driven actuators, i.e. a beam-type carbon nanotube (CNT) actuator and a shape memory alloy (SMA) [12, 13]. Both muscles are directly powered by hydrogen and oxygen purged into the system. The CNT paper actuators were shown to achieve transitions in strain around 0.02% within 30 minutes when they were alternately exposed to O_2 and H_2. With the SMA they demonstrated actuator stroke and power density comparable to a natural skeletal muscle and faster switching speeds than for the CNT actuators. This principle is dependent on the heating and cooling of the actuator, which would presumably necessitate shielding in biological applications to avoid e.g. protein denaturation. Recently, Biener et al. have analysed the actuation of nanoporous gold when it is subjected to ozone and carbon monoxide [14]. To be powered, these actuators all require the delivery of gas, which is why robotics rather than biological fields might be envisaged so far.

During the last ten to twenty years, polymeric actuator materials which are also called artificial muscles due to their biomimetic actuation behaviour have attracted growing interest. Various kinds of electroactive polymers (EAP) have been demonstrated and are still broadly researched [15, 16]. Every EAP mechanism shows specific actuation properties, which can be implemented into different kinds of applications, depending on the specific requirements. Despite their promising mechanical properties, very few EAPs - except for polymer gels which are mainly driven chemically - have been demonstrated to work with chemical energy [12, 17].

We show in this work the principle of chemically powering biomimetic actuators in liquid, where the actuation depends on the concentration of chemical agents in solution. Conducting polymers have attracted great attention to explore their potential for actuation. In particular, polypyrrole (PPy) achieves strong mechanical properties with moderate strains [18], can work under compression and tension and shows good biocompatibility [19-21]. PPy can be actuated with lower voltage compared to other commonly used EAP and actuator materials in general [18] and can thus work in the potential region of most chemical agents.

Since PPy can be designed into various actuator configurations, several different future applications are imaginable, ranging from smart artificial muscle implants [3], over environmental sensitive blood vessel repairs [22] and stimulus-responsive

actuator valves [23, 24] to microdevices for single cell studies [25]. Depending on future needs, several different applications might emerge.
In the subsequent sections, an insight into smart actuator materials and EAPs in particular is given, where different actuation mechanisms are compared. These parts will highlight the main reasons for the choice of PPy as actuator material in our work. Section 1.3 contains an outline of different drug delivery systems, from constant delivery to feedback loops. An overview concerning this application is given, because out of several possible future directions for chemically actuated PPy, this is presently an important and simultaneously still challenging field.

1.1 Smart actuator materials

The term "smart materials" is a wide concept of materials of which one or more properties can be altered in a controlled fashion by external triggers, such as electric- or magnetic fields, temperature, pH, stress, light or chemical agents [26]. Those substances sense external stimuli and respond accordingly in real or near-real time. The description applies to a wide variety of materials, e.g. piezoelectric ceramics, fluorescent and electroluminescent materials, magnetorheological fluids, halochromic materials or thermally actuated shape memory alloys, just to name a few. Since this thesis deals with smart actuators, we will briefly explain the main structures in this field. Actuators are devices that create mechanical motion when they are excited by certain stimuli. As opposed to several other actuator principles, like pneumatic actuators, hydraulic pistons or electrical motors, in smart actuators the material itself exhibits mechanical responses to external stimuli. Typical examples of stimulus-responsive actuator materials are listed below.

Piezoelectric materials
The piezoelectric and converse piezoelectric effects couple mechanical energy to electrical energy and vice versa. When an electric potential or field is applied to a piezoelectric material (e.g. natural crystals or synthetic piezoelectric materials), it can induce mechanical stresses or strains. The reverse effect is also possible and is used in sensors. Besides piezoceramics, also piezoelectric polymers were shown to work as smart actuators. Poly(vinylidene difluoride) (PVDF) / silver actuators optically driven via the piezoelectric effect have been shown employing a laser beam [27]. Several devices and structures include piezoelectric materials as high precision devices, microactuators, for vibration control, etc. [26]. Usually, high voltages (around 100V to kV depending on the geometries) are required to drive such actuators, with small strains up to ~1%.

Electrostrictive relaxor ferroelectrics
Electrostriction appears in materials which have high dielectric constants. The application of an electric field aligns polarized domains within the material, which remain aligned when the applied field is removed. Typically low strains in the order of 0.1% are reported with low hysteresis values (<5%) [26]. Relaxor ferroelectric polymers achieve higher strains >1% [18]. Generally, electrostrictive actuators require high fields around several kV/mm.

Thermally activated/ferromagnetic shape memory alloys (SMA) also known as smart metals or muscle wires, undergo a phase change with temperature (or stress) or a magnetic field which results in strain [28]. NiTi-alloys are most commonly used as thermally activated SMAs, but several other materials have been researched as well. Various forms are available, most of which work with a tensile force. Several systems exist for biological applications, mostly for catheters or stents [29]. SMAs usually run between fully contracted and fully extended without a large linear region in-between, but they achieve large forces, strains up to 5-6% and high power densities. The extent of hysteresis is usually significant (30 to 50 °C for common Ni-Ti SMAs), while material modifications have shown to decrease the hysteresis to 10-15 °C [26]. Thermally activated SMAs generally respond slower than magnetically actuated ones, because cooling is a slow process [29]. SMAs can be arranged into a wide range of geometrical configurations, which makes them attractive materials for many applications.

Shape memory polymers (SMP) can be triggered by electric- or magnetic fields, pH or temperature. Their working principle is similar to SMAs, but they have several advantages, like much lower cost, lower density and potential biocompatibility and -degradability [4].

Electrorheological fluids (ERF), magnetorheological fluids (MRF) and ferrofluids, which are liquids with fractions of particles, can experience dramatic changes in rheological properties, such as viscosity, in the presence of an external field [28]. For ERFs high electric fields are needed, while in MRFs and ferrofluids, the particles are controlled by a magnetic field. Electrorheological elastomers, also called electrovisco-elastic elastomers, and ferrogels employ a very similar principle of changes in rheology, but instead of suspending the particles in a liquid, an elastomer is taken, which changes its shear modulus in the solid state.

Nanoporous metals were recently demonstrated to yield strain amplitudes comparable to those of commercial ferroelectric ceramics. The effect is reported to be

caused by charge-induced changes in the surface stress, either evoked through an applied potential [30] or due to adsorbate-metal interactions [14].
Molecular actuators, -machines or -devices are systems based on molecules or molecular assemblies, which respond to external trigger stimuli (e.g. adenosine triphosphate (ATP) fuel, pH gradient, voltage or light) with a change in their state [31, 32]. Such molecular systems are either already present in nature and extracted or they are designed and synthetically assembled. One prominent example is the redox-induced shuttling of rotaxane [33]. We consider the bottom-up approach for artificial muscles with molecular actuators also an interesting prospective.

Electroactive Polymers (EAPs), which is a variety of smart plastic materials, will be presented in the next section.

1.2 Electroactive Polymers (EAPs)

Polymers have several characteristics that make them attractive: they are lightweight, fracture tolerant, pliable, and most of them are inexpensive. Strains can be two orders of magnitude higher compared to electroactive ceramics, densities are low, and certain polymer materials show faster responses than SMAs [15, 18, 34]. Limiting factors of polymer materials for the use as actuators can be low actuation forces, and their robustness. The research of polymer materials has opened up the possibilities to approach several new applications for actuators.
In electroactive polymers (EAPs), two principles for actuation can be distinguished. Electronic EAPs are driven by electric fields or coulomb forces, while ionic EAPs are based on the mobility of ions

Electronic EAPs

These actuators are driven by electrostatic forces and can, or even should, be operated in dry conditions. They usually exhibit high mechanical densities and large actuation forces, while the responses are comparably fast, within milliseconds. The main disadvantage of these materials is the high electric fields or actuation voltage needed (between 10-100V/μm, which leads to voltages of up to several kV). A compromise between strain and stress is often required. Section 1.2.2 explains some electronic EAPs in detail.

Ionic EAPs

For the actuators of this class, an electrolyte with mobile ions is required. The ions either cause a volume change inside the polymer or balance the charge at the interface between actuator and electrolyte. Voltages below 1 V up to several volts enable the actuation of these materials. Responses are slower compared to electronic EAPs, and lie in the range of a second to minutes. The response rate can be increased with several modifications. In aqueous electrolytes, however, it is important to not exceed the electrochemical stability window and e.g. induce hydrolysis at too high positive potentials.

Here we treat all of the mentioned materials with a focus on actuation. It is clear, however, that most of these materials can be used for a variety of other functionalities. For example, carbon nanotubes are due to their potentially high conductivities, attractive candidates for micro- and nanoelectronics [35, 36]. In assemblies on electrodes they can enable improved sensing for various species. Conducting polymers have been applied to various fields, e.g. polymer light-emitting diodes, electrochromic windows, energy storage and sensing devices [15, 37]. The basic component of ionomeric polymer-metal composites – polyelectrolyte membranes – serve as proton exchange membranes for fuel cells and ferroelectric polymers such as polyvinylidene fluoride (PVDF) are used as filter membranes. Polymer gels are utilised in biological fields, besides their actuator properties, to serve as extracellular matrices, smart surfaces, biocompatible- and protein adsorption preventing coatings, while their sol-gel transition can be used as an alternative to implantation of soft materials.

Subsequently, several EAP mechanisms which are important for reasons of comparison will be presented.

1.2.1 Ionic EAPs

In this section, several ionic EAPs are further illuminated to gain an insight into their most important properties, advantages and disadvantages.

Ionomeric Polymer-Metal Composites (IPMC)

IPMCs consist of a thin polyelectrolyte membrane with metal electrodes plated on both sides. Due to the negative charges of the polymer itself, only cations (e.g. H^+,

K^+, Na^+, Li^+, TBA^+, TMA^+) can penetrate the polymer. Those counter-ions balancing the negatively charged polymer backbone can move freely when a small electric field is applied [38, 39]. Today, the most widely exploited polyelectrolyte membranes are commercially available perfluorinated ionomers like Nafion® (DuPont), Aciplex® (Asahi Chemical) or Flemion® (Asahi Glass) or styrene/divinylbenzene-based polymers, which are stiffer since they are highly cross-linked. The compliant electrodes on both sides are composed of metal particles (Pt or Au) 3 - 10 nm in diameter, distributed within 10 - 20 μm depth of the polyelectrolyte membrane and a 1 - 5 μm thick gold layer (other coatings like Pt, Pd, Cu, Ag, Ni, and carbon nanotubes are possible) [40, 41]. Since most of the time commercial polyelectrolyte membranes are employed the costs are comparably high. Potentials of $\pm$1-4V are sufficient for actuation of IPMCs. When a potential difference is applied between the two electrodes, the actuator shows a fast bending motion towards the anode due to a field induced change in ion concentration, which attracts ions and solvent molecules to the cathodic side. In Nafion-based IPMCs, this fast movement is followed by a slow relaxation in the opposite direction. Several models are proposed for the actuation mechanisms [41]. A maximum strain of >3 % was achieved, while the typical strain is about 0.5 %. Due to drift after initial displacement IPMC usually require steady current to maintain a fixed position. The mechanism can not only be used for actuation but also for sensing, since application of stress results in a potential over the electrodes. One drawback of this actuation principle is that only bending motion can be achieved. However, IPMCs are a good choice for several niche applications due to the low actuation voltages required [42].

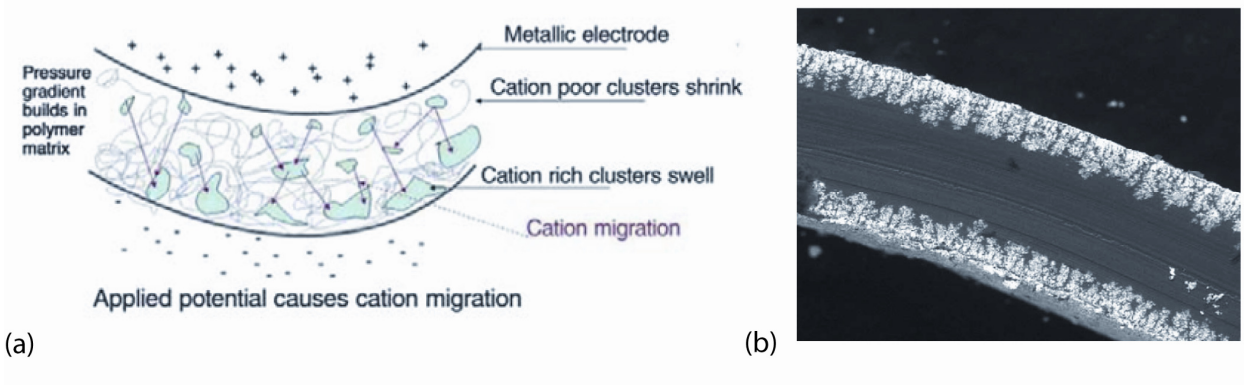

Fig. 1.1 (a) Principle of bending of IPMC actuators [34] and (b) Cut through an IPMC layer, the polyelectrolyte membrane in the middle, with penetration of metal particles from top and bottom [43]. This structure does not yet contain the plated metal electrodes.

Carbon Nanotube (CNT) actuators

A carbon nanotube can be thought of as a single graphite sheet wrapped into a cylindrical tube. When one CNT is present it is called single-walled nanotube (SWNT), while several such CNTs concentrically nested are called multiwalled nanotubes (MWNTs) (Fig. 1.2a). The diameter of SWNTs lies in the range of a few nanometers, depending on the structure, i.e. the way in which the graphene sheet is "rolled up". CNTs have several very interesting properties. Depending on their structure, they can either be semiconducting or metallic. Electrical and thermal conductivities are very high, greater than in copper and natural diamond, respectively [44, 45]. Additionally, also mechanical properties showed promising results so far. The calculated and measured Young's modulus and tensile strength for individual CNTs are around 0.64 TPa and 37 GPa [45, 46]. Fig. 1.2b shows a possible way to measure the mechanical properties of single nanotubes with an AFM tip. Due to the light weight, the density-normalised modulus and strength are much higher than for steel wire. These excellent mechanical values for single CNTs are not achieved though for assemblies of nanotubes, like nanotube sheets (also called buckypaper) and yarns.

Baughman and his team reported in 1999 the actuation of CNT sheet actuators in an electrolyte solution [47]. The actuation principle during non-Faradaic double-layer charge injection was proposed to be dependent as well on quantum mechanical effects (i.e. an increase in C-C bond length), at low levels of charge injection, as on electrostatic (coulombic) repulsion between neighbouring CNTs. During actuation, CNTs need to be immersed in an electrolyte. The application of a potential between the nanotubes and a counter electrode leads to double-layer charging of the CNT-electrolyte interface. The electronic charges within the nanotubes are thereby balanced by the accumulation of ionic charges on the surface of the CNTs in contact with the electrolyte [44, 45, 48-50]. Fig. 1.2 e and f illustrate the charging of single nanotubes and CNT clusters. The dependence of strain on potential is quasi-parabolic (Fig. 1.2g), due to the repulsive interaction between like charges. One can imagine that with a larger surface area, the charge injection can be increased and therefore also the actuation strain can be improved. Therefore, actuators including SWNTs are preferred over MWNTs, since the accessible solvent surface area of SWNTs is higher. A smaller modulus can also lead to higher strains [51]. Also, an increase in potential without exceeding the electrochemical stability window leads to a higher strain, which is why organic electrolytes [52, 53] or ionic liquids [48] are used instead of aqueous electrolytes. The achieved strain in the work of Baughman et al. is about 0.08% for a potential range of ± 0.9 V, while the stress generated during isometric actuation was reported to be 0.75 MPa [47]. Although these authors have interpolated the achievable strain to more than 1%, having the charge injection and

surface to volume ratios of single CNTs in mind, an actuator with such an active strain is not in sight [48]. In aqueous electrolyte, maximum actuator strains of up to 0.2 % were achieved for SWNT and MWNT sheets [54]. Values as high as 0.5% were reported for CNT yarns in TBATFB/acetonitrile electrolytes with applied voltages of ±2.5 V [52]. Fig. 1.2g shows the typical strain vs. potential dependence of CNT actuators in aqueous electrolytes and organic electrolytes, where it can be seen that most actuation strain is achieved at negative potentials with a minimum at about 0.2 to 0.3 V. Baughman reports that oriented MWNT yarns are able to generate isometric stresses up to 26 MPa based on a geometric cross-sectional area of the yarn [45], which is larger compared to unoriented nanotube sheets, but still a hundred times smaller than predicted for nanotube fibers with the modulus of individual SWNTs. The tensile modulus of MWNT yarns was measured to stay at values of 16 ± 5 GPa over a range of applied stresses from 35 to 70 MPa and at different applied potentials [52].

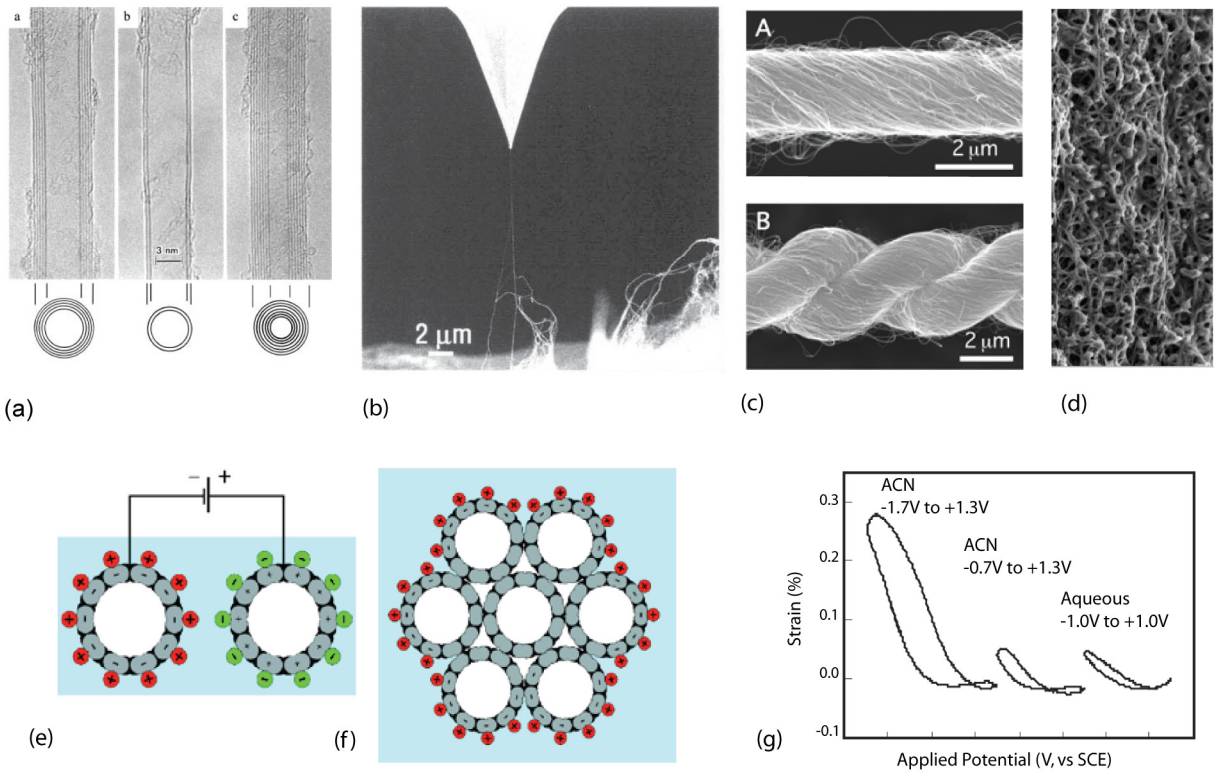

Fig. 1.2 (a) Electron micrographs of MWNTs with different numbers of nested CNTs [55], (b) SEM image of a SWNT tensile-loading experiment using an AFM tip [46], (c) CNT yarns (A) single and (B) two-ply [56], (d) electron micrograph of a buckypaper surface [57], (e) double-layer charge injection in CNT actuators for negatively and positively charged nanotubes, (f) shows the effect of decreased surface/volume ratios if CNT assemblies instead of single nanotubes are employed [47], (g) actuation strains of a buckypaper in different solutions, at different potentials [58].

Time scales on the order of seconds are typical in actuators that are approximately 30 μm thick, while in composite nanotube fibers the responses are even slower [18]. By using resistance compensation techniques or high voltage pulses in the range of 30 V, strain rates of 0.6%/s for isotonic conditions (constant mechanical load) [59] and stress rates of 180 MPa/s for isometric conditions (constant length) (which was calculated to result in a strain rate of 19%/s with a modulus of 0.95 Gpa) [60] were demonstrated. Possible actuator designs include buckypapers – free-standing or as bilayer or trilayer assembly – as well as yarns.
Other actuation mechanisms apart from the double-layer charge injection mentioned above include pneumatic [58], light-driven [61, 62] and fuel-powered [12] actuation as well as electrostatic actuation - which is used in nano-actuators [50], e.g. bearing-like nanoswitches [63] - and CNT hybrid actuators [50]. In pneumatic actuation, strains as high as 3% were achieved, with large hysteresis behaviour though.
Applications for CNT actuators might be envisaged in the field of aerospace where good temperature stability as well as light materials are important. Several problems, such as creep or low strain rates as well as actuation strain of macroscopic structures need to be solved before CNT actuators can be used for large scale applications. Applications that are envisaged include micro-robots, grippers, muscles to mimic insect, animal or human systems, as well as surgical robots [16].

Conducting Polymers (CP)

Conjugated or conducting polymers (CPs) are electronically conducting organic materials with conjugated structures. Upon application of a voltage or a current, the charges on the polymer, i.e. its oxidation state, can be changed. For most CPs, this charge on the polymer backbone is positive. A change in oxidation state of the polymer results in a flux of mobile solvated ions between the polymer and the surrounding electrolyte to maintain charge neutrality [64]. The ion flux accompanied by solvent is generally thought of as the main cause for the expansion and contraction of the polymers. Depending on the dopant anion, which was incorporated into the polymer during fabrication, the ion transport is dominated by anions or cations. If the dopant anions are small, they can leave and enter the polymer during actuation. In the other case, when dopant anions are large enough to be trapped inside the polymer, cation in- and efflux provides charge neutrality (Fig. 1.3a-c).
Since the first proposition of CP actuators in the 90' by Baughman and coworkers [65], continuous advances in performance and theoretical insights have been achieved. Today, a broad spectrum of actuators [25], theoretical background and model systems [16, 66-71] are available and more improvements are still to come. The most widely used CPs in actuator design include polypyrrole, polyaniline, polythiophene,

polyacetylene, as well as their derivatives [72] (Fig. 1.3d). Most work is however found on polypyrrole (PPy) actuators. Reasons for this might be that PPy is comparably stable in atmospheric and biological conditions [73, 74], whereas polyacetylene for instance reacts readily with oxygen, which appears to be reduced for PPy in electrolyte solutions [75]. Polyaninile (PANI) is mainly electroactive in acids below pH 3-4 and the actuation behaviour is strongly dependent on pH [76]. The actuation of polyaniline [17] was also demonstrated with changes in pH. PANI has three electrochemical states - leucoemeraldine, emeraldine salt and penigraniline - which is why the actuation shows two pairs of peaks when the potential is cycled. PPy on the other hand is electroactive over a broad range of pH [77] and can therefore work at neutral pH. The strain behaviour is linear and free of transitions, except for actuators which show both anionic- and cationic transport [78]. Due to the possibilities to achieve large strain ranges with low hysteresis values, CP actuators can be brought to a precise intermediate position and be held there, instead of being only switched between fully expanded and contracted states (Fig. **1.3**e-f).

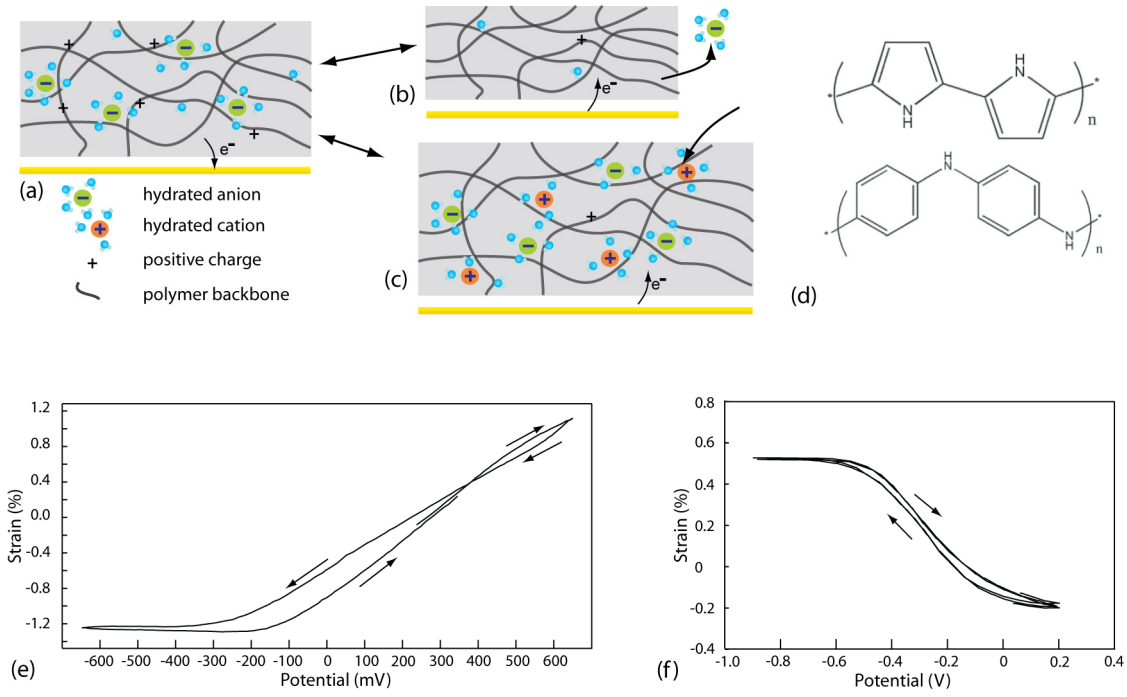

Fig. 1.3 Illustration of ion exchange in conducting polymers from the oxidised state (a) to the reduced (neutral) state when the polymer film is anion-exchanging (b) or cation-exchanging (c), (d) chemical structures of polypyrrole (top) and polyaniline (bottom) [34]. Strain vs. potential plots acquired during a potential sweep at 2 mV/s for an anion-exchanging PPy actuator (e) which expands (positive strain) for positive voltages and a cation-exchanging PPy actuator (f) which shows inverse behaviour. Arrows denote the sweep direction.

Total strains are typically around 1-3%, depending on the dopant ions, the electrolyte solutions, the force applied, as well as the actuation voltages [18, 25]. Larger actuator strokes were reported for instance by Kaneto and coworkers between 6-12% [79-81], by Smela et al. for lateral directions around 20-30%[82], using corrugated metal electrodes to 8-12% [83] or employing pentanol as co-surfactant for 5-6% [84] (see Table 1.1). CP actuators are usually driven with voltages in the range of ± 1 V in aqueous solutions and with higher voltages up to ± 5 V in organic solutions. Such large voltages are however not needed because smaller voltages also result in ample actuation. High tensile strengths can be achieved with CPs, typically in the order of several MPa. Increases up to >100MPa were reported in high quality electrochemically grown films and fibers and CPs with incorporated CNTs [85]. Reported tensile stresses and moduli are typically around several MPa and 0.05-0.8 GPa, respectively [18, 25]. Similar to CNT actuators, electromechanical coupling, i.e. the proportion of input energy transformed into work, is low (<1% as compared to 15-80% for DEAs) [18]. Typical strain rates are also small (~1%/sec), as for all ionic EAPs, because they are limited by ion transport and by internal resistances of the polymer and electrolyte. Increased voltages can be used to achieve faster actuation rates [86]. Other steps towards the improvement of strain rates above 10%/sec include corrugated metal contacts, porous polymers, smaller dopant ions, or thin films and fibers [83, 87-90]. The advantages of CPs over CNT actuators are their higher strains and lower cost, whereas CNT actuators achieve larger strengths and modulus.

PPy can be fabricated by electrodeposition onto conducting materials, and for microstructures patterning is possible by conventional microfabrication techniques [91]. Additionally, deposition onto non-conducting surfaces is possible by chemical polymerisation [92].

Several actuator geometries have been implemented, which shows the high versatility of this material. Thus the actuation is not restricted to one scheme, as it can be the case for other ionic EAPs. Possible designs include bilayer and trilayer devices, free-standing films, tubes, and yarns. Micro- and nanofabricated PPy actuators have also been shown in different configurations [22, 25, 73, 91, 92], for instance using flaps [93] (Fig. 1.4a), out-of-plane strain in micropatterns for microvalves [25, 82] or nanowires [94] and nanofibres [95]. Although most actuators are shown in liquid environment, several encapsulated CP actuators work in air [96, 97]. Table 1.1 shows an extract of different PPy actuators including different designs, doping ions and electrolytes. This table is by no means exhaustive, since several different actuator designs and actuators with lower or higher strains, stresses and moduli exist. Also, dry encapsulated films are not considered here. Actuators, for which strains and stresses are indicated, are mostly optimised with respect to these properties. Several publications do not report strain but rather changes in bending angle, grid length of

strain gauges, or tip distance. The table ought to give an insight into different actuator designs and structures, dimensions, ions used during fabrication and actuation as well as mechanical properties.

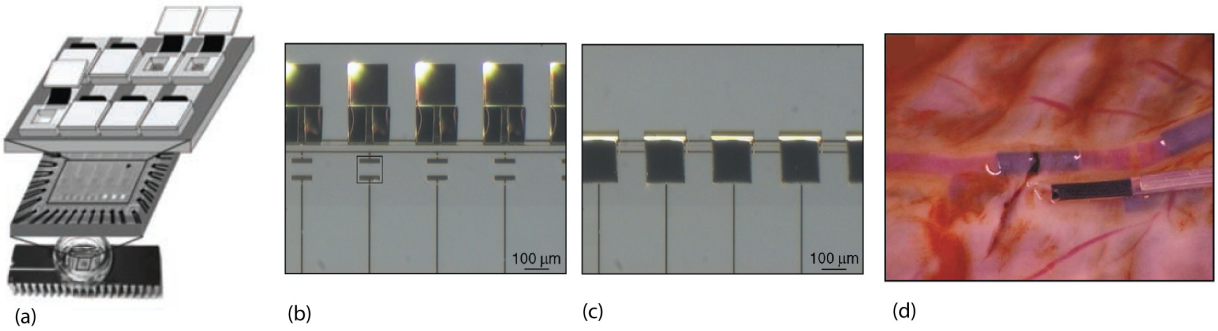

Fig. 1.4 Applications of PPy actuators in biological fields. (a)-(c) A cell clinic, which is an array of reservoirs for cells, which can be treated with different chemicals depending on the opening state of the reservoir, which is controlled by PPy flaps [22, 25, 98]. (d) Blood vessel repairs inserted *in vivo* [22].

An additional advantage of PPy is its biocompatibility. Most studies found that PPy is non-cytotoxic and *in vivo* only minimal tissue response was reported [19-21]. Additionally carboxy-endcapped polypyrrole has been proposed for improved bioactivity [99]. Due to its low voltage requirements, PPy does not need to be shielded from biological environments and it can work in body fluids, like blood plasma or urine, and in cell culture medium [73] (Fig. 1.4d). Overall, PPy is well suited to work in biomedical applications, because besides the mentioned characteristics it also works at body temperature and is light-weight [25]. Biodegradable/-erodible forms of conducting polymers have also been synthesised [100, 101].

Table 1.1 List of different possible actuator designs, dopant ions, electrolytes, and mechanical properties. [1] actuator strain under isotonic conditions, [2] actuator stress under isometric conditions

Actuator design	Dimensions (length, thickness)	Structure	Ion used	Strain typical[1]	Stress typical[2]	Modulus (MPa)	Ref
Microhinges	100 μm, 5 μm	Cr/Au/PPy	NaDBS	3-7%*	2N/m	-	[102, 103]
Bending beam	15 mm, 10 μm	Kapton/Au/PPy	NaDBS	-	-	-	[104, 105]
Film	7 mm, 13 μm	PPy	SO_3 in NH_4PF_6	6%	15MPa	-	[106]
Bending beam	20 mm, 10 μm	adherent film/PPy	$LiClO_4$	-	-	-	[107]
Film	10 mm, 12 μm	PPy	BF_4 in $NaPF_4$ or $NaBF_4$	9.5%	8-10MPa	-	[90]
Tube	15 mm, 15 μm	Au/PPy	DBS in NaDBS,NaCl ,LiCl,KCl	3-7%	>5MPa	150-260	[81, 108]
Film	50-80 mm, 10 μm	PPy	$TBAPF_6$	2.3%	>36MPa	-	[68]
Film	15 mm, 20 μm	PPy	BF_4,PF_6,CF_3 SO_3,ClO_4 in $NaPF_6$	12.5%	10-20MPa	-	[79, 80]
Film	17 mm, 12.5 μm	PPy	$LiClO_4$	-	-	100-500	[109]
Film	5-50 mm, 10 μm	Au corrugated /PPy	NaDBS in NaCl	5-12%	15-20Mpa	340	[83]
Bending monolayer	15 mm, 25 μm	PPy	$LiClO_4$	-		-	[110]
Film	15 mm, 20 μm	PPy	$Fe(CN)_6^{3-}$ in NaCl	1-2%	-	-	[111]

(Ionic) Polymer Gels (IPG)

Unlike other EAPs, polymer gels are not mainly triggered by electrical stimuli [112], but rather by alterations in pH, temperature, or chemical analytes, solvent composition and light [5]. These trigger signals evoke reversible phase transitions of the polymer gels, mainly due to changes in solubility or repulsion. Polymer gels are three-dimensional networks swollen by a large amount of solvent, and are classified into chemical- and physical gels depending on the nature of cross-links. The expansion and contraction of polymer gels take place due to active solvent uptake and release.

Polyelectrolyte gels, in which the polymer is ionizable, respond to changes in pH. Depending on the pK_a of the polymer, in a certain pH range the polymer chains become ionised and the gel swells due to ion-ion repulsion. The most prominent example of polyelectrolyte gels is polyacrylic acid, an anionic polymer, where an increase in pH leads to expansion of the gel. Besides anionic polymer gels including crosslinked polymethacrylic acid, polyacrylamide, and polystyrenesulfonic acid, also cationic polymer gels have been researched for actuation. Another group of synthetic polymers can respond to changes in temperature. When for instance the temperature around poly(N-isopropylacrylamide) is increased above the lower critical solution temperature (LCST), the polymer's water solubility is decreased, which leads to a collapse. Gels responding to temperature changes usually show more linear responses than pH-responsive gels, which show a rather step like behaviour. Collagen, a biological polymeric acid, was shown to be denaturated in concentrated salt solutions, like lithium bromide or urea and chemically actuated in length by acid-base transitions [113, 114].

Electrical actuation is either driven by the buildup of acidity or by the differences in ion diffusion rates in the gel and in the electrolyte [115, 116]. Between two plates, gel can undergo anisotropic contraction, expansion, or bending when an electric field is applied [117] (Fig. 1.5a). These effects can only occur for polyelectrolyte gels and not for uncharged hydrogels. Another bending mechanism was shown for polyelectrolyte gels in solution with oppositely charged surfactants [118]. A polyacrylonitrile gel surrounded by an electrode was shown to be electrically actuatable to tensile strains of 40%, by inducing a local pH change [119]. Actuator strain of polymer gels is mostly large, typically in the range of 10 to 50 % up to much higher values, however the established forces are small due to low elastic moduli (only several kPa) and for electrical actuation, voltages in the range of 3 to 10 V are needed. Compressive strengths range from tens to several hundreds of kPa for normal two-phase hydrogels (i.e. a polymer filled with a liquid) [6]. Developed stresses are generally higher for chemically driven gels when they are transferred between extremely different solutions, e.g. from strong acids to strong bases. Stiffer polymer gels were shown to

develop higher forces in response to chemical actuation, with a loss in strain though [120]. Mechanical properties are complicated during actuation, because of modulus and strength changes with water content and therefore, there are few systematic studies of the actuation response under load. Responses are generally rather slow (several (tens of) minutes), since the volume change depends on solvent in- and efflux, which is a diffusional process. Therefore, also strain rates are typically below 1%/sec, despite the large strains. Porous composites [121] or graft-type gels [122] have been developed to improve transition speed to a few minutes, and making the structures smaller also helps to largely reduce the actuation times [123].
Several approaches to improve mechanical properties have been demonstrated recently [6, 124]. These include double network hydrogels [125], introduction of sliding crosslinking agents [126], and reinforcement of gels with nanocomposites like inorganic fibers or plates [127], mimicking nature. With double network gels, compressive strengths up to 17 MPa at 90% water level have been demonstrated [125], which is nearly a factor 100 more than for usual gels. These values are however far above typical values of improved mechanical properties, where moduli are increased to tens of kPa while strengths around 1 MPa are shown [6]. Still, the actuation of such strong polymer gels has not yet been largely researched [128].

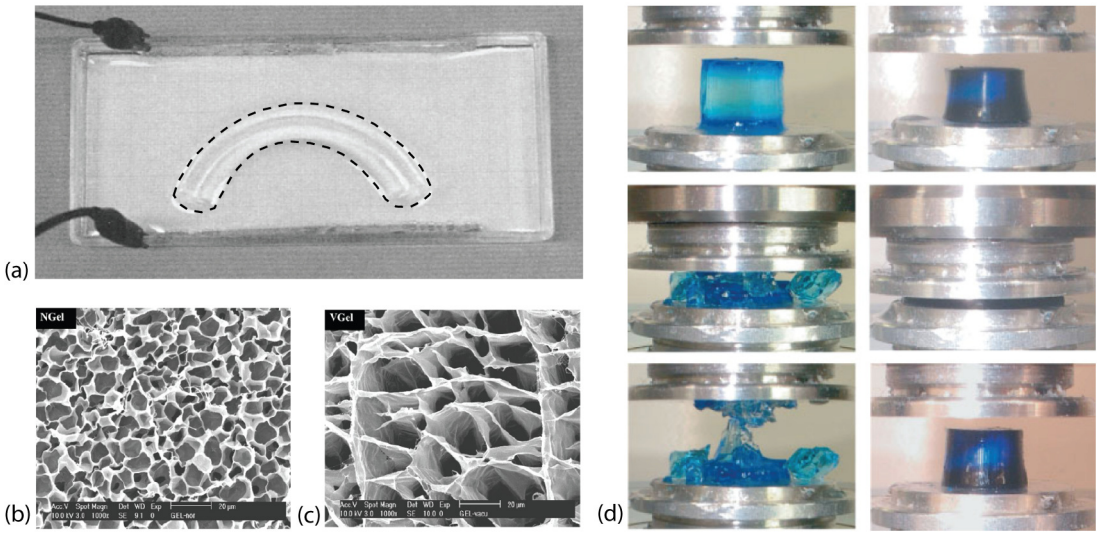

Fig. 1.5 (a) Polyelectrolyte gel which bends under the application of a dc electric field [117], (b) PNIPAAm gel as compared to (c) macroporous PNIPAAm gel [121] and (d) comparison of a typical two-phase gel (left) with a double network gel (right) under compressive stress [125]. The double network gel recovers its shape after elastic deformation, which is not the case for the two-phase gel.

Besides pH, temperature and electrical stimulation, hydrogels can also be designed to respond to antigen-antibody reactions or protein-ligand interactions, which also includes enzyme-substrate interactions [4, 129]. Several structures are biohybrid

hydrogels, which include an enzyme to actuate the hydrogel *via* pH transitions that are established due to the enzymatic reaction. Biohybrid hydrogels with calmodulin (CaM) – a calcium binding protein - were shown to undergo conformational changes upon binding of Ca^{2+} or certain peptides [130, 131]. These volume changes were reversed with the addition of EGTA, but not with a decrease in Ca^{2+} concentration. Optimally, the reponse should be reversible, which means that the switch can occur repeatedly. Using adenylate kinase-ATP with HPMA copolymers and PEG-base hybrid hydrogels a volume decrease of about 20% was achieved when the analyte concentration changed from 2mM to 8mM [132].

1.2.2 Electronic (dry) EAPs

Practically all electronic electroactive polymers, i.e. ferroelectric polymers, electrostrictive graft elastomers/-paper, electro-viscoelastic elastomers (similar to electro-rheological fluids), dielectric elastomer actuators (DEA), and liquid crystal elastomers (LCE), can not yet be employed in the kind of application we have in mind. Implementations for biomedicine exist, however restrictions appear mostly due to the high voltages or electric fields needed for actuation as well as due to the inherent actuation behaviour, which results in rather small versatility for actuator designs. Nevertheless, we shortly introduce some electronic EAPs to give an insight into their actuation principles and characteristics for comparison purposes.

Ferroelectric polymers do like other ferroelectric materials (nonconducting crystals or dielectric materials) exhibit spontaneous electric polarisation. This polarisation can be reversed and thus the dipoles are aligned by application of a high electric field, which results in a strain. (Piezoelectric materials have a very similar behaviour, but they do not spontaneously polarise). Such polymers can be actuated in air, vacuum and water, with high frequencies. Poly(vinylidene fluoride) (PVDF) and poly(vinylidene fluoride-trifluoroethylene) (PVDF-TrFE) are the most widely exploited ferroelectric polymers, where contractions of typically 3-7% in the direction of the electric field (typically 100 MV/m) have been achieved [15]. Introducing defects into PVDF-TrFE resulted in less hysteresis [133].

Dielectric elastomer actuators (DEA) exhibit thickness- and equi-bi-axial planar strain when an electric field is applied between two compliant electrodes that sandwich a dielectric elastomer. The strain is induced by electrostatic forces and can be very large in these devices (typically 10-100% and up tp 380% were reported), depending on the field strength [134, 135]. Additionally, high efficiencies can be reached (>30%) [136]. One disadvantage however is that dielectric EAP actuators

require very large electric fields (~100 V/μm) and the overhead in volume and mass due to prestrain is not negligible [18]. Thinner films of dielectric elastomers could help reduce the potential that has to be applied [137]. When high voltages are not an issue, several applications can certainly benefit from the use of DEAs [138, 139].

Liquid crystal elastomers (LCE) undergo a phase change when thermal or electrostatic energy is applied [140]. Bulk strain results from changes of order and alignment of liquid crystalline side chains which generates stresses in the backbone. While thermally actuated LCEs exhibit larger strains of up tp 40% (vs. ~4% in electrically actuated) [141, 142], their response time is slower than in electrically actuated ferroelectric LCEs due to the rate-limiting heat-transfer, and they require active cooling for relaxation (several seconds vs. several milliseconds) [143, 144]. Ferroelectric LCEs require up to two orders of magnitude smaller electric fields (several V/μm) than DEAs or ferroelectric polymers [142].

1.3 Drug delivery devices

Nowadays most drugs are still delivered at frequencies and doses based on average values. To individualise drug delivery, a great amount of research focuses on medical systems to deliver drugs in a controlled manner [145]. Thereby, the effectiveness and safety of drugs can be improved. It is important that drugs, as long as they are not released, stay intact and are protected from the body until needed. Also, the drug doses and delivery should be adjustable for patients with different needs, to avoid sidereactions of overdoses, etc. Sensing the environment could enable a simultaneous control of the drug release. Several implementations of individualised drug delivery are being explored [145-147].

Integrated medical feedback systems for example incorporate a sensor, a battery, an electronic chip, as well as a release mechanism for the drug. This principle is now already used in pacemakers where an oxygen sensor measures the oxygen content in blood and signals the actuator at which pace it should deliver electrical pulses. Such medical feedback systems have been proposed for the delivery of insulin in response to glucose levels in blood [23, 93, 148, 149] (Fig. 1.6a). Those devices require either a reservoir with an active pump [148], or one or more reservoirs which are opened when a signal is applied, where the release of the drug is driven by diffusion out of the reservoir [150].

A device that controlls drug release by programmable remote control but without sensor has been implemented [151]. A polypeptide is stored in an array of reservoirs and released in a controlled pulsatile manner by an electrothermal method, removing

the metallic membranes by local resistive heating from an applied current. The capability of varying the dose as well as release timing over six months was shown *in vivo* in canine models. A similar device used the electrochemical dissolution of gold membranes covering reservoirs to release a chemotherapeutic agent to an experimental tumor in rats [152]. The principle of controlled reservoir opening was also shown for an array of PPy flap valves [93] and in PPy membranes the rate of release was reported to be dependent on the applied potential [153]. The difficulties in those systems still lie in the size of the devices, i.e. the batteries needed, which make up a large part of the volume and weight.

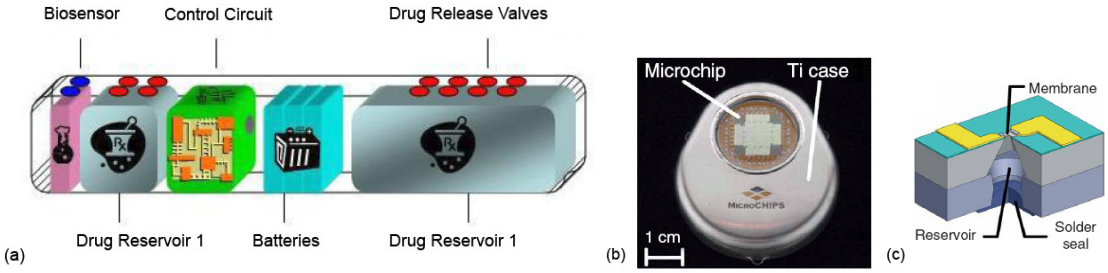

Fig. 1.6 (a) Schematics of an integrated medical feedback system with several separated entities in one device where the drug release is controlled by the opening and closing of pores [23]. (b) Example of a drug release device employing electrothermal removal of membranes to release a drug from an array of reservoirs as displayed in (c) [151]. In both examples batteries are needed.

To avoid the use of batteries, several systems have been researched which base on the passive transport of drugs, e.g. by diffusion or osmotic pumping: Similar to multireservoir devices mentioned above, a biodegradable polymer chip device was shown to release drugs in a pulsatile manner [154]. The team used membranes with different molecular weights to control the release rates of human growth hormone (HGH), dextran, and heparin. An obvious advantage over many other devices is the biodegradability, which eliminates a second surgery. Using nanoporous technology, membranes can be fabricated, which slowly release a drug from a large reservoir, the rate depending on the pore size as well as the surface modification [155, 156]. Semipermeable membranes were also used in artificial pancreas to provide a mechanical barrier between pancreatic cells and the host immune system, while being permeable for the chemical agents produced by the cells [157]. A drug-dispensing osmotic pump demonstrated by Wright et al. was activated where water enteres the device through a semipermeable membrane, which causes the osmotic agent to swell. This again pushes a piston to continuously dispense a drug from the drug reservoir [158]. Different hydrogel membranes or particles were demonstrated to release drugs due to molecule diffusion and constant or body-temperature dependent gel degradation [129].

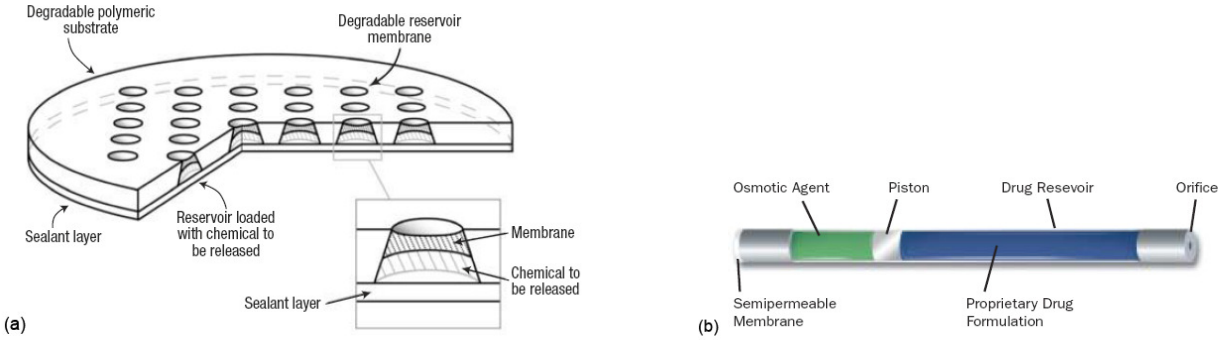

Fig. 1.7 (a) biodegradable polymer membranes with different thicknesses for the pulsed release of drugs from an array of reservoirs [154] and (b) osmotic pump to continuously release a drug from an orifice in the device [159].

Several microstructures have been researched to improve drug solubilisation and -availability, protection from drug hydrolysis and other types of chemical or enzymatic degradation. Examples include micelles, liposomes, liquid crystalline phases, polymer (micro)gels and –microcapsules and even nanotubes [160, 161].
The systems mentioned above include the advantage of working battery-less while continuously releasing a predefined amount of drug. If however the drug delivery should depend on the concentration of a certain chemical agent, materials have to be employed that (reversibly) change their state depending on their chemical environment. Approaches to such stimuli-responsive materials include polymer gel membranes or particles which change their porosity or structure depending on parameters like pH or the availability of certain molecules [5, 129, 160]. Else, an osmotic pump could be employed as external pump which constantly provides a drug (in this case insulin) via a transcutane catheter to a glucose-responsive microvalve [162]. A responsive hydrogel microvalve was shown to control the release of liquid in response to glucose [24]. In this example, however, the polarity was opposite to what would be needed for insulin delivery, i.e. more insulin when glucose concentration is higher.
More collective overviews over drug delivery, addressing also the transdermal transport, different pumps researched for the delivery and valve designs, as well as biocompatibility are given in [145-147].

1.4 Thesis outline

Currently, most smart actuators are driven by an external electrical potential from a power source like a potentiostat or a battery. For several reasons however, batteries are not always the best choice for powering actuators. For instance, batteries still belong to the most spacious and heavy parts in an electrical assembly and today's miniaturisation needs contrast with the energy consumption of actuators. Therefore, our goal was to broaden the range of chemically actuatable materials and to show the possibility of actuating PPy with redox agents in solution. PPy was selected due to its interesting and attractive properties like for instance the possibility of actuation with low voltages, high strength, broad strain vs. potential regions, compatibility with different (biological) liquids as well as the versatility with respect to actuator designs.

In chapter two of this thesis the actuation of PPy in response to redox chemicals in solution is, to the best of our knowledge, analysed for the first time. The principle of PPy actuation powered with chemical energy is described in section one of the next chapter. In section 2.2, the choice of the actuator design and of the system to measure strain responses, as well as the fabrication of the PPy bending actuators is explained. After giving a brief description of the electrochemical methods (2.3) and the measurement setup (2.4), the chemical actuation in anion- and cation exchanging PPy is demonstrated in sections 2.5 and 2.6, respectively. PPy with perchlorate (ClO_4^-) is shown to be actuatable with hexacyanoferrate and L-ascorbic acid, apart from kinetics just in the same way as with an external potential. In addition, section 2.5 also includes an analysis of reaction pathways for the redox agent induced actuation, and an investigation of the effects of changes in pH, electrolyte concentration as well as temperature on PPy strain. PPy with dodeclybenzenesulfonate (DBS^-) as large dopant anions is taken to demonstrate a reverse polarity of movements in section 2.6, also driven by changes in chemical energy.
Chapter 3 then presents an actuation principle which is partly chemical, partly electrochemical. With the same PPy(ClO_4) actuator as in chapter 2 we achieved considerable actuation within less than one second. This was possible during electrical shortcut to an oxygen cathode after reducing the PPy anode with L-ascorbic acid in solution.
Appendix A documents the model of the bending beam, and the equation for calculating strain from curvature is derived. We consider two cases, one for the actuator with only one metal layer on the backing layer and the second case for the backing layer coated on both sides with metal.

Appendix B contains the development of a PPy-based microfluidic valve fabricated in a very simple and cost-effective manner. The flow rate through the membrane valve was controlled through the applied electrical potential.

2 Strain response to redox agents in solution

Among the EAPs and smart actuators introduced in the previous chapters, ionic EAP actuators are best suited for actuator application in or near the human body due to the low potentials needed for actuation and their lightweight. Conducting polymers, polypyrrole (PPy) in particular, have caught our attention, because of the actuation properties as well as the biocompatibility and the various possible actuation configurations [25]. PPy can be actuated under high stress (typically up to 5 MPa, higher values were reported), features high stiffness (several hundred MPa), as well as moderate strains (typically 1-3%, higher strains of 12% in-plane and 30% laterally were reported) [18]. Limitations are found in strain rates (around 1%/sec) - as for all ionic EAPs - and electromechanical coupling. PPy can show linear responses of strain to potential with moderate to low hysteresis and is active in aqueous solutions in a wide range of pH, especially in neutral pH where several other conductive polymers are not actuatable [76, 77].

In this chapter we therefore present the possibility to induce strain in PPy with stimuli from the environment, i.e. redox agents in solution [163]. This principle is inspired by nature, where responses are mostly induced by chemical triggers, without the application of potential from an external electrical source, but rather directly including the conversion of chemical energy to work into the system.

After a brief introduction into the working principle of PPy actuators, we will discuss the different implementations that are possible. Following the description of the actuator fabrication, electrochemical methods, and the setup to observe the responses in the PPy films in sections 2.2, 2.3 and 2.4, we discuss the results obtained with the redox agents hexacyanoferrate and ascorbic acid in section 2.5. Comparison to the conventional actuation using a potentiostat yields a very good correlation, while linearity is given in all measurements, hysteresis can be as low as 6.5%, and the strain changes are repeatable. The origin of potential and strain responses are further analysed and compared to effects from electrolyte concentration-, pH-, and temperature variations. In section 2.6 we demonstrate that it is possible to change the polarity of the actuator by using large dopant anions. The resulting actuator also responds to hexacyanoferrate and ascorbic acid redox agents in solution.

2.1 Actuation principle of PPy actuators

Polypyrrole (PPy) is a chemical compound formed from connected pyrrole ring structures and its basic structure, like that of conjugated polymers in general, consists of carbon atoms connected by alternating single and double bonds (Fig. 2.1). For an in-depth discussion of the different proposed electropolymerisation mechanisms the reader is referred to the publication by Sadki et al. [164].

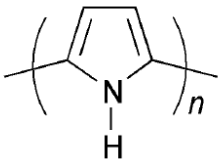

Fig. 2.1 Chemical structure of the polymer PPy which is formed from a number of connected pyrrole ring structures [164].

The product of the electropolymerisation onto a conducting substrate is not exactly the neutral non-conducting polymer as illustrated in Fig. 2.1 but the oxidised conducting form. This form is defined as *doped*, since the polymer chain carries a positive charge every 3 to 4 pyrrole units. The alternating single and double bonds allow net charge to be shared among the carbon atoms. This positive charge is counter-balanced by dopant anions A^- (Fig. 2.2). Oxidised and to a certain extent also reduced PPy is electrically conductive due to the mobile charges, which is the reason why conjugated polymers are also called conducting polymers. In the remaining text, PPy with dopant anions A^- is referred to as PPy(A).

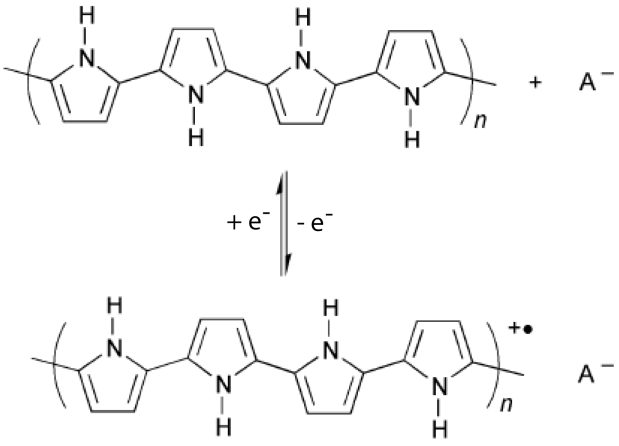

Fig. 2.2 The transition between neutral PPy (top) and partially oxidised PPy (bottom) with charge-compensating dopant anions A^- [164].

Upon application of a voltage or current, PPy can be switched between oxidised and neutral (reduced) states, i.e. more or less positive charges are present on the polymer backbone. The electronic structure of PPy allows charge to be removed and added relatively easily. A change in oxidation state of the polymer results in a flux of mobile solvated ions between the polymer and the surrounding electrolyte to maintain charge neutrality [64]. Depending on the size of the dopant anions incorporated during polymerisation, the in- and efflux is dominated by either anions or cations. If the dopant anions are small, they can enter and leave the polymer during actuation. On the other hand, charge compensation takes place by cations if the dopant anions become entrapped in the polymer matrix due to the large size and cannot leave during reduction. The two possible mechanisms are shown in Fig. 2.3. The volume change and thus actuation is, besides other effects [69, 165], primarily caused by the in- and efflux of ions with their solvation shell. In the case when water is the solvent, the hydration shell strongly increases the volume change. The number of water molecules depends on the anionic and cationic species.

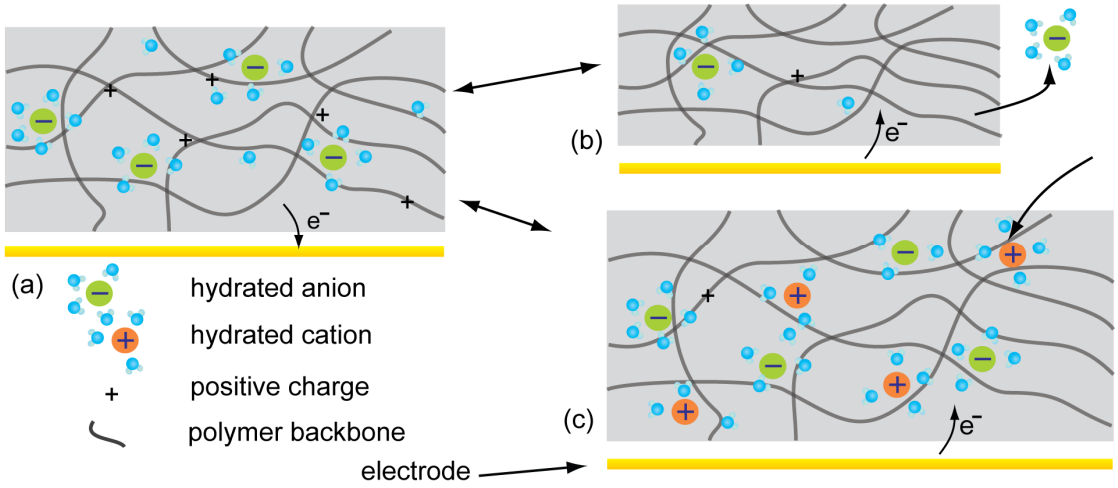

Fig. 2.3 Schematic illustration of the actuation mechanisms of PPy. When PPy is switched from the (a) oxidised state into the reduced state by transfer of electrons from a conducting substrate either (b) anions leave the polymer matrix or (c) cations enter the system to compensate the charge. In case (b) the PPy experiences a decrease in volume during reduction while in (c) the volume is increased (adapted from [25]).

Equations (2.1) and (2.2) describe the transitions illustrated in Fig. 2.3 from oxidised PPy^+ with anions A^- inside the matrix to reduced PPy with either anions released to the solution or cations incorporated into the film.

$$PPy^{+}\left(A^{-}\right)+e^{-} \leftrightarrow PPy + A^{-}_{sol} \tag{2.1}$$

$$PPy^{+}\left(A^{-}\right)+e^{-}+C^{+} \leftrightarrow PPy\left(A^{-}C^{+}\right) \tag{2.2}$$

The different dopants can affect besides the actuation direction also the material properties, such as morphology, conductivity, Young's modulus, and the actuation performance.
The transition from oxidised to reduced PPy and back can not only be evoked by electron transfer from a conducting substrate. An oxidising or reducing agent that interacts with PPy changes the oxidation state as denoted in Equation (2.3) [166], and with this it should induce ion exchange as shown in Fig. 2.4 for anion exchanging PPy [163].

$$Red + PPy^{+} \leftrightarrow Ox + PPy \tag{2.3}$$

The strain that results from the ion in- and efflux is supposed to be related to the established potential, in analogy to applying an external potential (e.g., using a potentiostat).

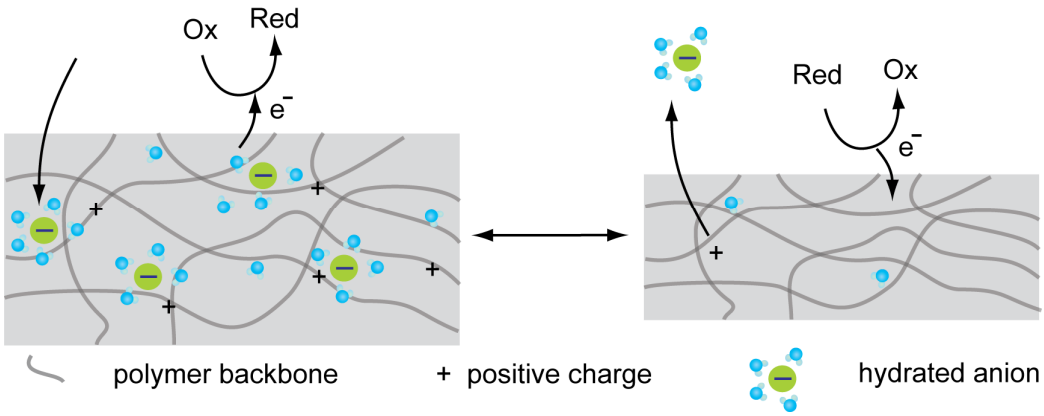

Fig. 2.4 Schematic illustration of the redox processes at an anion exchanging polypyrrole actuator. The reducing (Red) and oxidising (Ox) agents react at the polymer surface to induce anion A^- in- and efflux by changing the oxidation state of the polymer (adapted from [25]).

2.2 Actuator design and fabrication

The design of the setup has to enable the observation of PPy actuation and thus the characterisation of the response of PPy towards redox agents in solution. As already

mentioned in section 1.2.1 diverse implementations are possible to visualise strain in the polymer film. In our system we employed a bending beam actuator, which translates in-plane strain/stress into bending behaviour. The configuration is analogous to bi-metal strips, which bend due to thermal expansion [167]. This simple yet sensitive method has already been utilized in several papers [97, 103, 165, 168-173]. Fig. 2.5 illustrates the principle along with two different measurement methods: free-standing strips or tubes clamped into an automated force-displacement rig (Fig. 2.5b) [79-81, 83, 109] and PPy on strain gauges (Fig. 2.5c) [174-176]. One problem in using free-standing strips is to overcome the limitations due to charge percolation along the length of the strip [83]. Therefore, it is difficult to compare actuation using an external power source to chemically driven actuation. While in the first case the current has to run from both ends into the actuator strip, in the second mechanism, the electron transfer takes place at the whole actuator surface. A bending beam can also be implemented as micromechanical cantilever [102, 177], this however introduces additional mirco-scale effects, which complicates the analysis of the basic behaviour. Bending beam actuators are a cost-efficient way to analyse the strain in PPy since they require only a polymer backing with a very thin layer of inert metal and the movements can be analysed with standard camera equipment. Additionally, they are optimally suited for flow-through measurements, since the openings can be tightly sealed.

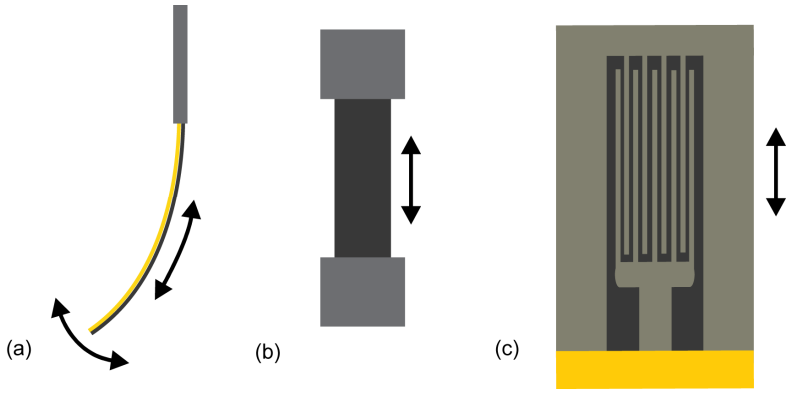

Fig. 2.5 Different configurations for measurement of PPy in-plane strain. (a) Bending actuator, (b) free-standing film, and (c) strain gauge.

As polymer backing, we chose polyimide (PI), due to its chemically stable properties and its broad availability from various vendors. Additionally, gold can directly be evaporated onto PI and forms a stable connection without adhesion layer. This fact reduces the possibility of side-reactions with chemically reactive materials, such as Cr.

Table 2.1 Various PI films from different vendors with their thicknesses, E-moduli and specific properties, which affect their suitability for use as backing in the bending beam actuator.

Vendor / Product	Thickness (μm)	E-modulus	Comment
Micronova / 825-14AM [a)]	25	2.9 GPa	Pre-bent
DuPont / Kapton 100HN [b)]	25	2.5 GPa*	Straight
DuPont / Kapton 50HN [b)]	12.7	2.5 Gpa*	Too deficient/difficult handling
DuPont / Kapton E [b)]	25	5.52 GPa*	Too stiff
St Gobain / 2345-1 [a)]	25	-	Au peels off during cutting
Mc Master Carr/7648A723 [a)]	25	-	Helical bending

* as indicated by vendor, else measured using a Zwick/Roell Z005 tensile tester.

[a)] PI tape where the adhesive was removed

[b)] PI film which is ready for use

Table 2.1 displays different PI films that were tested for their compatibility as backing for the bending beam actuator. We either directly used PI films and coated them with a gold layer or we employed PI tape, where we manually removed the adhesive before the Au coating step. The PI tapes were generally better suited due to their fabrication process dependent pre-bending, which simplifies the analysis of the sample curvature. Not all selected tapes were ideal, however, because either the Au layer peeled off during cutting (which is supposed to result from a surface treatment of the tape) or the films bent helical. Other substrates employed in the literature include mylar [77], polyethylene [165] or PVDF [178]. Mylar is not ideally suited as substrate of bending beams, because problems with fragility of the material as well as cracking of the gold were reported to arise [77].

Polyimide (Kapton®) tape (Micronova Manufacturing) of 25 μm thickness, where the adhesive had been removed using acetone, was coated on one side with gold of 400 Å thickness by vacuum evaporation (0.7 Å/s with a current of 60 mA) (Fig. 2.6a,b). No additional adhesion layer was included, since the gold layer adhered well to the PI film and we did not want any additional material in the system which is not inert. The polyimide/gold (PI/Au) films were cut into 1.4 mm wide strips using a sharp blade and electrically connected with adhesive copper tape, as illustrated in Fig. 2.6b. On an area of 23.8 mm^2, PPy was galvanostatically deposited onto the gold layer (Fig. 2.6c). For this, pyrrole monomer was first passed over neutral alumina (Al_2O_3) until colorless before use and stored at 4°C. The aqueous polymerisation solutions were prepared with the respective electrolyte, either $NaClO_4$ (sodium perchlorate,

Sigma-Aldrich) or NaDBS (sodium dodecylbenzenesulfonate, Sigma-Aldrich), and pyrrole (Sigma-Aldrich, 98%). Ultra high quality water (>18Mohm·cm) was used throughout the experiments. For PPy(ClO_4) the solution was gently purged with nitrogen before polymerisation for mixing and to reduce the oxygen content. Nitrogen purging was not done for PPy(DBS) due to strong bubble formation with the surfactant inside the solution. The polymerisation solutions were always composed directly prior to synthesis to reduce the possibility of pyrrole degradation.

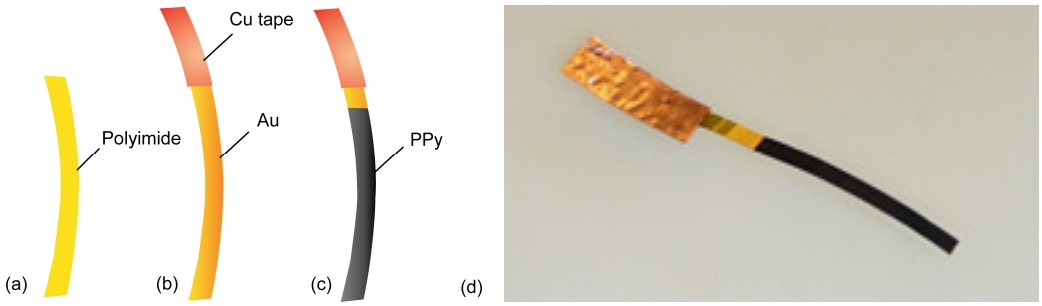

Fig. 2.6 Fabrication process of the PPy bending actuators. (a) Adhesive is removed from the PI tape, (b) an Au layer of 400Å is evaporated onto the PI film and contacted with a Cu tape, (c) PPy is polymerised onto the PI/Au strip. (d) Finished bending actuator sample.

We employed galvanostatic depositions, since this method gave reproducible results in actuator properties in our system. Other teams report that PPy properties (conductivity, structure) are improved and more reproducible when potentiostatic [91] or potentiodynamic deposition techniques are used [179]. These conclusions are however dependent on the properties under analysis. The polymerisation solutions are given in the corresponding sections for anion-exchanging and cation-exchanging PPy. After deposition and before starting the measurements the samples were conditioned to achieve a constant actuator performance. The samples were cycled 15 times at 150 mV/s (-0.65 V to +0.8 V vs. Ag/AgCl in 0.5 M $NaClO_4$ for PPy(ClO_4) and -0.9 V to +0.2 V vs. Ag/AgCl in 0.5 M NaCl for PPy(DBS)) until a stable CV was reached and further equilibrated in the respective measurement solution for one hour. During deposition and conditioning, the actuators, i.e. working electrodes (WE), were suspended freely from an alligator clip between a platinum counter (CE) and an Ag/AgCl reference electrode (RE, Radiometer Analytical), the gold-coated side facing the platinum counter electrode. The current and voltage for polymerisation as well as for cyclic voltammetry (CV) were controlled by a Model 283 Princeton Applied Research (EG&G) potentiostat/galvanostat or a VersaStat3 (Princeton Applied Research).

2.3 Electrochemical methods

For polymerisation, conditioning, as well as during measurements, we are using different electrochemical methods, which are briefly explained in this section. In general, electrochemistry is concerned with the interrelation of chemical and electrical effects [180]. An electrochemical cell consists of at least two electrodes, a working electrode (WE) and a reference electrode (RE). While the WE is the electrode under scrutiny, the RE behaves as an ideal nonpolarised electrode with constant potential, in our case a silver/silver chloride (Ag/AgCl) RE is used. If a current is required to pass through the WE and the cell resistance is relatively high, an additional counter electrode (CE) is needed (Fig. 2.9a). During polymerisation, we applied a constant current between WE and CE. This method is called galvanostatic or chronopotentiometric. If instead of current the potential is controlled to be constant between WE and RE, we are working in a potentiometric or chronoamperometric mode.

2.3.1 Cyclic Voltammetry

During cyclic voltammetry (CV), a triangular potential time waveform (Fig. 2.7a) is applied to the WE and the current passing through the electrode is recorded. The WE potential is varied between two turning potentials with a constant scan rate v = dE/dt. For a CV diagram, the potential and current values corresponding to the different points in time are plotted in a graph (Fig. 2.7b).

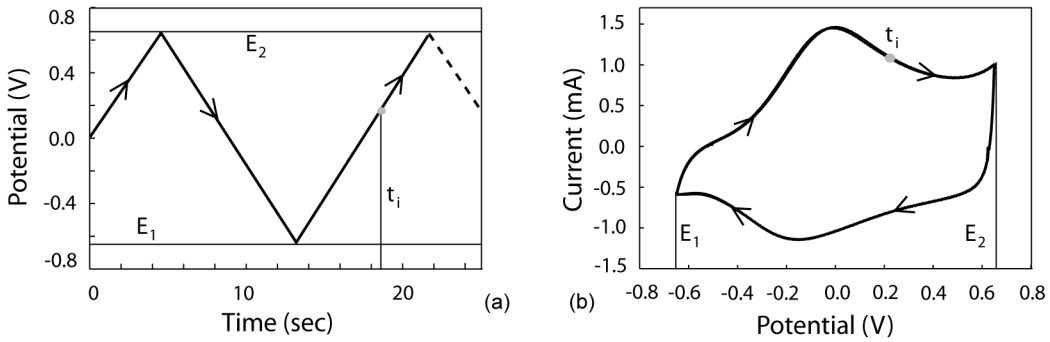

Fig. 2.7 Illustration of cyclic voltammetry: (a) triangular potential waveform applied to the working electrode (WE). The potential is varied between a lower potential E_1 and a higher potential E_2 with a constant scan rate v = dE/dt. At each time point t_i the potential and the corresponding current value are plotted into a graph, the cyclic voltammogram (b). Here the CV of a PPy film as in Fig. 2.19b taken at 150 mV/s is shown.

By definition anodic currents (currents during the positive potential scan half) are plotted in positive direction. The CV displays the different faradaic and non-faradaic processes at the WE. Usually, peaks in a CV appear due to redox processes. Fig. 2.7b shows the CV of a thin PPy film acquired at a scan rate of 150 mV/s. During the anodic scan (from potential E_1 to E_2), the polymer is being oxidised, which is reflected in a positive current peak, whereas the negative current peak corresponds to a reduction of the PPy. The characteristics of a CV usually vary when the scan rate is changed or with different film thicknesses. For thicker films, the current peaks are broader since the redox processes do not occur simultaneously throughout the whole film (compare to Fig. 2.13a).

2.4 Measurement setup and data acquisition

The different measurements were performed in a custom-made PMMA-flow cell (Fig. 2.8) with input- and output tubing (Ismatec) which enabled the liquid exchange driven by a tubing pump (Ismatec) set at 2.5 ml/min, which does not affect the bending of the beam. The flow rate is high enough to provide a satisfying exchange rate but low enough to avoid interferences to the strip bending.

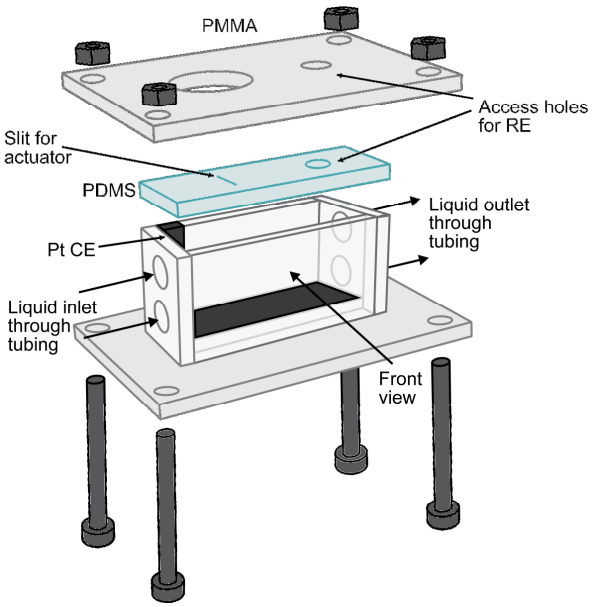

Fig. 2.8 Illustration of the flow cell setup. The cell (1 ml volume) is assembled from PMMA pieces, sealed with a PDMS cast and fixed with PMMA panels and screws. The PDMS cast has access holes/slits for the bending actuator, the reference electrode (RE) as well as the Pt counter electrode (Pt CE). The liquid is flushed into and out of the PMMA cell using tubes, which are not displayed. The whole cell is turned such that the front view window can be observed from the top.

For proper footing of the strip while the liquid is flushed and to seal the cell, the strip was inserted into a slit of a polydimethylsiloxane (PDMS) sealing, which also had access slits/holes for the counter and the reference electrodes. The length of the strip inside the flow cell was adjusted to 12 mm. The Pt-foil counter electrode needed to be as large as possible, therefore it covered the bottom of the flow cell and a part of the sidewall.
Two different configurations were employed for the characterisation of the system. First, the bending actuator properties were characterised in a three-electrode setup with potential scans applied by a potentiostat (Model 283 Princeton Applied Research (EG&G) potentiostat/galvanostat) (Fig. 2.9a). These measurements provide a reference to further compare the two actuation methods. Subsequently, the responses to redox agents in solution were acquired in a two-electrode setup where the established potential is measured between WE and RE (FLEXREF, World Precision Instruments, Eref = -59 mV/SCE) along with the actuator bending (Fig. 2.9b). The potential data is collected over a multimeter (Keithley 2000) with 0.1 mV resolution using custom LabVIEW software sampling at 1 Hz.

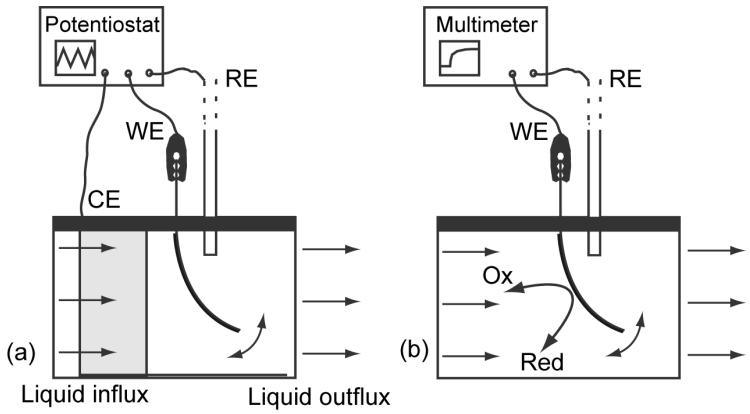

Fig. 2.9 Schematic illustrations of (a) the three-electrode setup for actuator characterisation where the potential is externally applied by a potentiostat and (b) the two-electrode setup for measurements of the established potential resulting from the reaction of redox agents at the PPy.

A digital video camera (1200x1600) connected to a microscope and controlled over PC with PSRemote (Breeze Systems) recorded the actuator movement (Fig. 2.10a-c). The strips are tilted about 2° to improve the contrast for the image analysis. A ruler was included in the field of view for initial calibration. Analysis of the recorded voltage and images was performed using custom Matlab subroutines. The curvature of the strip was extracted by fitting a circle to the strip outline minimising geometric error using nonlinear least squares (Fig. 2.10d-e).

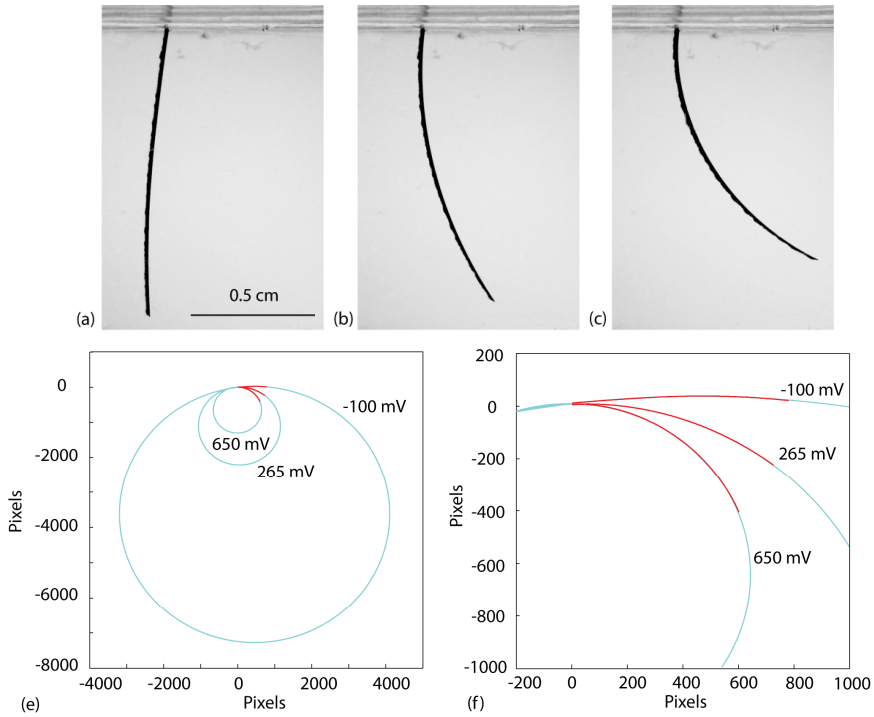

Fig. 2.10 (a-c) Image acquisition and (d-e) curvature evaluation by fitting circles to the outline of the actuator using Matlab of PPy actuator at three different potentials (a) -100 mV, (b) +265 mV, and (c) +650 mV.

To calculate the actuation strain from the measured curvature, classical beam theory can be used. In appendix A the whole model is explained. It was previously shown that the curvature of bending actuators made from polypyrrole on a PI/Au layer [168] or only a gold layer [103] can be expressed by the Timoshenko equation [167] for a uniformly heated bimetallic strip:

$$\begin{aligned} \frac{1}{R} - \frac{1}{R_r} = \kappa - \kappa_r = \frac{6 \cdot \alpha_{PPy} \cdot (1+m)^2}{h(3(1+m)^2 + (1+mn)(m^2 + \frac{1}{mn}))}, \\ m = \frac{h_{PI}}{h_{PPy}}, n = \frac{E_{PI}}{E_{PPy}}, h = h_{PI} + h_{PPy} \end{aligned} \tag{2.4}$$

with R being the radius and κ the curvature of the strip, while R_r and κ_r are the radius and curvature of the rest state before actuation. E_{PI} and E_{PPy} are the E moduli of the PI substrate and the PPy layer, respectively, h_{PI} and h_{PPy} are the corresponding thicknesses, and α_{PPy} is the actuation strain of the PPy layer. The strain in PPy, α_{PPy}, is assumed to be constant over the whole thickness. This equation can be deduced from the equilibrium conditions of the normal forces and the bending moments (see Appendix A for further explanations). The Au layer was

neglected in the model calculations due to its small thickness (40 nm) compared to the other layers. The strain, which is the relative change in length of the polymer due to oxidation/reduction when the layer is not adhering to PI/Au, can then be calculated from the curvature data points that were measured. A positive strain refers to bending to the PI side (Fig. 2.10).

2.5 Characterisation of anion exchanging PPy

As mentioned in section 2.1, two different actuation principles are possible, depending on the size of the incorporated anion. Here, we analyse the responses of PPy actuators with perchlorate (ClO_4^-) as dopant anion. Perchlorate is a comparably small anion and therefore PPy(ClO_4) is an anion-exchanging polymer film (Fig. 2.4), which can be actuated in aqueous solutions and shows a large continuous strain window [109, 174, 176].
Parameters used for calculations are as follows: the E modulus and Poisson ratio of the polyimide are given as 2.9 GPa and 0.34, while the thickness h_{PI} is 25 μm. We measured a tensile modulus of 0.102 GPa $\pm$ 8 MPa for our PPy(ClO_4) films (Zwick/Roell Z005 tensile tester, at 10%/min), which corresponds well to values reported for anion-exchanging PPy films (80 - 110 MPa for low forces) [109]. Variations in modulus might introduce inaccuracies on the calculated strain, i.e. decreasing the modulus about 8 MPa leads to an increase in strain of around 7%. The thickness h_{PPy} is taken as 13.1 μm which corresponds to a charge density during polymerisation of 2.3 C/cm^2 using a conversion factor of 5.7 μmC^{-1}cm^2 [181], which was verified for our system using white light interferometry (Zygo) of Au-sputtered PPy samples.

2.5.1 PPy(ClO_4) actuator performance using an external power source

In order to put the redox-controlled actuation properties of PPy into practical use, it is beneficial when the actuator exhibits (i) a large total strain, (ii) low charge consumption during actuation, (iii) a broad linear region, (iv) a small to no hysteresis in strain, and (v) no drift during measurements.
The charge or current, which is used to change the potential of the PPy during actuation, should be held low. Under this condition, the number of redox molecules, that are required to react at the polymer to load it to a certain potential, can be

reduced. This will eventually lead to shorter response times. Hysteresis and drift should be avoided to ensure the same strain values for forward and reverse potential transitions and in the course of time.

To achieve a large net strain, the polymerisation should be carried out under low current and low potential [176, 182]. A possible explanation which was given is that PPy films produced at higher potentials form a more crosslinked network, which restricts anion movement into and out of the polymer, which consequently limits mechanical deformation. A low polymerisation potential can be achieved by using a low current, and high molarities of $NaClO_4$ and pyrrole [182-184]. Thus the molarity of $NaClO_4$ and pyrrole were both set to 0.2 M, which leads to a potential of about 0.69 V with a polymerisation current of 6 mA/cm^2. It is interesting to see that, although the net strain increases with lower polymerisation potential, the charge density used to switch the oxidation states stays similar, which was observed by Pyo et al. [176]. An increase in total polymerisation charge should result in the same net strain, but in larger curvature changes because the films are thicker (see the model in Appendix A). This is however only true up to a certain thickness, where a maximum in bending is achieved [103]. In this case, the errors introduced in the data readout and analysis can be reduced. The increased PPy film thickness simultaneously results in an increase of switching charge though. This trade-off in mind we found a charge density of 2.3 C/cm^2 to be a good choice.

Only few publications report on the hysteresis and linearity behaviour of anion exchanging PPy during potential cycling. The microstrain of a PPy(ClO_4) actuator was measured in [176] and compared to PPy(Cl) and PPy(NO_3). The strain changes of PPy film actuators with various dopants (BF_4^-, PF_6^-, $CF_3SO_3^-$, ClO_4^-) tested in different electrolytes showed good linearities but the hystereses were not negligible, even with different scan window sizes employed [79, 80]. The effect of monomer and electrolyte concentration and current density on the actuation of PPy(CF_3SO_3) in aqueous $NaPF_6$ electrolyte was analysed by Chu et al. [182, 183]. An increase in both monomer and electrolyte concentration as well as a decrease in polymerisation current density increased the actuation strain. The linearity regions did not change significantly while hysteresis was observable with all fabrication parameters at a scan rate of 2 mV/s. Several other parameters have been considered for the observation of mass changes during cycling of PPy films. Varela et al. [185] reported the mass change of thin PPy(ClO_4) films in different solvents and showed that in water the mass change vs. applied potential shows least hysteresis. The total mass changes are however larger in acetonitrile (ACN), methanol (MeOH), N,N-dimethylformamide (DMF) and ethanol (EtOH), although the electroactivity in water is greatest. The mass changes of PPy(Cl), PPy(NO_3), and PPy(ClO_4) were shown to depend on the thickness of the polymer layer [186], i.e. thicknesses of below 0.1 μm partly yielded cation transport. The electrolyte can also influence the mass change of PPy(Cl) and

result in anionic or mixed anionic and cationic transport [78, 187]. Different fabrication- or scan parameters were not considered in those publications.
To test the linearity, strain extent and hysteresis in our system, the actuators were subjected to voltage scans in different ranges (Fig. 2.11). The results were examined to be reproducible with at least three different actuators. The scan rate was set at 2 mV/s, since the transition time during operation with redox agents is assumed to lie in this range. Optimally, the system should display a linear strain over the range where abundant redox pairs are available under mild conditions. Fig. 2.11a displays the strain response when the potential window is set from -0.65 V to +0.65 V. Extending the higher end of the potential window might lead to overoxidation, especially with such a slow scan rate [188-193] .

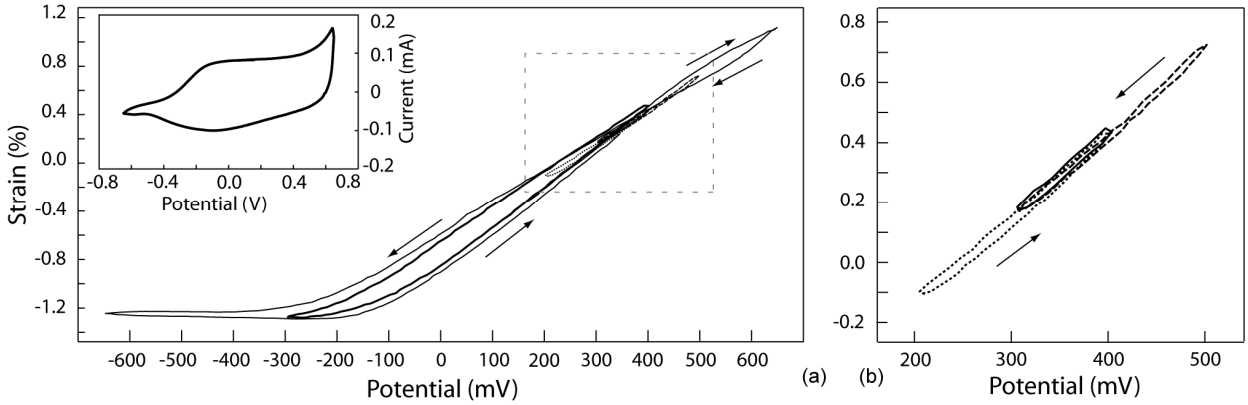

Fig. 2.11 Linearity and hysteresis measurements of PPy(ClO_4) bending actuators in 0.5 M $NaClO_4$. The voltage is applied by a potentiostat vs. an Ag/AgCl reference electrode with a scan rate of 2 mV/s. A positive strain corresponds to expansion of the polypyrrole film. The liquid exchange rate in the flow chamber is 2.5 ml/min. The inset shows the CV recorded at 2 mV/s corresponding to the potential scan for the strain analysis.

Although strain vs. potential in forward and reverse scans is linear in the interval from about -150 mV to 650 mV, hysteresis of 13.2 % is present and shows a transition at about 400 mV. It is possible that besides ion movement, structural changes in the matrix and reorganization of the liquid in the film take place [69, 194]. In addition, because of the large potential window and the slow scan rate, cations could also play a role in volume changes [78]. Reduction of the scan window size, as indicated in Fig. 2.11a and b, lead to reduced hyteresis. For example, ranges of 700 mV and 200 mV result in hystereses of 11.4 % and 6.5 %, respectively. Further reducing the scan window to 100 mV leads to a hysteresis of 9.7 %.

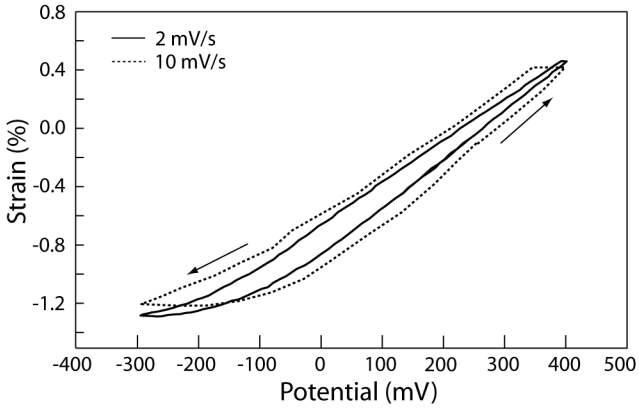

Fig. 2.12 Increase in scan rate – linearity and hysteresis measurements of $PPy(ClO_4)$ bending actuator in 0.5 M $NaClO_4$. The voltage is applied by a potentiostat vs. an Ag/AgCl reference electrode with a scan rate of 2 mV/s and 10 mV/s respectively.

An increase in scan rate from 2 mV/s to 10 mV/s leads to doubling of the hysteresis (Fig. 2.12), which shows that the amount of oxidation and reduction of the PPy does not only depend on the potential window, but also on the scan rate. Since the charge consumption at higher scan rates is decreased, so is the actuation strain, because it depends on the consumed charge [195]. Other reasons include transport kinetics of anions or the relaxation inside the polymer network [69, 71].

2.5.2 Reproducibility of $PPy(ClO_4)$ actuation

To have a good starting point for further measurements with the redox agents, the strain behaviour of the $PPy(ClO_4)$ actuators should be reproducible. First, we considered the cyclic voltammograms (CVs) directly after fabrication. The positions of the peaks as well as the peak currents in the CVs are fairly consistent for the given deposition recipe as can be seen in Fig. 2.13a. Some variability might result from slight differences in strip width or immersed strip length in the deposition solution and thus variances in deposition area. Another effect which is not relevant for further measurements but is still visible in this data set is the immersion depth during CV since this effect changes peak currents.

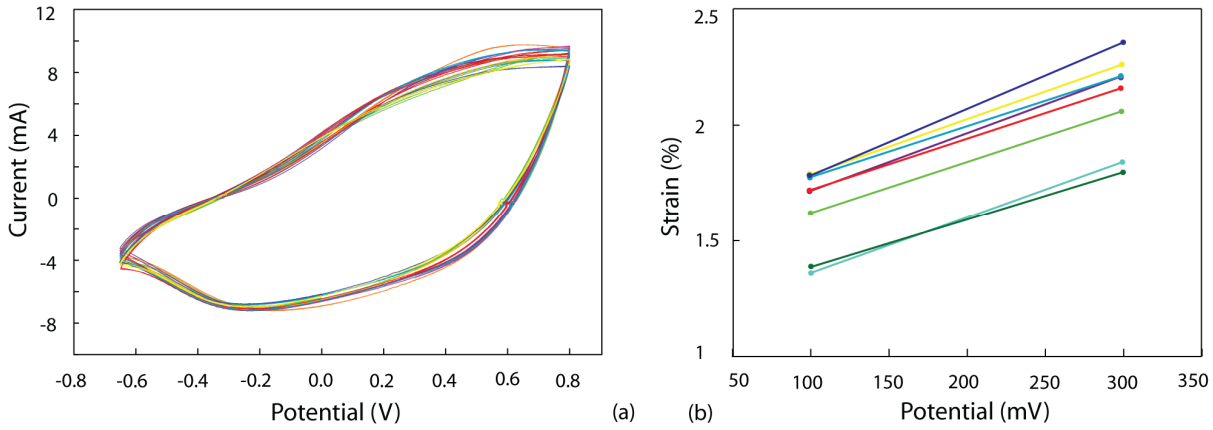

Fig. 2.13 Reproducibility of the system in (a) CVs taken at 150 mV/s of PPy(ClO_4) actuators in 0.5 M $NaClO_4$ for 14 different samples. Always 14^{th} and 15^{th} cycle of conditioning cycles are taken. (b) Absolute strain values at 100 mV and 300 mV for 9 different samples.

The absolute strain values at 100 mV, i.e. the strain relative to the straight film but without correction to the rest state, for the different actuator samples (Fig. 2.13b) are 1.664±0.184%. Since the strain values during measurements are taken relative to the strain at rest state of each actuator, the remaining shift is eliminated at that point. The strain slope for the actuators is 0.4587±0.0307% / 200mV. Inaccuracy in strain can originate from the different steps during the whole process, i.e., from fabrication, over setup and data acquisition to computational fitting. We however assume that it is mainly due to variations in actuator fabrication [105], since we are working with a permanent setup with stable lighting and the length of the strip inside the flow cell is not crucial, since we readout the curvature, which is length-independent.

2.5.3 Actuator response to the hexacyanoferrate(III/II) redox couple

To study the effects of redox agents on the PPy(ClO_4) films, we first employed the hexacyanoferrate(III/II) pair. As displayed in Equation (2.5), hexacyanoferrate(III) can be reduced to hexacyanoferrate(II), which simultaneously oxidises a substrate, in our case PPy (Equation (2.6)). If hexacyanoferrate(II) is predominant in the solution, the reaction proceeds to the left of equation 2.6 and PPy is reduced, whereby its potential is lowered.

$$Fe(CN)_6^{3-} + e^- \leftrightarrow Fe(CN)_6^{4-} \tag{2.5}$$

$$Fe(CN)_6^{3-} + PPy \leftrightarrow Fe(CN)_6^{4-} + PPy^+ \tag{2.6}$$

The electrochemical potential of a redox pair in solution can be described by the Nernst equation

$$E = E_0 - \frac{RT}{zF}\ln(\frac{a_{red}}{a_{ox}}) = E_0 - \frac{59.16mV}{z}\log_{10}(\frac{a_{red}}{a_{ox}}) \tag{2.7}$$

where E^0 is the standard electrode potential, R the universal gas constant, T the absolute temperature, F the Faraday constant, z the number of electrons transferred in the reaction and a_{red} and a_{ox} are the chemical activities for the reducing and oxidising agent. The potential E is established at a metal electrode in a redox solution and a similar potential is established at PPy (see Fig. 2.15 for further explanation).

The change in potential due to the reactions of reducing and oxidising agents leads to a related change in strain of the bending actuator.

For the subsequent measurements the polymerised and conditioned actuators were clamped into the flow cell, which was flushed with a constant liquid flow. The aqueous solutions contained 0.5 M $NaClO_4$ and the corresponding redox chemicals. For each new step, the actuation solutions were fully replaced. The pH of the measurement solutions was measured with a pH meter (SevenEasy, Mettler Toledo) and showed a value of pH 6.1 ± 0.2. Temperature was measured with a digital thermometer (TES-1303, TES Electrical Electronic Corp.) by positioning the sensor next to the strip. The temperature close to the actuator stayed stable at 21.6 °C ± 0.1 °C during experiments.

Fig. 2.14a displays the potential and the corresponding strain of an actuator, which is established under the effect of different ratios of the hexacyanoferrate(III/II) couple (hereafter referred to as $C_{Fe(III)}/C_{Fe(II)}$) at a total molarity of 10 mM. Higher molarities can not be used due to the low solubility of $KClO_4$ (1.5g/100ml at 25°C). At the beginning, when hexacyanoferrate(II) is predominant, PPy is being reduced and the potential drops from the rest potential of about 265 mV to 168 mV. The potential drop triggers anion efflux and thus a decrease in strain. As expected, when increasing the concentration of $K_3Fe(CN)_6$ relative to that of $K_4Fe(CN)_6$, the potential and strain response is reversed, i.e. PPy is oxidised which results in a positive strain. The potentials adjusted by $C_{Fe(III)}/C_{Fe(II)}$ at 1:9, 5:5, 9:1 and 9.9:0.1 mixtures were 202 mV, 253 mV, 304 mV, and 343 mV, respectively. The potentials established at the polypyrrole follow a quasi-Nernstian behaviour with a slope of 46 mV for potential vs. $\log(C_{Fe(III)}/C_{Fe(II)})$. On a gold surface, the potentials

established with the same redox ratios yield a slope of 59 mV (Fig. 2.15), which means that the PPy actuator does not behave like a normal metal electrode [166]. For steps 2 to 5, the times to reach 95 % of the final asymptotic values were 140, 80, 130 and 280 seconds, respectively. The shortest response time is gained with $C_{Fe(III)}/C_{Fe(II)}$ of 5:5 during step 3. Step no. 2 might be slower since the concentration of hexacyanoferrate(III) is lower. On the other hand, steps 4 and 5 are expected to be faster, due to the higher concentration of the oxidising agent. A possible explanation why steps 4 and 5 are not faster is that charging the PPy film away from its rest potential results in slower kinetics.

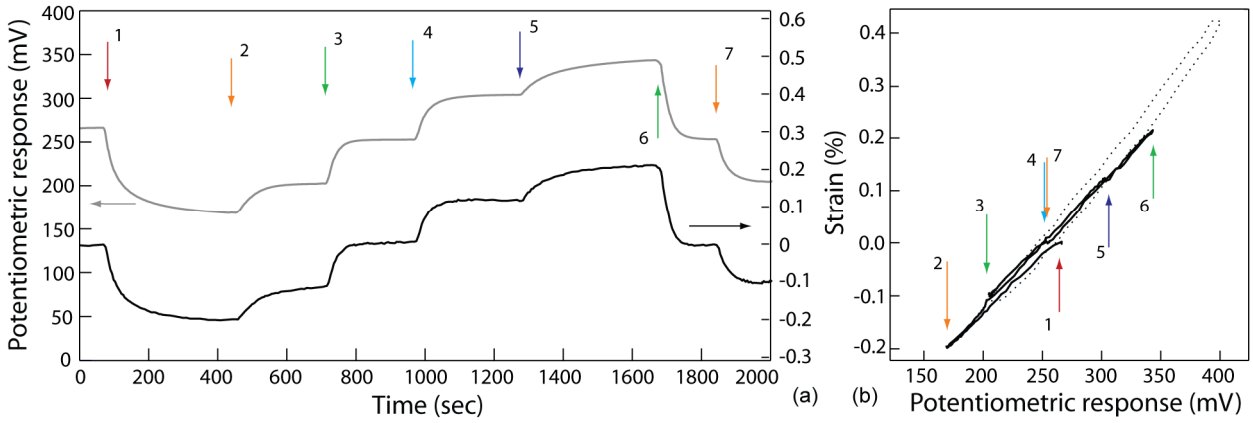

Fig. 2.14 PPy(ClO_4) bending actuator in 0.5 M $NaClO_4$ actuated with different ratios of the hexacyanoferrate(III/II) couple at a total molarity of 10 mM. The ratios of $C_{Fe(III)}/C_{Fe(II)}$ are (1) 0.1:9.9, (2) 1:9, (3) 5:5, (4) 9:1, (5) 9.9:0.1, (6) 5:5, and (7) 1:9. Arrows denote the exchange of solutions inside the flow cell. The new solution always fully replaces the previous solution and liquid exchange rate is 2.5 ml/min. (a) Potential and strain as a function of time and (b) strain versus potential to visualise the linearity; the dotted line corresponds to the measurement from Fig. 2.11b.

The response time might also be influenced by the exchange rate of the liquid inside the flow cell. Measurements with PI/Au strips, as described on the next page, however showed that delays due to liquid exchange were negligible in comparison to the reaction kinetics of polypyrrole (Fig. 2.16). It is assumed that the limiting factor for the response time is the reaction of redox agents at PPy since strain change and thus ion exchange can be driven at faster rates (Fig. 2.11).

The 5:5 and 1:9 mixtures lower the potential and strain again to the same values as during the forward passage. As demonstrated in Fig. 2.14b the linearity pointed out in section 2.4.1 is also achieved when the actuator is driven by redox reactions and the strain vs. potentiometric response does not show relevant hysteresis. The direct comparison to the actuator performance using an external power source as depicted in Fig. 2.14b indicates that the strain values from both actuation mechanisms coincide.

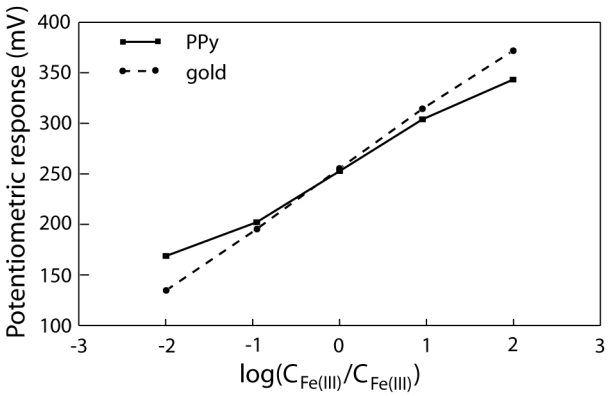

Fig. 2.15 Potentiometric responses of PPy and gold electrodes vs. the concentration ratios of oxidising to reducing agent $C_{Fe(III)}/C_{Fe(II)}$. The gold sample shows a Nernstian response with a slope of 59 mV, which is in contrast to the quasi-Nernstian response of the PPy sample where the mean slope is only 46 mV. This indicates that PPy does not behave like a normal metal electrode.

To get a feeling for the characteristics of the response times inside the flow cell, the same measurements as seen in Fig. 2.14 were conducted with PI/Au strips without the PPy layer. Hexacyanoferrate shows fast kinetics on Au, therefore the time response will be largely influenced by the liquid exchange in the flow cell. Fig. 2.16 displays the potentiometric responses towards different ratios $C_{Fe(III)}/C_{Fe(II)}$. The response times (95% of the final asymptotic values) of the PI/Au strip were much faster compared to the PI/Au/PPy strip, namely 28 sec, 32 sec, 45 sec, and 58 sec for steps 2 to 5, respectively. The liquid exchange is repeatable and reproducible, as shown by the second forward passage in Fig. 2.16 and by additional measurements, which are not displayed here. Thus we can conclude, that the kinetics of the PI/Au/PPy actuators are fully dependent on the PPy layer.

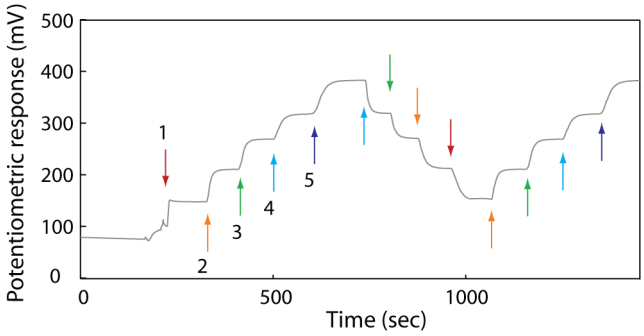

Fig. 2.16 Potentiometric response of a PI/Au strip without PPy layer in the flow cell under the influence of different $C_{Fe(III)}/C_{Fe(II)}$ ratios as in Fig. 2.14 at a total molarity of 10 mM. Arrows denote the exchange of 0.5 M $NaClO_4$ solutions with redox agents inside the flow cell. The new solution always fully replaces the previous solution and liquid exchange rate is 2.5 ml/min.

The repeatability of the PPy actuator was measured by continually cycling between two solution potentials, i.e., $C_{Fe(III)}/C_{Fe(II)}$ of 9:1 and 1:9 at a total molarity of 10 mM. The potential and strain return to the same values for every cycle as can be observed in Fig. 2.17, thus the system shows high repeatability and a cycled elastic actuation without irreversible component, i.e. drift, superimposed on the response. The hysteresis of 14.2 % is higher than what was observed in Fig. 2.14b. As experiments with the potentiostat showed (Fig. 2.11 and Fig. 2.12), hysteresis was higher for smaller scan ranges as well as for faster scan rates. These observations can explain the behaviour in the redox-induced actuation. In Fig. 2.14, the total potential range is larger and the transitions occur stepwise, which overall corresponds to a slower transition.

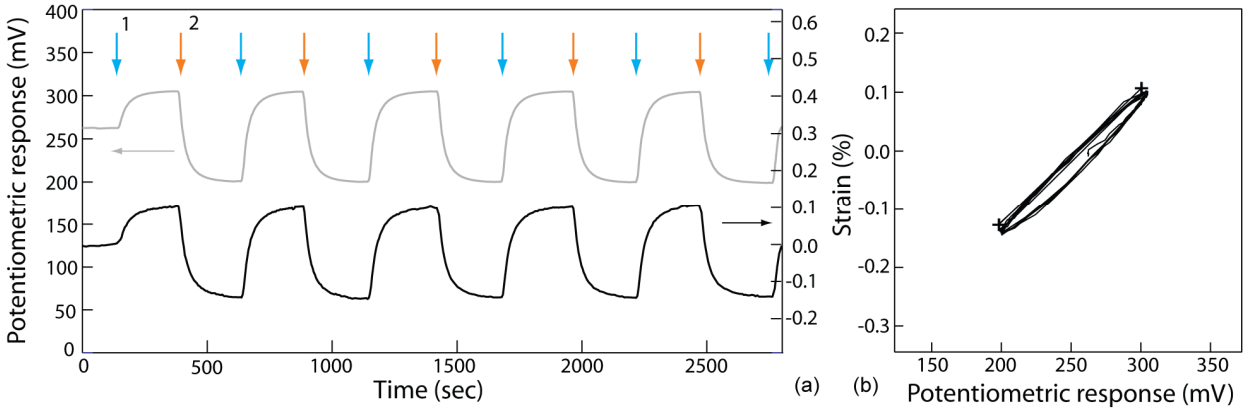

Fig. 2.17 Repeatability of the system - PPy(ClO_4) bending actuator in 0.5 M $NaClO_4$ actuated with $C_{Fe(III)}/C_{Fe(II)}$ of (1) 9:1 and (2) 1:9 at a total concentration of 10 mM. Arrows denote the exchange of solutions inside the flow cell. The new solution always fully replaces the previous solution and liquid exchange rate is 2.5 ml/min. (a) Potential and strain as a function of time and (b) strain versus potential to visualize linearity, the crosses mark potentials which were applied by the potentiostat.

2.5.4 Hexacyanoferrate(III) concentration dependence

The actuator response cannot only be established with redox couples in solution, which change the potential and strain corresponding to their relative ratio, but also using redox moieties, which establish a potential dependent on their oxidation capability. Thus polypyrrole was subjected to varying concentrations of hexacyanoferrate(III). Fig. 2.18a displays the strain and potential variations in time,

when $C_{Fe(III)}$ changes from 100 uM to 10 mM. Again, transitions are clearly visible and the strain is linearly correlated to the potential, as illustrated in Fig. 2.18b.

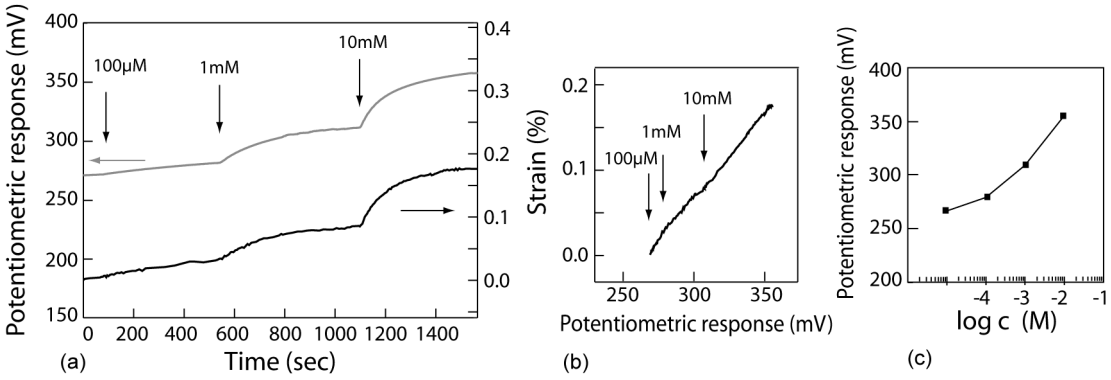

Fig. 2.18 (a) Potentiometric and strain responses of a PPy(ClO_4) bending actuator to hexacyanoferrate(III) of concentrations (1) 100 μM, (2) 1 mM, (3) 10 mM in 0.5 M $NaClO_4$ as a function of time. Arrows denote the exchange of solutions inside the flow cell. The new solution always fully replaces the previous solution and liquid exchange rate is 2.5 ml/min. (b) Strain versus potentiometric response for the visualisation of linearity. (c) Potential values consecutively established after 470 seconds in dependence of the analyte concentration $K_3Fe(CN)_6$. The leftmost data point corresponds to the rest potential.

Kinetics are, however, rather slow and a stable potential is only reached after about 900 seconds for 10 mM of redox analyte, while the time to reach 95 % of the final asymptotic value is about 570 seconds. The transition speed in these measurements is overall much slower than for a redox couple, as we have seen in Fig. 2.14. With only one redox agent, the potential reaches a quasi-equilibrium state after a longer period of time compared to a redox pair, because the redox moiety in solution is far from an electrochemical equilibrium. In this case, a thinner polypyrrole film would help decreasing the response time [166], due to the lower charge needed to load the polymer to the final potential. The CVs in Fig. 2.19 indicate that a PPy film fabricated with 0.23 C/cm^2 total charge displays a much lower current during cycling than the film fabricated with 2.3 C/cm^2 total charge, when all the other fabrication parameters are equal. The peaks in the CV of the thicker film are broader and less characteristic compared to the thin film since the redox processes do not occur simultaneously throughout the whole film. In experiments, where the polymers were externally charged from 150 mV to 350 mV and back (Fig. 2.19c), a 13.1 μm thick film (which corresponds to a total charge of 2.3 C/cm^2) consumed about 7.1 mC and 6.6 mC whereas for a film polymerized with 10 times less total charge about 0.45 mC and 0.57 mC was used respectively.

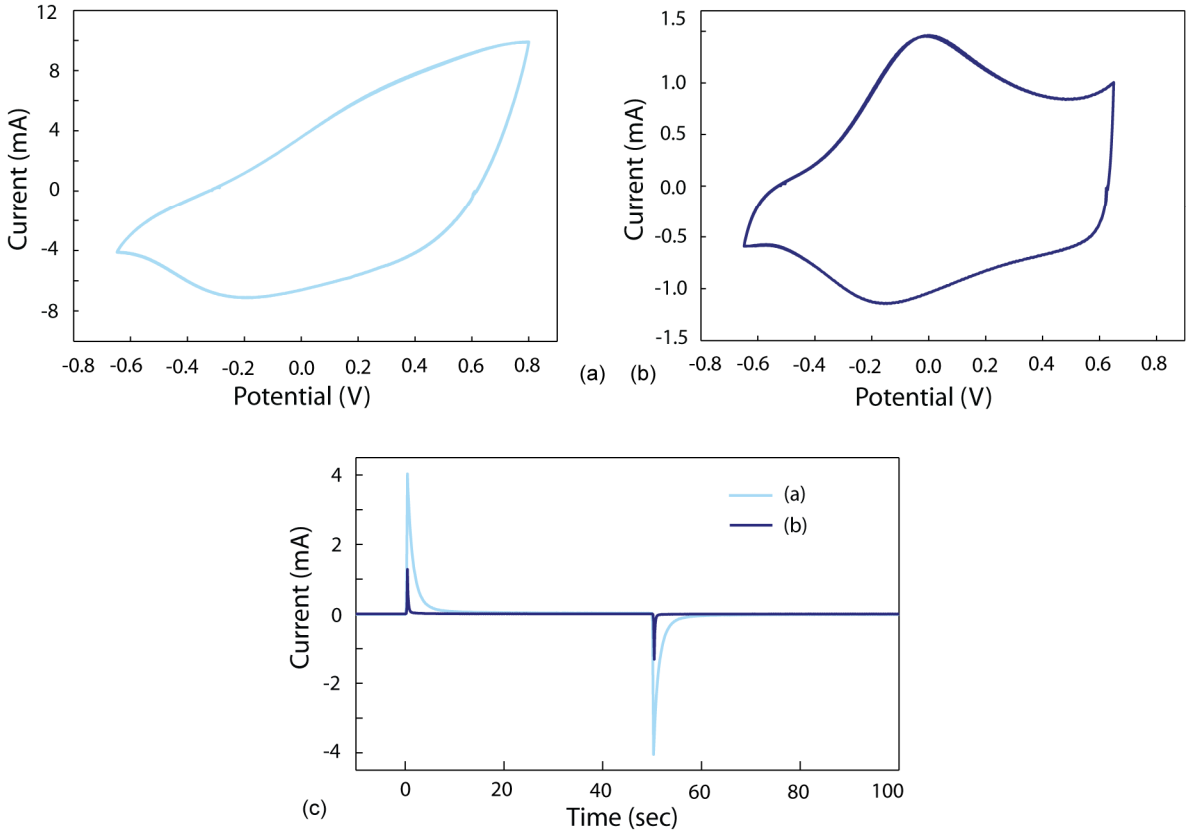

Fig. 2.19 Cyclic voltammograms taken at 150 mV/s in 0.5 M $NaClO_4$ of $PPy(ClO_4)$ actuators with total charges used for polymerisation of (a) 2.3 C/cm^2 and (b) 0.23 C/cm^2. 9th and 10th cycle of conditioning cycles are displayed. (c) Step answers of the films as in (a) and (b) for potential steps from 150 mV to 350 mV and back.

As displayed in Fig. 2.20, the responses of PPy actuators with thinner films to different concentrations of hexacyanoferrate(III) are faster compared to 13.1 μm thick films in Fig. 2.18. The time to reach 95 % of the final asymptotic value is roughly 200 seconds for 10 mM of redox analyte. For Au without PPy layer, this value is about 50 seconds, which is largely defined by the flow cell. During the time used for reaction, the thinner PPy actuator is charged up to higher potentials. If both films are left in the redox solutions for longer times, the potentials of the actuators reach equal values. In this situation, the thickness is irrelevant for the established potential.

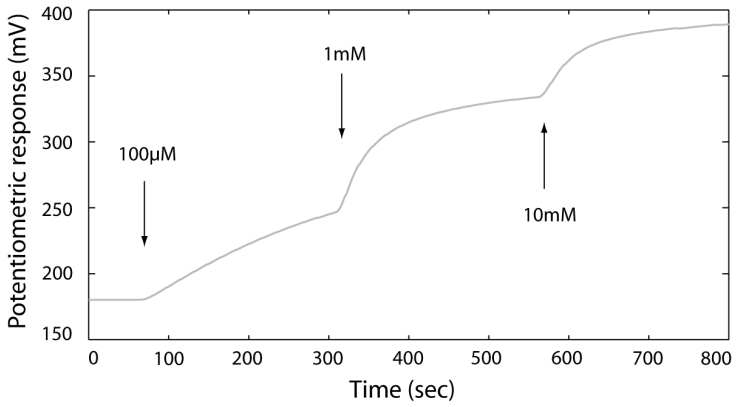

Fig. 2.20 Potentiometric responses of a PPy(ClO_4) bending actuator fabricated with 0.23 C/cm^2 total charge to hexacyanoferrate(III) of concentrations (1) 100 μM, (2) 1 mM, (3) 10 mM in 0.5 M $NaClO_4$ as a function of time. Arrows denote the exchange of solutions inside the flow cell. The new solution always fully replaces the previous solution and liquid exchange rate is 2.5 ml/min.

Fig. 2.18c illustrates the potentials that are established with the different concentrations after 470 seconds. Since $K_3Fe(CN)_6$ is an oxidising agent, only values above the intrinsic potential of the PPy(ClO_4) actuator of 265 mV can be established. Hence it is supposed that in this system for concentrations lower than about 100 μM the slope of both potential and strain versus concentration is not linear and depends on the polymer's intrinsic potential.

2.5.5 Principle of redox reaction and strain change

We have considered the strain of the PPy actuators in relation with the potential that is established in response to the redox active species. This behaviour was interpreted as the result of the redox reaction at the polymer surface accompanied by a change in potential which induces ClO_4^- ion in- or efflux and thus swelling or shrinking of the polymer (Fig. 2.21a). However, polypyrrole can function both as ionic and electric conductor [196] and shows an open-circuit potential that depends on both the concentration of electrolyte ions and redox ions in solution [166, 197].
In case of an electronic and ion-exchange equilibrium the potential of a PPy film can be described by equation (2.7) [70, 197-200]:

$$E = E^0 + \frac{RT}{F} \ln \left[\frac{Poly^+}{Poly} \right] + \Delta\varphi_D \tag{2.8}$$

where E^0 is the standard potential of the $Poly^+/Poly$ system at the equilibrium concentrations of the oxidised and reduced forms, $Poly^+$ and Poly, respectively. The Donnan potential, which is the potential drop across the polymer-electrolyte interface, is given by

$$\Delta\varphi_D = \pm\frac{RT}{F}\ln\left\{\frac{x}{2a}+\left[1+\left(\frac{x}{2a}\right)^2\right]^{1/2}\right\} \tag{2.9}$$

for a (1,-1)-valent electrolyte with x being the concentration of polymer backbone charges and a the activity of ions in the electrolyte solution. In the case of $PPy(ClO_4)$ the Donnan potential is positive, while for a cation exchanging PPy film it is negative.

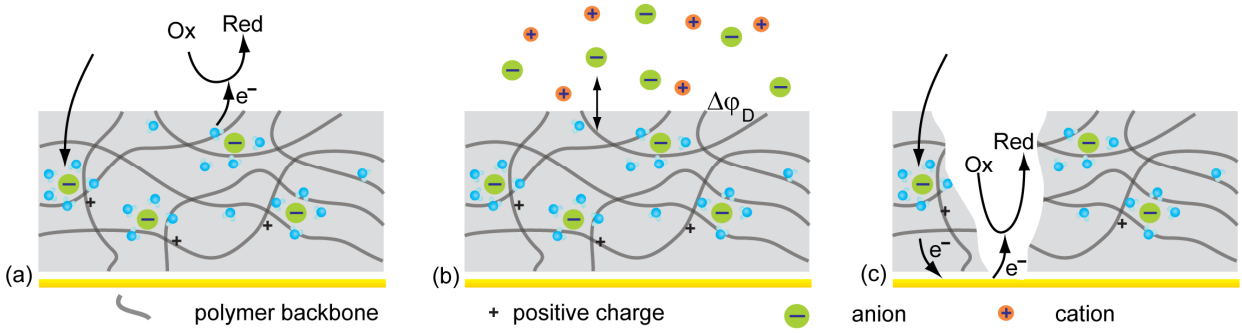

Fig. 2.21 Schematic illustrations of the different reaction pathways: (a) the potential is established by the reaction of the redox agents at the PPy film which induces electrolyte ion exchange, (b) the potential as well as to some extent the strain of the PPy actuator are defined by the concentration change of the redox agents due to influence on the Donnan potential and (c) the redox reaction takes place at the gold electrode with subsequent ion exchange.

Since the open circuit potential of PPy can depend on the concentration of the electrolyte ions and/or the redox couples in solution, it is important to show that the potential changes are not produced by the simple concentration change of the redox agents and are thus not induced by changes of the Donnan potential at the polymer solution interface [70, 201] (Fig. 2.21b), but are rather induced by the charge transfer at the PPy surface.

Bockris and Diniz [196] showed that in a polypyrrole membrane immersed in a solution of the hexacyanoferrate(III/II) couple an electric current can be induced by applying a potential difference over the membrane, which displays the possibility of a redox reaction at the polymer. Redox sensitivity of PPy and its derivatives was also shown in several other publications [166, 197, 202-204]. If the potential change would result from the increased activity of ions in the electrolyte solution, the potential would decrease with an increase in concentration, due to the definition of the Donnan

potential. This is not the case as can be seen in Fig. 2.18. Additionally, we have verified that total concentrations of the hexacyanoferrate redox couple of 1 mM and 10 mM with $C_{Fe(III)}/C_{Fe(II)}$ of 5:5 result in the same potential and strain, only the kinetics are different.

Another possible process, which we however consider an unlikely route of reaction, is that redox ions first move into the membrane and then react at the gold electrode to establish a potential (Fig. 2.21c). Firstly, Curtin et al. [205] showed that the replacement of ClO_4^- by $[Fe(CN)_6]^{3-}$ in a PPy(ClO_4) film is virtually negligible. Secondly, an ion exchange of the dopant with the redox anion results in most cases in a different electrochemical behaviour, in the case of $[Fe(CN)_6]^{3-}$ as dopant the actuator exhibits mixed anion- and cation exchange during CV in NaCl as well as in $NaClO_4/K_3Fe(CN)_6$ solutions [111]. The CVs of PPy(ClO_4) in 0.5 M $NaClO_4$ before and after measurements with $K_3Fe(CN)_6$ added do not vary, as shown in Fig. 2.22a. CVs of PPy($Fe(CN)_6$) in 0.5 M $NaClO_4$ or in 0.5 M $NaClO_4$ with 0.01 M $K_3Fe(CN)_6$ added exhibit totally different CV results as compared to PPy(ClO_4).

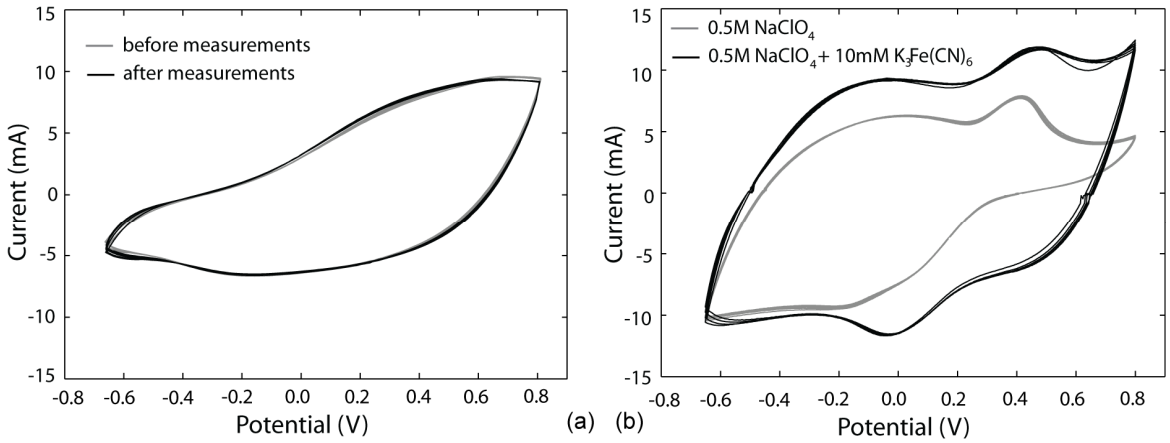

Fig. 2.22 Cyclic voltammograms taken at 150 mV/s of (a) PPy(ClO_4) in 0.5 M $NaClO_4$ before and after measurements with $K_3Fe(CN)_6$ and of (b) PPy($Fe(CN)_6$) in 0.5 M $NaClO_4$ and 0.5 M $NaClO_4$ + 10 mM $K_3Fe(CN)_6$.

Since the PPy actuators display constant actuation performance and the CV curves before and after the experiments do not display variations, we presume that no replacement of ClO_4^- by $[Fe(CN)_6]^{3-}$ occurs. Hence it is not likely that the redox reaction takes place at the gold electrode after hexacyanoferrate ions have diffused into the polymer layer, which was also concluded for poly(N-methylpyrrole) (PMPy)[204, 206].

The redox agents could also, instead of diffusing through the PPy film, directly react at the gold electrode at places where the polymer film is disrupted or has holes. We therefore analysed the integrity of each PPy film and did not observe any disruptions or holes (Fig. 2.23b). Only at the clamping positions, some films showed cracks due to the high mechanical stresses at these points (Fig. 2.23a). The solution however did not get in contact with these clamped parts. Hence we assume that the reactions we measured did not originate from redox reactions at the gold electrode.

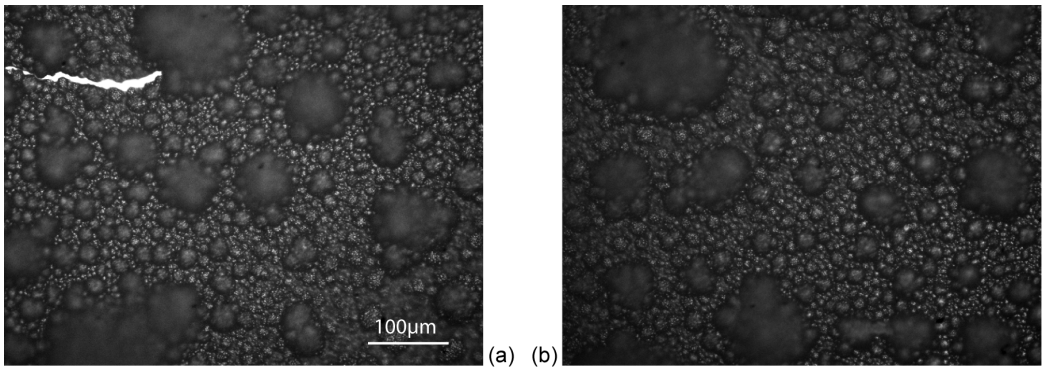

Fig. 2.23 Light microscopy images of PPy(ClO_4) film surface with (a) a disruption due to mechanical clamping and (b) with an intact surface. The length scale is the same in both images.

Considering all of the above-mentioned arguments, we infer that the strain changes observed during the measurements in the previous sections result from the ion exchange due to a change in potential of the PPy film, which is caused by the reaction of the redox agents at the polymer film surface.

Various other redox species possibly can not be used in this system due to possible interferences with the polymer matrix besides the redox reaction. Redox ions that are prone to replace ClO_4^- can behave differently than hexacyanoferrate. Sulphate (SO_4^{2-}) for example, which acts as anion of various redox salts and can be a product of different redox agents, has a considerable impact on PPy(ClO_4) and therefore the redox-induced actuation could be interfered by other effects [205, 207]: possible interference of sulphate(IV) ions with PPy can be the replacement of ClO_4^- or Cl^- with SO_4^{2-} [205, 207] or steric/electrostatic interactions, due to which Cl- ions remain in the film if SO_4^{2-} is present in the solution [78]. Redox salts with SO_4^{2-} as anion or other redox ions that are prone to replace ClO_4^- have to be dealt with. It is therefore important to note that no general statements can be made whether redox agents are able to properly influence PPy actuators.

2.5.6 Ascorbate concentration dependence

To assure that PPy cannot only be actuated with the hexacyanoferrate couple, we analysed the responses to L-ascorbic acid (L-AA), a biologically relevant agent. Fig. 2.24 shows the reaction mechanism from L-AA to dehydro-L-ascorbic acid (DHA). The oxidation reaction of L-AA is pH dependent, i.e. the first step of reaction to the ascorbyl radical (not shown in Fig. 2.24), which involves the release of one proton, is favoured by a more alkaline pH. The increase of L-AA concentration in an unbuffered solution leads to a more acidic pH, whereby the oxidation process is slowed down, i.e., the potential at the electrode is not linearly correlated to the L-AA concentration Thus, the measurement solution was buffered to maintain the activity of L-AA with a 20 mM acetic acid/sodium acetate buffer, pH 4.5 at 21 °C.

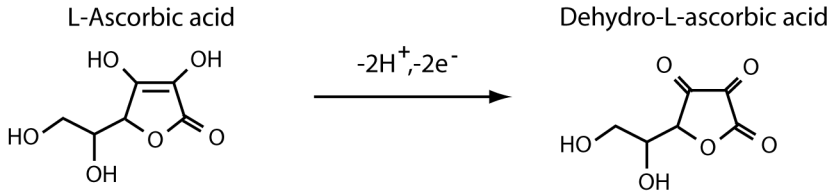

Fig. 2.24 Reaction of L-ascorbic acid to dehydro-L-ascorbic acid (which is not an acid). The intermediate step af ascorbyl radical formation is not included [208].

The polypyrrole actuator was subjected to different concentrations of ascorbic acid in acetate buffer and perchlorate electrolyte. Fig. 2.25a and b indicate a linear response of strain proportional to the PPy film potential, which is established by the reducing agent. Hence, L-AA is also able to influence the strain in the actuator by changing the oxidation level of polypyrrole through reaction at the polymer. When low concentrations of redox analyte are used, the reaction rate is slow and during the time used for measurements, a stable potential is not yet fully established. Thus in Fig. 2.25c it can be observed that for the reaction time of 430 seconds, the slope of potential versus concentration is not linear until a concentration of about 500 μM is reached. With lower concentrations the established potential might still be partially dependent upon the polymer's rest potential. For normal L-AA levels (0.03-0.085 mM in serum and 0.07-0.15 mM in urine) in the human body, the intrinsic potential of the actuator therefore has to be increased or the actuation has to be carried out in solutions with higher pH. Higher pH can be used to decrease the reduction potential and increase the reactivity of L-AA, since the first step of reaction is favoured in more alkaline solutions, as mentioned above. We tried to use phosphate buffer to control the pH to between 7 and 9 and to achieve lower reaction potentials. The phosphate buffered solution however resulted in a slight variation of the CV (a small

second cathodic peak appeared) and therefore we could not be sure if there were changes inside the PPy film. Ion exchange is not expected when using phosphate buffer [205], which is why not the ions but rather the pH is assumed to be the cause. Although pH was reported not to influence the volume change in PPy during CV [77], changes in the oxidation state of the PPy, which could affect the CV [209, 210], can not be excluded. This phenomenon however needs further analysis.

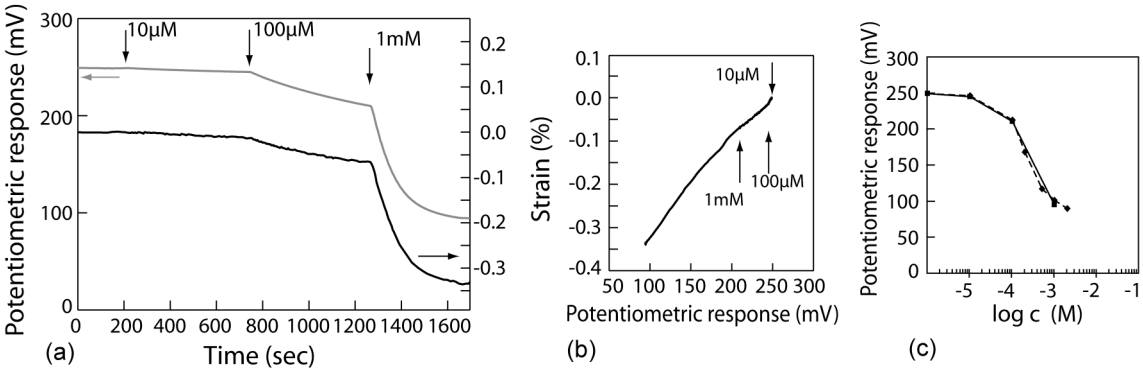

Fig. 2.25 (a) Potential and strain responses of a PPy(ClO_4) bending actuator in 0.5 M $NaClO_4$ and 20 mM acetate buffer pH 4.5 as a function of time actuated with L-ascorbic acid of concentrations (1) 10 μM, (2) 100 μM, (3) 1 mM. Arrows denote the exchange of solutions inside the flow cell. The new solution always fully replaces the previous solution and liquid exchange rate is 2.5 ml/min. (b) Strain versus potentiometric response for the visualisation of linearity. (c) Potential values consecutively established after 430 seconds in dependence of the analyte concentration for two samples. The leftmost data point corresponds to the rest potential.

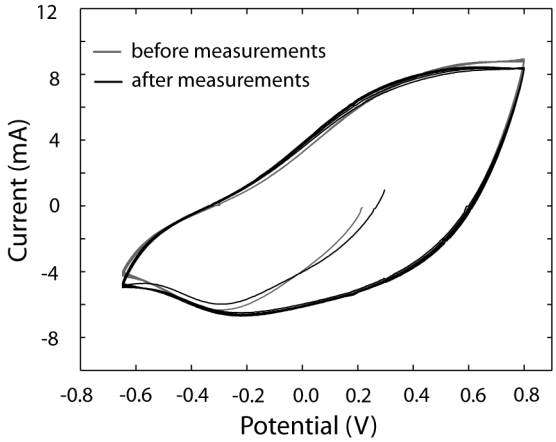

Fig. 2.26 Cyclic voltammograms taken at 150 mV/s in 0.5 M $NaClO_4$ of PPy(ClO_4) actuators before and after the actuation measurements using L-AA in acetate buffer.

In PPy(Cl) films - which are very similar to PPy(ClO_4) films with respect to ion exchange behaviour [186] and morphology [211] - it was shown that ascorbic acid does not replace the dopant anions [212]. The CVs in Fig. 2.26 indicate that the electrochemistry of the films is not changed after measurements with L-AA in acetate buffer. Thus also in the case of L-AA we assume that the strain and potential changes result from the redox reaction at the PPy surface and not from redox reaction at the Au electrode or actuation through a change ion activity.

2.5.7 Influences of electrolyte pH, concentration, and temperature on PPy(ClO_4)

So far the responses of the PPy actuators towards redox chemicals were considered. Variations in pH, electrolyte concentration and temperature could however also effect a strain response. Although these parameters were measured to be or held constant during the redox measurements, it is important to see the influence of pH, temperature and electrolyte concentration.
Various groups have already shown the effects of pH changes on actuation properties of polypyrrole [77, 172, 213]. In this section, the influence of pH on potential and actuation of PPy is presented in our system using the flow cell. Treatment in acidic solutions leads to protonation of the nitrogen atoms in PPy [214, 215] and therefore an increase in potential and influx of anions for charge neutrality. It has been reported that anion content-pH curves showed that with increasing pH from 0 to 13 two stages of Cl^- expulsion from the film exist [215] – one in the range of pH 2-4 and one in the pH range 9-11. This led to the consideration of two proton transfer steps:

$$PPy^+HA^- + H^+ + A^- \leftrightarrow PPy^+HH^+2A^- \qquad \text{(pKa ~ 2-4)} \qquad (2.10)$$

$$PPy^+HA^- + OH^- \leftrightarrow PPy + H_2O + A^- \qquad \text{(pKa ~ 9-11)} \qquad (2.11)$$

where PPy represents a PPy chain segment of 3-4 pyrrole rings. Schematically, the process of protonation, deprotonation can be presented as follows:

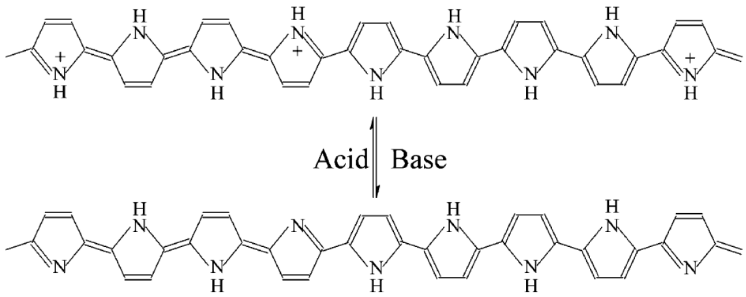

Fig. 2.27 Acid – base transitions of PPy film [216].

Fig. 2.28 displays pH induced responses of the potential as well as the strain in a 0.5 M $NaClO_4$ solution. The pH was adjusted with appropriate amounts of NaOH and $HClO_4$, respectively. Acidic solutions lead to a higher potential and strain, whereas the opposite effect is found in more alkaline solutions. It is visible that a hundredfold increase or decrease of hydrogen ion concentration does by far not influence the actuator as much as either hexacyanoferrate or ascorbate. We noticed that the potential and strain responses of PPy in our system are slightly smaller compared to reported values in the literature [210, 213]. Possible reasons involve the following parameters: differences in electrolyte concentrations, the thickness of the polymer and the extent of pH. The sensitivity of the potential towards pH decreased when the film thickness was increased from a few hundred nanometers to some tens of micrometers [77, 210]. Since potential is related to strain or volume changes also in the case of protonation/deprotonation, decreased sensitivity is also expected for strain in our system since the thickness of the film is 13 μm. This decrease in sensitivity was explained by the fact that protonation or deprotonation is not likely to proceed throughout the whole film for thicknesses larger than about 10 μm [210]. Therefore also strain is comparably small.

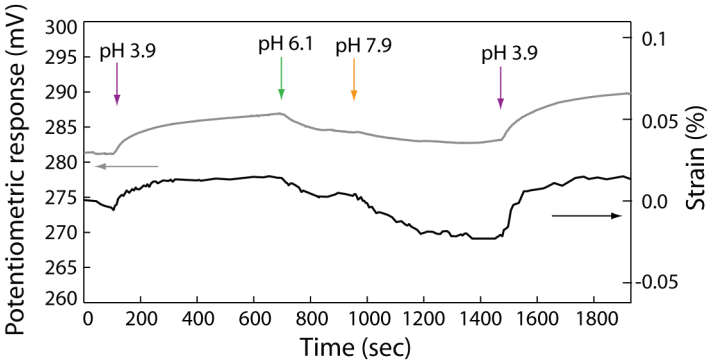

Fig. 2.28 Influence of pH changes on the potential and strain of the PPy(ClO_4) bending actuator which was fabricated as for the previous measurements. Arrows denote the exchange of solutions inside the flow cell. The new solution always fully replaces the previous solution and liquid exchange rate is 2.5 ml/min.

For electrolyte concentration and -temperature changes, the PI strips had to be coated with gold on both sides, to minimise contact of the PI with the solution (refer to section 2.4.8 for more details) and to introduce more symmetry in the backing substrate. The second gold layer was included into the strain calculations (see Appendix A).

As already elaborated in section 2.5.5, PPy is an ionic conductor and therefore its potential as well as the volume depend on the concentration of electrolyte ions. We see in Fig. 2.29a that at high molarities an increase in concentration leads to a decrease in potential and simultanously an increase in strain. This behaviour is different from the redox agent driven potential- and strain changes we have observed in the previous chapters. Here, the increase in electrolyte concentration leads to a change of the Donnan potential of the polymer film, but not the redox state of the film [197]. Fig. 2.29b shows that at low molarities, the slope of strain to potentiometric response is very small [198], since the polymer becomes more impermeable to the electrolyte.

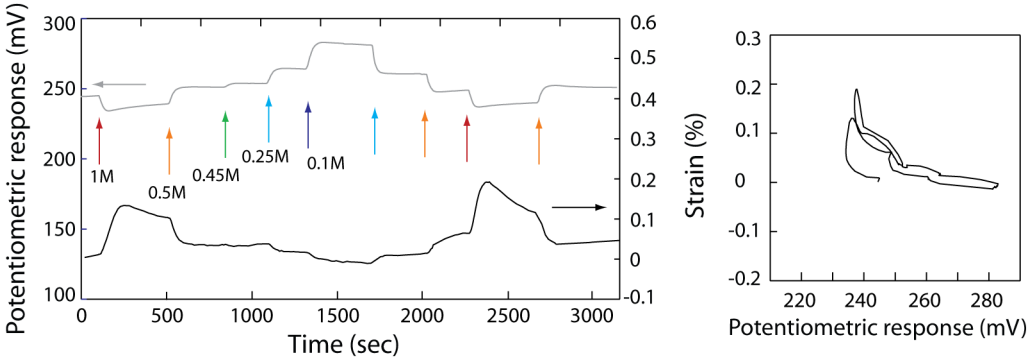

Fig. 2.29 Influence of electrolyte concentration changes on the potential and strain of the PPy(ClO_4) bending actuator which was fabricated with an additional Au backing layer. Arrows denote the exchange of solutions inside the flow cell with concentrations of (1) 1 M, (2) 0.5 M, (3) 0.45 M, (4) 0.25 M, (5) 0.1 M.. The new solution always fully replaces the previous solution and liquid exchange rate is 2.5 ml/min.

Temperature was measured with a digital thermometer (TES-1303, TES Electrical Electronic Corp.) by positioning the sensor next to the strip. The temperature close to the actuator stayed stable at 21.6 °C ± 0.1 °C during experiments. For temperature response measurements, the temperature was controlled by pre-cooling or heating of the measurement solution which was then flowed into the fluid cell. Fig. 2.30 displays the transitions in potential and strain when colder (17 °C) and warmer (29 °C) solutions are flushed into the system. What is mostly discussed in literature about temperature is its effect on the polymer properties when it is varied during

polymerisation [217]. We assume that variations in strain result from different thermal expansion coefficients in PPy and the backing layer.

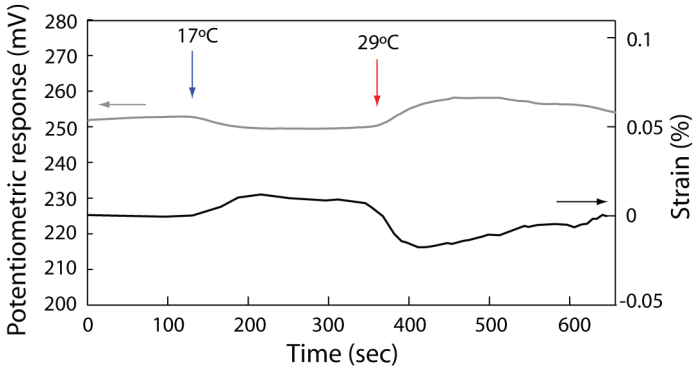

Fig. 2.30 Influence of temperature changes on the potential and strain of the PPy(ClO_4) bending actuator which was fabricated with an additional Au backing layer. Arrows denote the exchange of solutions inside the flow cell with temperatures of (1) 17 °C and (2) 29 °C with a temperature at the start of 21,6 °C. The new solution always fully replaces the previous solution and liquid exchange rate is 2.5 ml/min.

Considering the results above, we re-emphasize that neither pH, nor electrolyte concentration and temperature can be the sources for strain change we have observed with the redox agents.

2.5.8 Control measurements with PI/Au strips

To be able to fully exclude any influences of the PI/Au strip itself we did several control measurements. The strain mentioned in the following section is calculated with the same constants as above, as if the strip had an additional PPy layer, to enable a straightforward comparison of the results.
It is well known from literature, that strain changes in PPy are induced by applied potentials. Therefore, compared to Fig. 2.11 in section 2.5.1 we see in Fig. 2.31a using a PI/Au/PPy bending beam actuator that application of potentials to the bare PI/Au strip does not yield any strain change. Also in the case of redox agents, e.g. hexacyanoferrate(II/III), the bare strip does not show a response in strain, as visible in Fig. 2.31b. The results for changes in temperature, electrolyte concentration, and pH are given in Fig. 2.31c-e. Variations in both concentration and temperature lead to movements of the bare strip, probably due to ion diffusion and water uptake and

due to the different thermal expansion coefficients in PI and Au, respectively. On the other hand, pH does not visibly influence the strain. Due to these influences, the concentration and temperature changes for PPy bending beam actuators in the previous section were analysed with PI films covered on both sides with Au layers of 40 nm thickness, which suppresses the influences of the substrate.

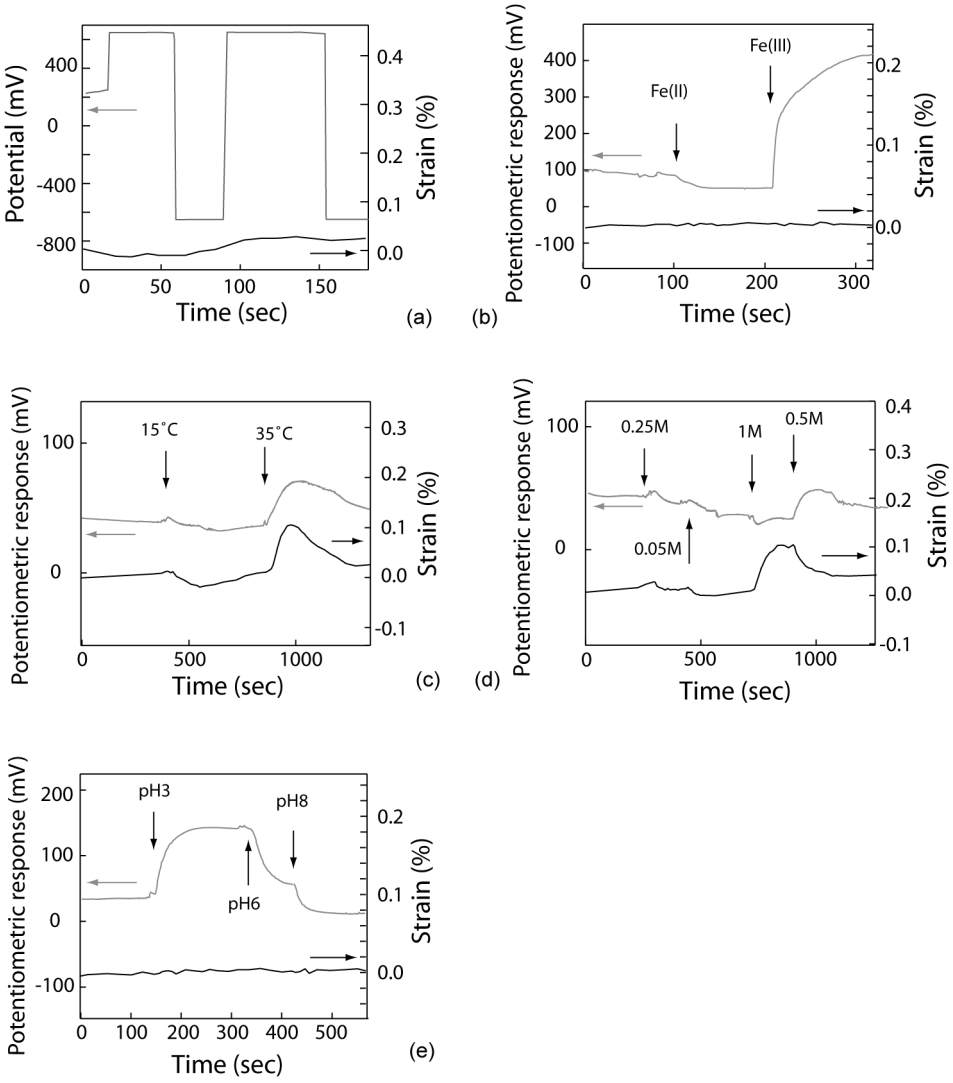

Fig. 2.31 Influences of (a) applied potential, (b) hexacyanoferrate(II/III), (c) temperature, (d) electrolyte concentration, and (e) pH on a bare PI/Au strip in the flow cell in 0.5 M $NaClO_4$.

2.6 Characterisation of cation exchanging PPy

To show the possibility of redox agent driven actuation in the reverse direction (Fig. 2.32), dodecylbenzenesulfonate (DBS^-) is the counter ion of choice. Besides its linear actuation properties [81, 104], PPy(DBS) is known to be biocompatible [218] and can be operated in NaCl and KCl solutions as well as other electrolytes with small cations.

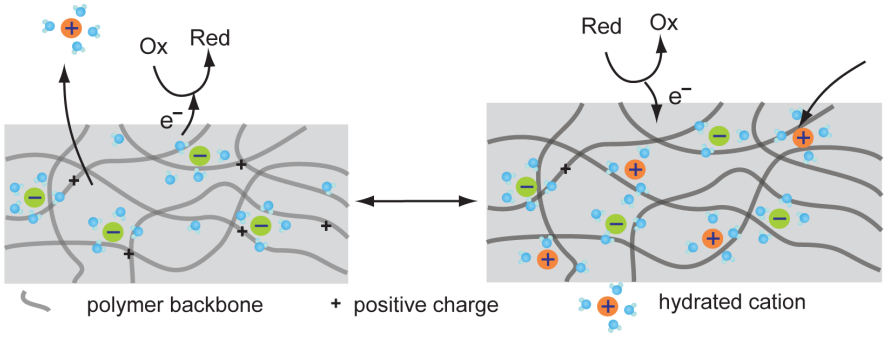

Fig. 2.32 Schematic illustration of the redox processes at a cation exchanging polypyrrole actuator. The reducing (Red) and oxidising (Ox) agents react at the polymer surface to induce cation in- and efflux by changing the oxidation state of the polymer (adapted from [25]).

Usually, in-plane strain values around 1-2%, 0.5 to 1 cm tip movement for 1.5 cm long bilayer strips or bending angles of 10° to 30° for 2 cm long bilayers were reported [77, 81, 104, 105, 219]. A comparison of strain, tip movement and bending angle is rather difficult. Several improvements in strain were reported for PPy(DBS) films, for instance strains up to 3.5% in PPy/PEDOT/PPy actuators [220], 2-7% for tubular linear actuators [81] and up to 20-30% out-of-plane strain for layer thicknesses around 1 μm were reported [82].

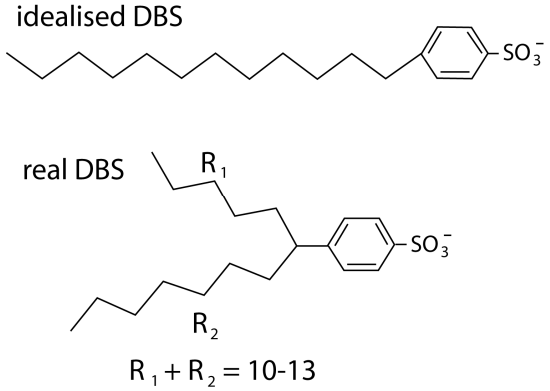

Fig. 2.33 Structures of dodecylbenzenesulfonate (DBS) ions in their idealised form and the actual structures of the commercially available product, as analysed in [91].

DBS^- is a surfactant, also called amphiphilic molecule, which means that is has a hydrophobic and a hydrophilic end. It is made up of a carbon-alkyl chain attached to a benzene ring. The structures of idealised and commercially available DBS, which consists of structural isomers, are given in Fig. 2.33.
The actuators for the cation-exchanging PPy were fabricated as described in section 2.2 with polymerisation conditions as given in the next section. The parameters used for calculations of the strain of PPy(DBS) from the curvature measurements are as follows: the E modulus and Poisson ratio of the polyimide are as in section 2.5 given as 2.9 GPa and 0.34, respectively, while the thickness h_{PI} is 25 μm. Literature estimates for the modulus of PPy(DBS) are 0.15-0.25 GPa in the reduced state and 0.45 GPa in the oxidised state [219]. For a PPy tube the reported moduli are 0.15 and 0.26 GPa for reduced and oxidised states respectively [108]. We used a modulus of 0.25 GPa for our calculations, since we are working with both states, i.e., oxidised and reduced PPy. Christophersen et al. for example [103] used values of 0.12, 0.2, and 0.4 GPa for their modelling of PPy(DBS) microactuators. The tensile modulus of the PPy(DBS) films was not measured, because the gold backing could not be fully removed from the PPy film and the fims coiled up. The strain calculations with a modulus of 0.25 GPa are comparable to the strain measured for a freestanding PPy(DBS) film [81]. The tubular linear actuators analysed in this publication showed higher total strains from 2% up to 7%, which was accounted for by the cylindrical structure and presumably the larger surface to volume ratio. The choice of the modulus for model calculations could introduce inaccuracies on the total strain. We are however mainly interested in the strain behaviour and changes in strain, where the total strain extent plays a minor role.
The thicknesses h_{PPy} are taken as 14.4 μm or 6.3 μm which correspond to charge densities during polymerisation of 2.3 C/cm^2 or 1 C/cm^2, respectively, using a conversion factor of 6.25 μmC^{-1}cm^2 [83, 219].

2.6.1 PPy(DBS) actuator performance using an external power source

The fabrication method for PPy(DBS) was also adjusted to the different actuation properties needed. During polymerisation with NaDBS, fabrication parameters other than those for the PPy(ClO_4) actuators have to be chosen, because the two anions - ClO_4^- and DBS^- - behave differently.

At first, the fabrication parameters were selected to achieve a large strain and low charge consumption during switching (Fig. 2.34a). As reported earlier for PPy(DBS) [104] and also for PPy(pTS) [221], lower deposition current density and thus lower polymerisation voltage leads to higher net strain. One disadvantage however of low deposition current is the increased charge consumption during actuation [104]. The deposition current was set to 2 mA/cm^2, which results in a voltage of 0.67 V for 0.2 M NaDBS and 0.1 M pyrrole. Here, the pyrrole concentration was not set to a value higher than 0.1 M to reduce the charge consumption during actuation [105].
The strain vs. potential thus resulting exhibits two linear regions, the first with a larger slope between -0.5 V and -0.2 V and the second one with a smaller slope between -0.2 V and 0.2 V (Fig. 2.34a). At negative potential, the slope tends towards zero. The transition in hysteresis experienced at 10 mV/s shifts to a different range at 2 mV/s. To see the influences on the hysteresis, linearity, and charge consumption, several fabrication parameters were varied one by one (Fig. 2.34b-e). The polymerisation current density, which is known to largely influence the net strain as well as the charge during actuation [104], was increased from 2 mA/cm^2 to 15 mA/cm^2 (Fig. 2.34b). Higher current densities resulted in rising of the potentials to values above 3 V and to actuators which barely moved. As expected, the current during cycling for this fabrication method is lowered, especially the capacitive current at higher oxidative potentials (Fig. 2.35b), while the net strain is smaller.
The inset of Fig. 2.34b shows an actuator which was also fabricated with 15 mA/cm^2 but due to the high current in the system, the normal 1 cm^2 Pt CE evolved large bubbles, which largely decreased the active surface area whereby the potential was increased up to 2.5 V. This was not the case when we used a coiled Pt wire electrode with an active surface area of about 2.5 cm^2. Generally, such high potentials are assumed to lead to overoxidation of the polypyrrole, but seemingly the overall actuation performance as well as the CV are not remarkably deteriorated. Maw. et al [104] analysed the polymerisation at current densities up to 40 mA/cm^2 without mentioning overoxidation of their actuators. The linearity behaviour of the high voltage sample is improved to one linear region, which even expands to values above 0.2 V as indicated in Fig. 2.36b and also the peaks in the CV shifted to more positive values (Fig. 2.35a). The exact reasons for this straightening are not known and have not been further analysed. It is however assumed that the film density is a relevant parameter. Since an increased current density and thus an increased polymerisation potential lead to an improved linearity and hysteresis behaviour, lower Py and electrolyte concentrations, which also result in a higher potential, were analysed.

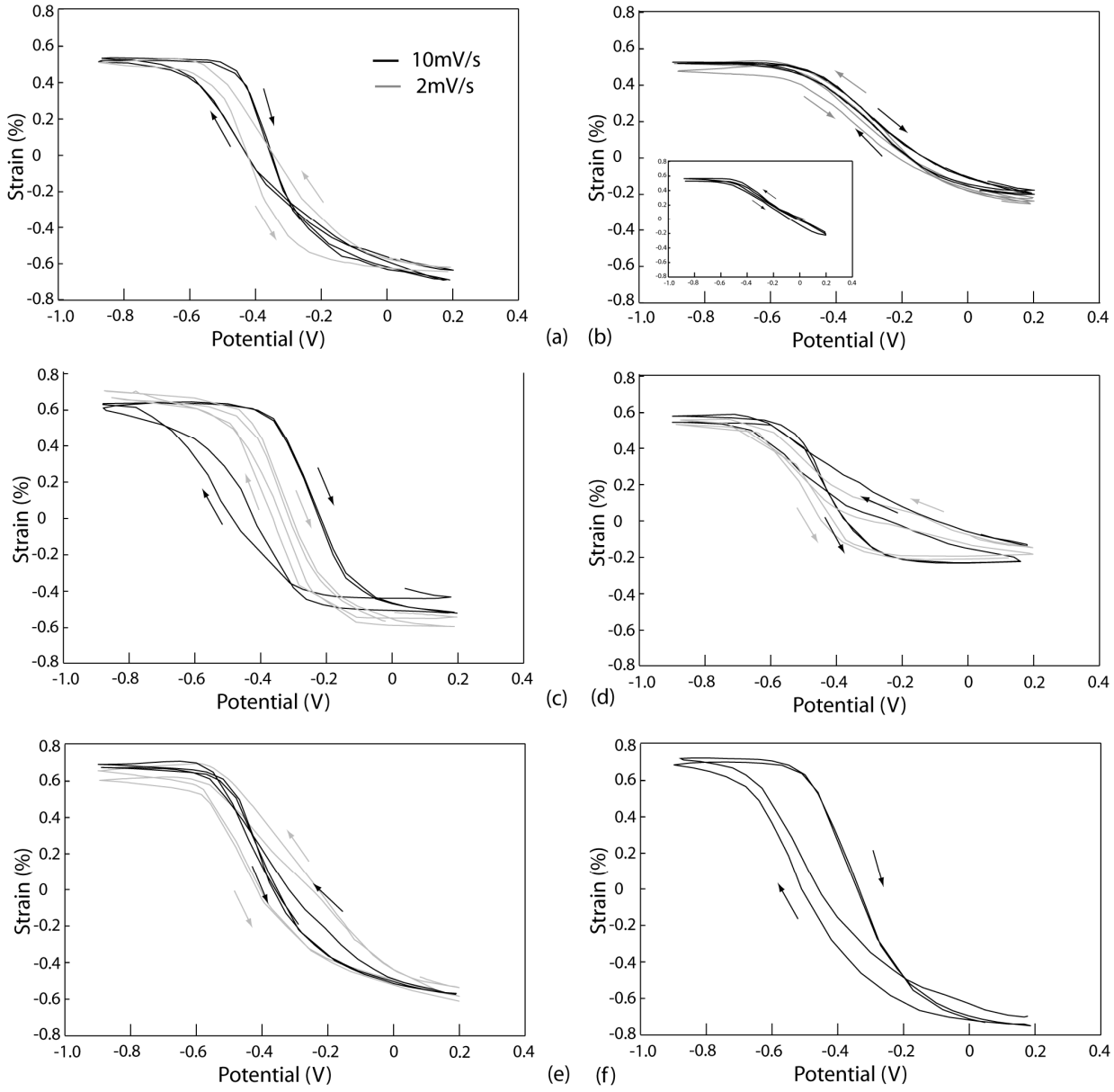

Fig. 2.34 Linearity and hysteresis measurements of PPy(DBS) actuators. Several parameters are varied during polymerisation, where the unchanged parameters are as in (a) 0.1 M Py, 0.2 M NaDBS, 2 mA/cm^2, 2.3 C/cm^2, and cycling electrolyte concentration 0.5 M NaCl. Increase in current density to 15 mA/cm^2 (b), decrease in Py concentration to 0.05 M (c), decrease in NaDBS concentration to 0.05 M (d), decrease in total charge used during polymerisation to 1 C/cm^2 (e), and cycling electrolyte concentration of 0.1 M (f). The voltage is applied by a potentiostat vs. an Ag/AgCl reference electrode with a scan rate of 10 mV/s and 2 mV/s. Inset in (b) shows measurements of a sample produced with 15 mA/cm^2 with a smaller active counter electrode surface and thus higher potential.

The linearity, was slightly improved for lower Py concentrations (Fig. 2.34c) while the net strain was as high as in Fig. 2.34a. The potential range over which actuation is observed is smaller and more hysteresis occured. As expected, the charge consumption during actuation is smaller (Fig. 2.35c) [105]. The decrease of NaDBS concentration during synthesis worsened both the linearity and hysteresis, as well the total strain (Fig. 2.34d). Lower electrolyte concentrations during CV did not show improvements for neither linearity, nor strain. Instead, larger hysteresis occurred during the potential scan, probably since the redox processes of the films in less concentrated electrolytes are slower [222].

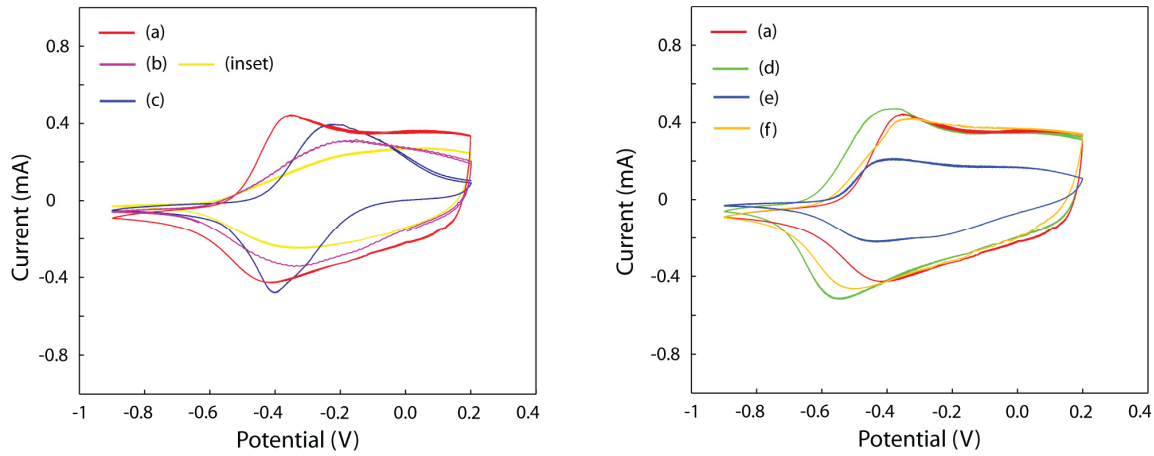

Fig. 2.35 CVs of the samples as in Fig. 2.34a-f taken at 10 mV/s in the flow cell vs. Ag/AgCl.

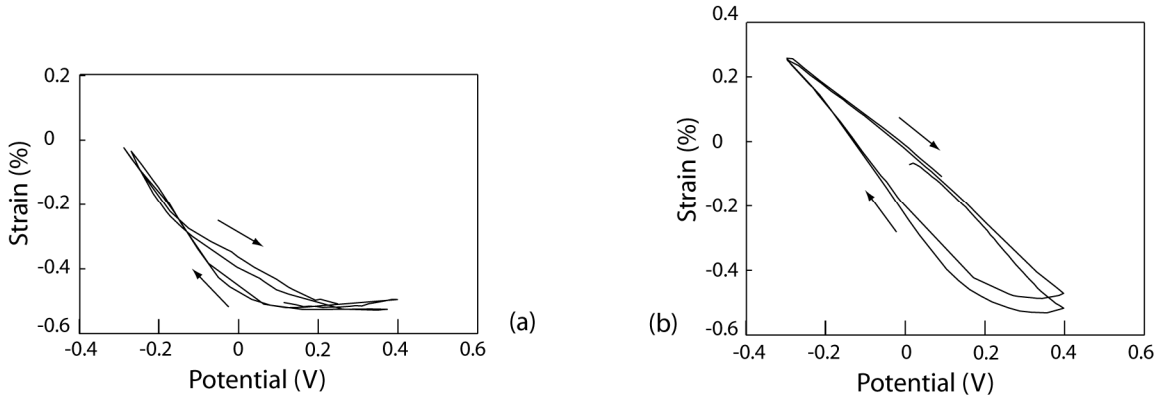

Fig. 2.36 Hysteresis measurements of PPy(DBS) actuators in 0.5 M NaCl at higher potentials. The fabrication parameters correspond to Fig. 2.34(a) and Fig. 2.34(b) (inset). The voltage is applied by a potentiostat vs. an Ag/AgCl reference electrode with a scan rate of 2 mV/s.

Also in the case of PPy(DBS), not much is known about linearity and hysteresis dependence on fabrication parameters. The tip displacement at -1.1 V and +0.4 V and charge consumptions were analysed for different polymerisation currents and electrolyte concentrations by Maw et al. [104, 105]. They however have not analysed

the strain during potential cycling and have therefore no data on linearity or hysteresis. Yamato et al. [81] have analysed the strain response of tubular PPy(DBS) actuators with different diameters as well as the influence of different salts in the measurement solution. Shimoda et al. [77] looked at pH dependence of strain where they however use a much thinner PPy(DBS) layer and did not consider different fabrication parameters. The strain during cycling was compared for PPy(OBS) and PPy(BBS) freestanding films loaded with a constant stress of 0.5 MPa in 0.1 M NaCl [219]. They also showed the mass changes of 0.2 μm thin PPy films with several alkyl benzenesulfonates. Optical beam deflection technique (also called 'mirage effect' technique or probe beam deflection) has been used to research ionic diffusion processes in PPy(DBS) in different electrolytes (KCl, $KClO_4$, CsCl, NaCl, $LiClO_4$, LiCl) during cycling [223]. The mirage deflection signal showed most linearity with NaCl, LiCl, and $LiClO_4$ while least hysteresis was achieved with KCl, $KClO_4$, and CsCl. EQCM measurements of PPy(DBS) mass changes were performed in various electrolytes ($KClO_4$, KCl, CsCl), where KCl and CsCl show the most linearity, while in $KClO_4$ additional anionic exchange appears at voltages higher than -0.25 V [224]. Baker et al. [194] analysed the mass transport by EQCM of PPy(PSS), which also exhibits cation transport similar to PPy(DBS), in various different electrolytes and analysed the linearities and hystereses.
Our results provide more insight on strain behaviour during cycling when certain fabrication parameters, like current density, dopant- or pyrrole concentrations, are altered. The current density was found to have the biggest influence on linearity and extent of strain.

2.6.2 Actuator response to redox agents

Also in the PPy(DBS) system we chose the hexacyanoferrate couple as well as L-AA to actuate the system. Fig. 2.37 displays the results measured with an actuator of the type as in Fig. 2.34e, i.e. 0.2 M NaDBS, 0.1 M Py, current density 2 mA/cm^2 and a total charge density during polymerisation of 1 C/cm^2. The potential and strain are analysed in response to different concentrations of hexacyanoferrate(III) as well as the redox couple. In the beginning of the measurements, the strain nicely follows the potentiometric response, which is given by the different concentrations $C_{Fe(III)}$. Above 300 mV however the strain goes into saturation and does not increase any further, as can be observed in Fig. 2.37b. When the actuator is subjected to a lower concentration $C_{Fe(III)}$ of 10 μM, the potential decreases as expected but the strain does not change. This is also the case when the redox couple with $C_{Fe(III)}/C_{Fe(II)}$ of 1:9 and 9:1 is repeatedly flushed into the flow cell. When comparing to Fig. 2.36a, it is

obvious that the actuators also feature this hysteresis behaviour when actuated with an external power source. Since the potentials of the hexacyanoferrate(III/II) couple fall into the range where the slope of the strain is zero, the actuators as used for these measurements are not suited for these redox agents. The same effects are also observed with PPy actuators fabricated with higher current densities. Yet, this does not mean that these actuators cannot be used at all for redox-induced actuation. Redox agents with a lower standard potential, such as L-ascorbic acid, nicotinamide adenine dinucleotide (NADH), methylene blue or cysteine, for instance, can work in the linear region of the actuator.

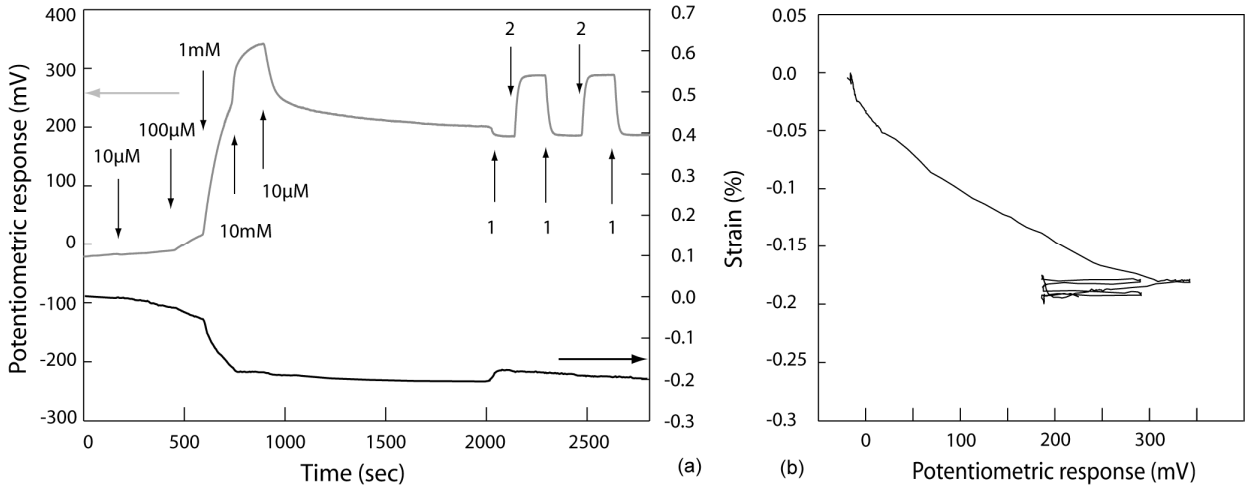

Fig. 2.37 (a) Potentiometric and strain responses of PPy(DBS) bending actuator to hexacyanoferrate(III) with concentrations of 10 μM, 100 μM, 1 mM, and 10 mM and to the hexacyanoferrate(III/II) redox couple with $C_{Fe(III)}/C_{Fe(II)}$ of (1) 1:9 and (2) 9:1 at a total concentration of 10 mM in 0.5 M NaCl as a function of time. The fabrication parameters are as in Fig. 2.34e. Arrows denote the exchange of solutions inside the flow cell. The new solution always fully replaces the previous solution and liquid exchange rate is 2.5 ml/min. (b) Strain versus potentiometric response for the visualisation of linearity.

Another issue which is addressed with these measurements is the recovery time. When the actuator is exposed to a lower concentration, in this case $C_{Fe(III)}$ is lowered from 10 mM to 10 μM (Fig. 2.37), the potential decreases very slowly. Further analysis of this effect is shown in Fig. 2.38, which displays the potentiometric response with different concentrations $C_{Fe(III)}$. The decrease to 1 mM from 10 mM results in a stable value after about 160 seconds. If however the concentration is further decreased, no stable potential is reached within the same time. Concentrations of 10 μM up to 100 μM exhibit a very slow response for both concentration increases and decreases, which indicates that these actuator types are best suited for concentrations $C_{Fe(III)}$ above 100 μM. Also here, thinner films might improve kinetics of responses to lower concentrations of redox agents.

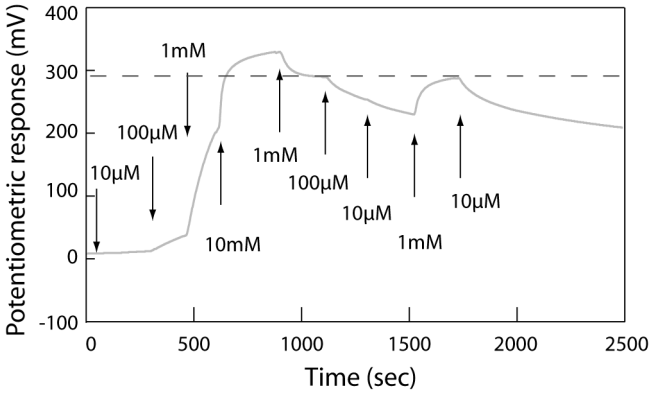

Fig. 2.38 Potentiometric responses of PPy(DBS) to different concentrations of hexacyanoferrate(III) inside the flow cell. The dashed line marks the potentiometric response for 1 mM reagent. The arrows denote the exchange of solutions inside the flow cell. The new solution always fully replaces the previous solution and liquid exchange rate is 2.5 ml/min.

The response to reducing agents is tested with L-AA. Since the rest potential of PPy(DBS) actuators is much lower than for PPy(ClO_4) actuators, the pH of the solution had to be increased up to pH 9.1 with a phosphate buffer to increase the reactivity of L-AA. Transitions were not detected for 1 mM or 10 mM L-AA in pH 4.5 solutions. The strain- and potentiometric responses to 10 mM L-AA in phosphate buffer are shown in Fig. 2.39, which demonstrates that the actuation of PPy(DBS) can be induced in the direction of more negative potentials.

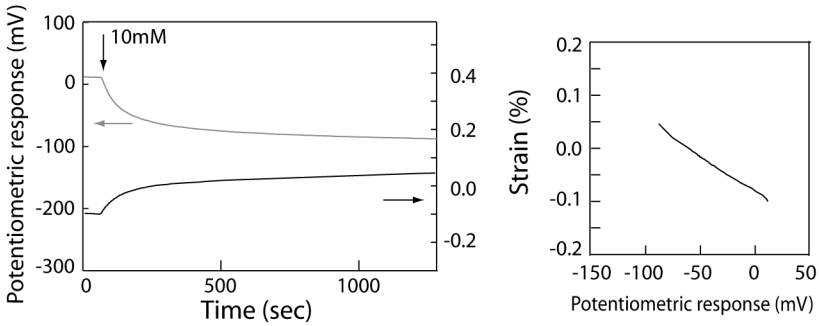

Fig. 2.39 (a) Potentiometric and strain responses of PPy(DBS) bending actuator to L-AA with a concentration of 10 mM in 0.5 M NaCl and 0.1 M phosphate buffer (pH 9.1 at 21°C) as a function of time. The arrow denotes the exchange of solutions inside the flow cell. The new solution always fully replaces the previous solution and liquid exchange rate is 2.5 ml/min. (b) Strain versus potentiometric response for the visualisation of linearity.

2.7 Conclusion

In this chapter we demonstrated that PPy can be actuated by redox agents in solution and shows a strain response which is directly related to the established redox potential of the polymer. To visualise the actuation of the PPy films, a bending beam setup was designed, which enables simple and low-cost fabrication and measurements. First, the behaviour of PPy(ClO_4), an anion exchanging polymer film, was analysed. The actuators could be used in a certain potential window where the strain response of forward and reverse scans is linear and, depending on the scan window size, hysteresis is as low as 6.5%. Two types of redox species were employed, namely hexacyanoferrate and L-ascorbic acid. It was demonstrated that the potential can be established using either a redox couple or a redox moiety. Furthermore, the actuator performance in a redox-driven system displayed linear behaviour in forward and reverse transitions, high repeatability and hysteresis values of 14.2% and lower. The redox-driven strain changes were comparable to the electrically driven actuation. This opens up the opportunity to ease the design and characterisation steps of chemically powered actuators by simply using an external power source. The strain induced by the different redox agents ranged from -0.2% to 0.2%, values which are a multiple smaller than the total strain that can be achieved. This is due to the fact that the potential range where strain is linear – from about -200 mV to above 650 mV – is much larger than the potential range served by the redox agents. Refined fabrication parameters might eventually result in further improved actuator characteristics. For a particular redox agent with its characteristic potential range, the actuator properties could be modified to exhibit improved sensitivity as well as maximum strain and minimum hysteresis in this specific potential window. Several teams demonstrated that fabrication parameters or dopant ions can influence the ion exchange behaviour, potential dependent PPy mass change or actuation [78, 105, 202, 225]. Response times for redox couples – in the range of 80 to 280 seconds – were shorter than those for redox moieties. Depending on the concentration, potentials induced by redox moieties approached a stable value only after several minutes. When the film thickness was tenfold smaller, the response times for molarities of 1-10 mM were reduced to the range of 100 seconds. Freestanding films with the same thickness of 1-2 μm are expected to demonstrate even faster kinetics, because of the larger surface to volume ratio.

We analysed the different pathways that a redox agent could take to induce the responses we have observed and concluded that the most probable route is the potential-dependent anion exchange after reaction of redox ions at the PPy. We also showed that in our measurements, electrolyte concentration-, pH- and temperature changes were not the driving factors for the actuation of PPy.

By replacing ClO_4^- with DBS^- dopant ions for PPy polymerisation, the actuation direction was inverted. We demonstrated that the strain behaviour of PPy(DBS) can be customised to a certain extent by choosing different fabrication parameters. For instance, the strain range was expanded to more positive values when a higher current density was used for polymerisation. With these actuators, strain responses were achieved with hexacyanoferrate(III) as well as L-ascorbic acid. It is possible that PPy(PSS), which is also a cation-exchanging film, could be used in more positive potential windows, as indicated in EQCM measurements [78].
One issue with this way of actuation is the slow recovery time when concentrations of redox agents are decreased. A possible approach to solve this difficulty if the recovery time is more important than the rise time, is to increase the leakage current from the PPy such that the rest state of the PPy can be reached faster. This however slightly slows down the reaction time.
If the PPy actuators ought to be used in a system, where a fast response is much more important than concentration dependence of the strain, another principle may provide a better solution. The next chapter treats such an approach where the PPy actuator functions as artificial muscle with one chemical and one electrochemical half-cycle.

3 Fuel-powered artificial muscle

So far the work has focused on the strain responding linearly to different redox agents in solution. This principle can find its applications in actuators which have to respond to their environment in dependence of molecule concentrations. Another possible implementation of PPy actuators which are responding to their environment is the direct use of two fuels which react at two different electrodes, just as in a fuel cell, to actuate an artificial muscle at a faster pace. This principle veers toward biological muscles, where a fuel (i.e. glucose, ATP) is constantly delivered to the muscle while a single electric twitch can make the muscle contract [13].

3.1 Introduction

We have shown in the previous section that it is possible to chemically actuate PPy with redox agents in solution. Although the actuation can be effected at a faster rate when a potentiostat is used, the strain rate in the redox actuated system is low. In hydrogels, which exhibit volume changes when triggered by changes in pH, temperature or specific interactions to a molecule, low actuation rate is also an issue [6]. Porous composites [121], graft-type gels [122] or smaller structures [123] have been developed to improve transition speed to a few minutes. Other smart actuators like piezoelectric materials or liquid crystal elastomers can respond much faster, but are usually actuated by electrical energy. Ionic electroactive polymers (EAPs) such as carbon nanotubes or conducting polymers show moderate to high strain rates, depending on the applied potential [16]. PPy has the attractive properties of being actuatable with a potential from an external power source as well as from redox agents in a solution. In the proposed system, we take advantage of combining these mechanisms. The PPy actuator is inserted into a fuel cell in the function of an anode. During one half-cycle, the potential at the PPy film is established by the redox agent in the anodic compartment. In the second half cycle, the actuator is shortcut to the cathode, which electrochemically charges the PPy to a more positive potential. Although in the second half-cycle, electrochemical instead of purely chemical energy is transferred to the PPy, no external power source is needed.

3.2 Fabrication Process

The fabrication of the strip is equal as in section 2.5 for the PPy(ClO_4) actuator, since the actuation behaviour for these samples is well known due to the previous measurements. The PPy film is used as the anodic part of a fuel cell whereas a self-breathing oxygen cathode completes the system. This cathode consists of a E-TEK ELAT® gas diffusion layer with Pt particles as catalyst, a stainless steel mesh as current collector, as well as an air-diffusion PMMA piece to enable air flow to the gas diffusion layer. The two electrodes are separated by a Nafion 212 proton exchange membrane (DuPont). A reference electrode (RE) is placed inside the anodic compartment to measure the potential of the PPy film. The inter-electrode-circuit is opened and closed with a switch. Images can be acquired from the side with an illuminated background for good contrast. The whole setup is displayed in Fig. 3.1.

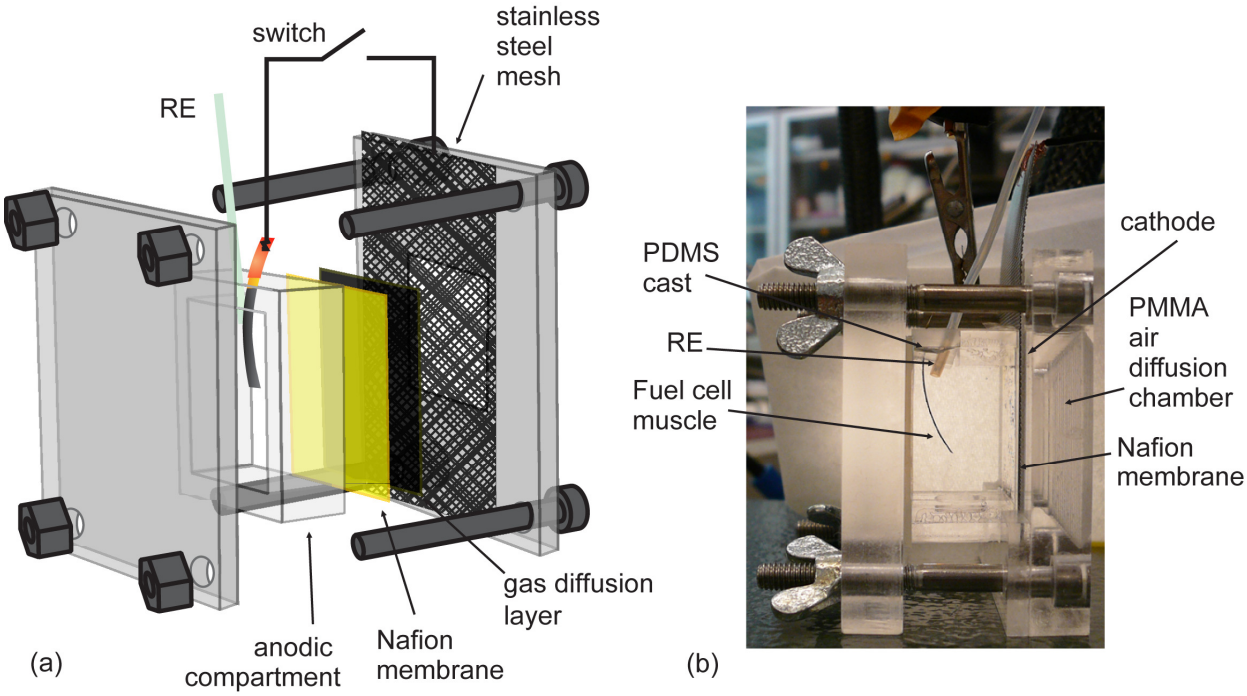

Fig. 3.1 Illustration (a) and picture (b) of setup for fuel-cell actuator. The illustration shows the anodic and cathodic sides, which are ionically connected to each other by a Nafion membrane and electronically by a circuit. The anode consists of a chamber with electrolyte and the fuel while the cathode is a gas diffusion layer in direct contact with the membrane. The electrical connection is made through a stainless steel mesh, which is pressed against the gas diffusion layer and which enables air diffusion.

3.3 Experimental results

We saw in previous sections, that PPy can be oxidised and reduced by redox agents in solution. In analogy to a fuel cell, PPy can thus work as a cathode as well as an anode, when the chemical environment is switched. In this setup, the PPy actuator is kept as the anodic side, separated from an oxygen-cathode. The bending beam actuator was immersed in 0.5 M $NaClO_4$ in 20 mM acetate buffer (pH 4.5 at 21 °C) and 1 mM L-AA.
Both electrodes, anode and cathode, are electrically charged by the fuels inside the chambers while the circuit is open. L-AA in the anodic compartment reduces the polymer. During this reduction, the dopant anions (ClO_4^-) inside the polymer matrix are expelled to maintain the charge neutrality in the film. This leads to a decrease in volume and thus bending of the actuator towards the PPy. The actuator is chemically powered and generates a potential by acting as a fuel-cell electrode. It generates and capacitively stores electrical energy, and at the same time causes actuation. Unlike an ordinary fuel cell, the charge is stored on the electrode and not transferred to the second electrode to establish current in an electronic circuit. On the cathodic side, oxygen in air is reduced in the presence of Pt. Use of this oxygen cathode with a hydrogen anode in a fuel cell setup resulted in an overall open-circuit potential of 0.9 V. The direct measurement of the cathode potential vs. a reference electrode is however difficult, because the cathode is not inside a compartment filled with a solution. The value depends on the connection of the Nafion membrane to the carbon cloth as well as the pH of the anodic electrolyte. In our system, the potential established at the PPy when it is shortcut to the cathode is 410 mV vs. Ag/AgCl, which corresponds to a value of roughly 610 mV vs. NHE. The reactions ideally taking place at the anode and cathode are indicated in equations 3.1 and 3.2, respectively.

$$L - AA \rightarrow DHA + 2e^- + 2H^+ \tag{3.1}$$

$$O_2 + 4H^+ + 4e^- \rightarrow 2H_2O \tag{3.2}$$

So far, the processes described herein take place under open-circuit conditions. When the inter-electrode circuit is closed, current can freely flow and the anodic side is driven towards a more positive potential (Fig. 3.2). While electrons are recombined with holes in the electronic circuit, protons (H^+) are exchanged through the Nafion-membrane from the anodic to the cathodic compartment. The artificial muscle thus works in part chemical and electrochemical, depending on the actuation cycle.

When the connection between the electrodes is broken again, the fuel-cell muscle is recharged and returns to the deflection of the initially charged state. These cycles are presented in Fig. 3.2. The kinetics during the reaction with L-AA are slow. However, when the actuator is connected to the cathode, a fast transition takes place and drives the actuator's potential up 100 mV within one second (the values reached within milliseconds are not indicated here because the measurement setup was designed for seconds as the lowest resolution). Only after that, equilibration to the final potential takes place at a slower pace. The strain of the muscle (calculated as in the previous section) corresponds the potential transitions (Fig. 3.2b). The half-cycle where PPy is reduced does not display the same kinetics or values as experienced before with L-AA in the flow cell (Fig. 2.25). A possible reason is that the anodic compartment in these measurements was not stirred, while inside the flow cell the continuous flow can be compared to stirring of a solution. Depletion of L-AA is not considered due to the large size of the anodic compartment.

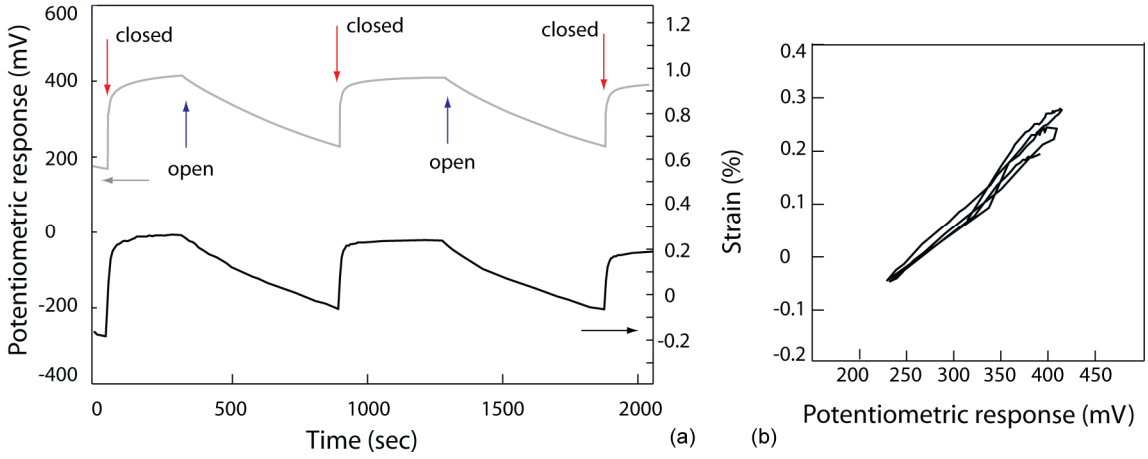

Fig. 3.2 (a) Potential and strain responses of a PPy(ClO_4) fuel-cell bending actuator in 0.5 M $NaClO_4$, 20 mM acetate buffer pH 4.5, 1 mM L-AA as a function of time. Arrows denote the points where the electrical circuit to the oxygen cathode is opened and closed. (b) Strain versus potentiometric response for the visualisation of linearity.

3.4 Conclusion

We demonstrated an approach to improve the response time of a PPy actuator by using it as an anode in a fuel cell. A strain response of 0.23% was reached within one second. The process of recharging is still comparably slow (several minutes). Also here, improvements in the reaction kinetics for instance by making the surface to

volume ration larger or by catalysing the chemical reaction have to be envisaged. In one cycle, chemical energy is directly converted to mechanical energy on the polymer itself while in the second half-cycle the actuator is powered electrochemically over the cathode. So far, the two compartments are separated by a proton exchange membrane. Several approaches for membrane-less fuel cells to be directly used inside or near the human body were reported during the last years [226]. Such specific electrode reactions can also be employed in our system to avoid the use of a membrane.

4 Conclusion and Outlook

4.1 Conclusion

For future applications, ways of driving conducting polymer actuators different than by an external power source directly connected to the polymer might become important, e.g. if batteries and external power sources should be avoided for internal prostheses or biological applications in general. To this end, we have studied the principle of actuating polypyrrole (PPy) with redox agents in solution, i.e. hexacyanoferrates and L-ascorbic acid. Actuation of anion-exchanging films, PPy(ClO_4), and cation-exchangin films, PPy(DBS), was achieved and investigated with different redox agents in solution and further compared to actuation by a potentiostat. To improve the strain rates of chemical actuation we showed that it is possible to employ the PPy actuators in a fuel cell setup.
The actuation behaviour of anion exchanging PPy with perchlorate (ClO_4^-) dopant ions was first measured with an external potential applied from a potentiostat. These results then served as a reference for comparing the chemical and electrochemical actuation methods. PPy(ClO_4) showed a strain response with a broad active potential window. The actuators can be used between -100 mV and 650 mV vs. Ag/AgCl where the strain response in forward and reverse scans is linear and, depending on the scan window size, hysteresis is as low as 6.5%. The redox-induced strain responses were analysed with hexacyanoferrate, a redox pair with a well-defined stable potential, and L-ascorbic acid, a biologically relevant molecule, also known as Vitamin C. Strain and potential were established using either a redox couple or a redox moiety. Except for kinetics, the actuator performance in the redox-driven system and the system with an external power source connected is comparable. Response times for redox couples, which are in the range of 80 to 280 seconds, are shorter than those of redox moieties. It was shown that a thinner film can help reducing the reaction time. Using the hexacyanoferrate couple, a transition in strain from -0.2% to 0.2% is achieved with high repeatability and no drift. The strain is rather small, because we did not fully exploit the total strain available from the actuator when it is driven in a larger potential window, which can be a goal of future

research. Besides redox-driven chemical actuation, we also considered influences of pH, electrolyte concentration, and temperature on the strain, which did not result in comparable actuation performances. Additionally to these measurements of possible side-effects, the pathway of actuation by redox agents was examined. We concluded that neither the exchange of redox ions with dopant ions nor the reaction at gold are probable mechanisms in our system.
Since several applications might depend on the reverse actuation with certain chemical species, we also examined the possibility to chemically actuate PPy(DBS). Following the analysis of strain vs. potential dependent on different fabrication parameters, we showed that actuation with hexacyanoferrate(III) and L-ascorbic acid is possible. Due to strain saturation at high potentials hexacyanoferrate(II) could not be used for this polymer. Generally, kinetics either in forward or reverse transitions were slow and therefore need to be addressed. One solution was indicated with thinner films, another solution for fast actuation was presented in the third chapter, where a PPy actuator was used in a fuel cell setup.
PPy(ClO_4) was operated as anode in a fuel cell with an oxygen cathode. The polymer was reduced by L-ascorbic acid in the compartment when the electrical circuit between anode and cathode was opened. As soon as the two electrodes were connected, the cathode charged the PPy up, which resulted in a corresponding strain change within one second. This setup with one chemical and one electrochemical cycle also demonstrates the versatility of PPy.

4.2 Outlook

We showed in this work that it is possible to chemically power biomimetic actuators in liquid, where the actuation depends on the concentration of chemical agents in solution. Certain limitations were experienced in this system and therefore we list potential follow-up research.
For a particular redox agent to be used in the system, a larger total strain, and concomitantly improved sensitivity, should be achieved. In this thesis it was shown that actuation behaviour is related to the fabrication, and strain in a larger potential window was gained with higher polymerisation currents. Additionally, several teams demonstrated the influences of fabrication parameters or dopant ions on the ion exchange, PPy mass or actuation [78, 105, 225]. The co-polymerisation of PPy with another conducting polymer might lead to a shift of the active strain windows [202].
The response rates for the films used in our measurements were in the range of several minutes. We saw however when a potentiostat was used, that much faster rates for strain changes can be gained. So the strain rates in the chemically actuated

system are not restricted by the ion-exchange but rather by the redox reaction at the PPy. We demonstrated that charging kinetics are faster with a thinner PPy film. Therefore, PPy actuators with larger surface to volume ratios should help enable faster reactions. Nanofiber structures with a high surface to volume ratio can supposedly be charged and actuated at a faster pace. The fabrication of nanofibers was demonstrated for PANI [227] and could also be thought for PPy. Generally, nanostructured CPs could yield similar characteristics to CNT actuators with higher strains [3].

In this work, we utilised hexacyanoferrate and L-ascorbic acid as redox pair and redox moieties. This kind of chemical actuation is however not limited to redox active species. The addition of enzymes to the system could expand the actuation mechanism to various chemical molecules, like glucose for instance. We have analysed the strain response to glucose with glucose oxidase (GOx) as enzyme and benzoquinone (BQ) as mediator in solution. As displayed in Fig. 4.1, a contractive strain is experienced on the addition of glucose, which leads to reduction of the PPy. These preliminary results indicate that it is possible to use the chemical energy of glucose, which is abundantly present in the human body (biological concentrations are 0.4 mM to 26.7 mM), to power the actuation of PPy. In further steps, the incorporation of GOx and a mediator into the polymer film has to be implemented. This was already accomplished for glucose sensors or fuel cells with PPy films [228-230].

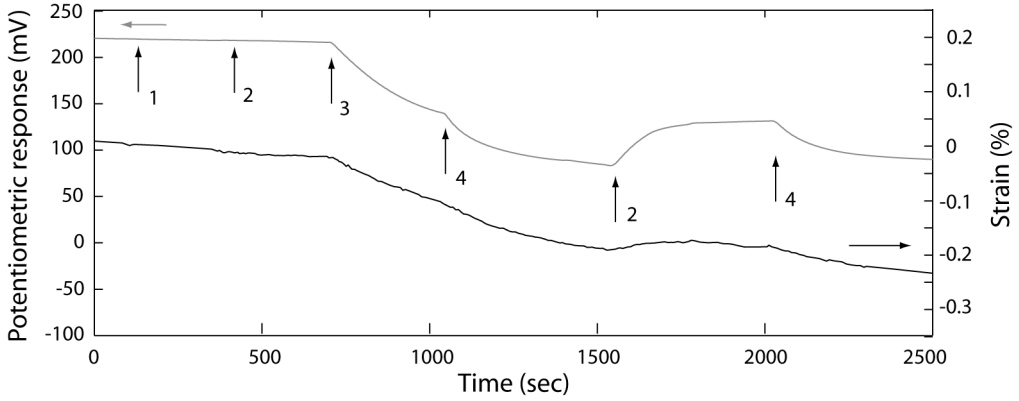

Fig. 4.1 Potential and strain responses of a PPy(ClO_4) bending actuator in 0.5 M NaCl and 50 mM phosphate buffer pH 7, with (1) glucose oxidase (GOx) and (2) GOx and benzoquinone (BQ) added, as a function of time actuated with glucose of concentrations (3) 1 mM, (4) 10 mM. Arrows denote the exchange of solutions inside the flow cell. The observed drift in strain might be due to side-reactions of the chemicals in solution.

On one hand, the energy from glucose could be used in systems such as the fuel cell actuator we presented in chapter 3, where mechanical strength and faster kinetics are relevant. On the other hand, the PPy actuator could be designed to sense different glucose concentrations, and convert this information into a certain strain. Thereby, chemically actuated PPy may broaden the choice towards stronger actuators with various design possibilities for integrated medical feedback systems, which are so far mostly approached by hydrogels. Although several approaches exist e.g. for glucose controlled closed-loop insulin delivery with hydrogels [231], problems like wrong polarity [24, 232], leakage [233], or cross reactivity of other saccharides [231] are still present.
Overall, the chemical actuation of PPy, or even conducting polymers in general, can open up new possibilities to directly use the available fuels in biological systems [3].

Appendix A – Model formulation for strain calculation

To calculate the strain from the curvature that is measured during experiments, classical beam theory was used. The bending of a beam consisting of two or three composite materials can be applied to model the system [103, 168, 234]. The only difference to several similar mechanical systems is that the bending is not evoked by external forces but rather by an intrinsic actuation strain.

The model has the following assumptions:

- The total beam thickness is small compared to the radius of curvature.
- The plane cross-section remains a plane.
- The profile of the beam has to be symmetrical in the z axis.
- The different materials are firmly connected to each other such that no sliding takes place.
- The change in the PPy thickness is much smaller than the lateral dimensions of the strip and the curvature along the width of the bilayer can be neglected.
- All layers are elastic, such that the relationship between stress and strain is given by the elastic or Young's modulus.
- Strains and stresses are isotropic in the x- and y-directions.

Fig. A.1a illustrates the two layers of PPy and PI. The PPy layer exhibits an actuation strain α_{PPy}, which is the relative change in length $\Delta l/l$ when the layer is not laminated to the PI. The PI layer shows no active change in length, thus $\alpha_{PI} = 0$.

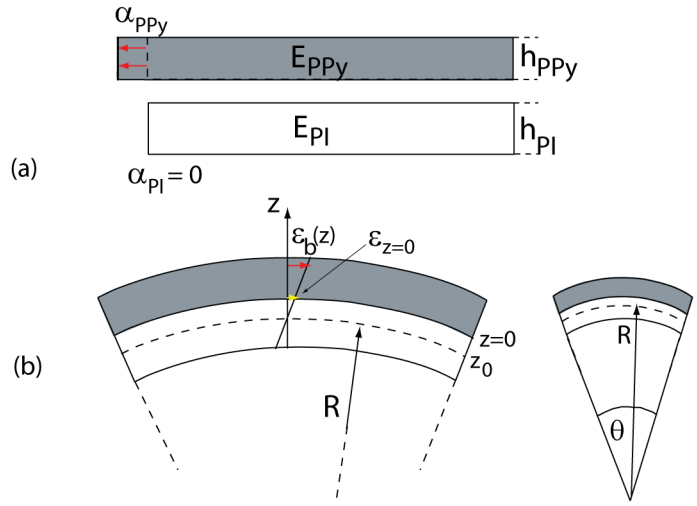

Fig. A.1 Schematic illustration of the bending beam in a sideview of the beam: (a) Actuation strain α_{PPy} in the PPy layer upon electrochemical oxidation for ClO_4^- doping and reduction for DBS^- doping, respectively, when it is free-standing and not laminated to the polyimide layer. (b) Laminating the two layers together results in a bending strain $\varepsilon_b(z)$ which is linearly dependent on z. The dimensions are not to scale.

The thin gold layer (40nm) can be neglected in the calculations, which will be shown later in this section. Due to the actuation strain α_{PPy} the beam displays a bending motion when the two layers are connected, which is shown in Fig. A.1b. At equilibrium the net forces F_{net} at any cross section A must be zero

$$F_{net} = \int_A \sigma(z) dA = 0 \tag{4.1}$$

The stress $\sigma(z)$ is isotropic in the x- and y-directions, as already mentioned in assumption no. 8. This equation can further be split into the contributions of the PPy and the PI layers

$$F_{net} = \int_{A_{PPy}} \sigma_{PPy}(z) dA + \int_{A_{PI}} \sigma_{PI}(z) dA = 0 \tag{4.2}$$

Due to the elastic behaviour of both layers, the stresses can be written as a function of the strains. In the PI layer, the stress is only dependent on the geometric bending strain $\varepsilon_{b,PI}(z)$, while in the PPy layer, the stress depends on the the actuation strain α_{PPy} in addition to the bending strain $\varepsilon_{b,PPy}(z)$.

$$\sigma_{PPy}(z) = E_{PPy}(z) \cdot (\varepsilon_{b,PPy} - \alpha_{PPy}) \tag{4.3}$$

$$\sigma_{PI}(z) = E_{PI}(z) \cdot \varepsilon_{b,PI} \tag{4.4}$$

with the geometric strain $\varepsilon_b(z)$, which increases linearly from the line of zero strain at z_0 as shown in Fig. A.1b. E_{PPy} and E_{PI} are the elastic moduli of the PPy and PI layers, respectively. The bending strain $\varepsilon_b(z)$ is the normalized difference of the segment length at z and the segment length of the line of zero strain, i.e. the length of the beam when no bending is present

$$L_0 = R \cdot \theta \tag{4.5}$$

$$L_z = (R + z - z_0) \cdot \theta \tag{4.6}$$

$$\varepsilon_b(z) = \frac{L_z - L_0}{L_0} = \frac{z - z_0}{R} \tag{4.7}$$

where θ is the angle that encloses the segment (Fig. A.1b). This means that the strain is always relative to the length of the PPy layer in the straight position. We can rewrite this equation to

$$\varepsilon_b(z) = \varepsilon_{z=0} + \frac{z}{R} = \varepsilon_{z=0} + z \cdot \kappa \tag{4.8}$$

Here, $\varepsilon_{z=0}$ is the strain at $z=0$, which arises due to definition of z to be zero at the interface rather than at the line of zero strain z_0 and $\kappa = R^{-1}$ is the curvature of the beam.

The net moments M_{net} also have to be zero at equilibrium just as the net forces in eq. 4.1.

$$M_{net} = 0 = \int_{A_{PPy}} \sigma_{PPy} \cdot z dA + \int_{A_{PI}} \sigma_{PI} \cdot z dA \tag{4.9}$$

Expanding and rearranging the two equations for F_{net} and M_{net}, while the moduli for both layers as well as α_{PPy} are assumed to be constant over z

$$F_{net} = 0 = \int_{A_{PPy}} E_{PPy}\left[\left(\varepsilon_{z=0} + \kappa \cdot z\right) - \alpha_{PPy}\right] dA + \int_{A_{PI}} E_{PI}\left(\varepsilon_{z=0} + \kappa \cdot z\right) dA \tag{4.10}$$

$$\begin{aligned} &\varepsilon_{z=0} \cdot E_{PPy} \cdot b \cdot h_{PPy} + \varepsilon_{z=0} \cdot E_{PI} \cdot b \cdot h_{PI} + \frac{1}{2} E_{PPy} \cdot \kappa \cdot b \cdot {h_{PPy}}^2 - \frac{1}{2} E_{PI} \cdot \kappa \cdot b \cdot {h_{PI}}^2 \\ &= E_{PPy} \cdot b \cdot \alpha_{PPy} \cdot h_{PPy} \end{aligned} \tag{4.11}$$

$$M_{net} = 0 = \int_{A_{PPy}} E_{PPy}\left[\left(\varepsilon_{z=0} + \kappa \cdot z\right) - \alpha_{PPy}\right] \cdot z dA + \int_{A_{PI}} E_{PI}\left(\varepsilon_{z=0} + \kappa \cdot z\right) \cdot z dA \tag{4.12}$$

$$\begin{aligned} &\frac{1}{2}\varepsilon_{z=0} \cdot E_{PPy} \cdot b \cdot {h_{PPy}}^2 - \frac{1}{2}\varepsilon_{z=0} \cdot E_{PI} \cdot b \cdot {h_{PI}}^2 + \frac{1}{3} E_{PPy} \cdot \kappa \cdot b \cdot {h_{PPy}}^3 + \frac{1}{3} E_{PI} \cdot \kappa \cdot b \cdot {h_{PI}}^3 \\ &= \frac{1}{2} E_{PPy} \cdot b \cdot \alpha_{PPy} \cdot {h_{PPy}}^2 \end{aligned} \tag{4.13}$$

with b as the width of the beam, which can be cancelled. The resulting matrix form is

$$\begin{bmatrix} E_{PPy} \cdot b \cdot h_{PPy} + E_{PI} \cdot b \cdot h_{PI} & \frac{1}{2} E_{PPy} \cdot b \cdot {h_{PPy}}^2 - \frac{1}{2} E_{PI} \cdot b \cdot {h_{PI}}^2 \\ \frac{1}{2} E_{PPy} \cdot b \cdot {h_{PPy}}^2 - \frac{1}{2} E_{PI} \cdot b \cdot {h_{PI}}^2 & \frac{1}{3} E_{PPy} \cdot b \cdot {h_{PPy}}^3 + \frac{1}{3} E_{PI} \cdot b \cdot {h_{PI}}^3 \end{bmatrix} \cdot \begin{bmatrix} \varepsilon_{z=0} \\ \kappa \end{bmatrix} = \begin{bmatrix} E_{PPy} \cdot b \cdot \alpha_{PPy} \cdot h_{PPy} \\ \frac{1}{2} E_{PPy} \cdot b \cdot \alpha_{PPy} \cdot {h_{PPy}}^2 \end{bmatrix} \tag{4.14}$$

The two unknowns $\varepsilon_{z=0}$ and κ can be found by solving the two equations with a matrix division. When the left-hand matrix is A and the right-hand matrix is B,

$$\begin{bmatrix} \varepsilon_{z=0} \\ \kappa \end{bmatrix} = A^{-1} B \tag{4.15}$$

The calculations were performed using Mathematica and the resulting equation was transformed using the variables m, n, and h,

$$\begin{aligned} &\frac{1}{R} - \frac{1}{R_r} = \kappa - \kappa_r = \frac{6\alpha_{PPy}(1+m)^2}{h(3(1+m)^2 + (1+mn)(m^2 + \frac{1}{mn}))}, \\ &m = \frac{h_{PI}}{h_{PPy}}, n = \frac{E_{PI}}{E_{PPy}}, h = h_{PI} + h_{PPy} \end{aligned} \tag{4.16}$$

which is also known as the Timoshenko equation for actuation strain due to thermal expansion. From this formula, the strain can be easily calculated, when the curvature

of the beam is available from measurements. Here R_r and κ_r denote the radius and curvature of the beam at the rest state before actuation.

As already mentioned above, the calculations for the conversion from curvature to strain were carried out without taking into account the third (gold) layer. By adding a third term to the equations for equilibrium force and momentum

$$\begin{aligned} F_{net} = 0 = & \int_{A_{PPy}} E_{PPy}\left[\left(\varepsilon_{z=0} + \kappa \cdot z\right) - \alpha_{PPy}\right] dA \\ & + \int_{A_{Au}} E_{Au}\left(\varepsilon_{z=0} + \kappa \cdot z\right) dA + \int_{A_{PI}} E_{PI}\left(\varepsilon_{z=0} + \kappa \cdot z\right) dA \end{aligned} \tag{4.17}$$

$$\begin{aligned} M_{net} = 0 = & \int_{A_{PPy}} E_{PPy}\left[\left(\varepsilon_{z=0} + \kappa \cdot z\right) - \alpha_{PPy}\right] \cdot z dA \\ & + \int_{A_{Au}} E_{Au}\left(\varepsilon_{z=0} + \kappa \cdot z\right) \cdot z dA + \int_{A_{PI}} E_{PI}\left(\varepsilon_{z=0} + \kappa \cdot z\right) \cdot z dA \end{aligned} \tag{4.18}$$

and further rearranging as well as solving the matrix equation with Mathematica again, we gain

$$\kappa - \kappa_i = \frac{1/h_3 \left(n_1 n_2 m_1^3 m_2 + \left[n_1(m_2+1)\right] m_1^2 + \left[n_1(n_2 m_2^2 + m_2^2 + 1)\right] m_1\right)}{\left[\frac{1}{12} n_2^2 - \frac{7}{6} n_2 + \frac{1}{12}\right] m_2^4 + \left[\frac{1}{3}(n_1(n_2 m_1 - m_1) + n_2 - 1)\right] m_2^3 + \left[0.5(n_1(n_2 m_1^2 - m_1^2 + 1) + n_2 + 1)\right] m_2^2 + \left[\frac{1}{3}(n_1(n_1 m_1^3 - m_1^2) + n_2 + 1)\right] m_2 + \frac{1}{3} n_1(m_1^3 + m_1^2 + m_1) + \frac{7}{12}},$$
$$m_1 = \frac{h_1}{h_3}, m_2 = \frac{h_2}{h_3}, n_1 = \frac{E_1}{E_3}, n_2 = \frac{E_2}{E_3}$$

(4.19)

It can be shown, that the error thus included is around five percent and does not vary from sample to sample. In our system, we had a gold thickness of 40 nm and assumed a bulk modulus of 53 GPa as reported in literature for thin gold films [235]. For samples with gold layers deposited on both sides of the PI substrate, the gold layers were included in the calculations of the strain. This case was used during the measurements for responses to temperature and electrolyte concentration changes, to introduce more symmetry in the backing substrate (see section 2.5.8).

Appendix B – PPy microfluidic valve

The design and fabrication of a microfluidic valve was considered for future application as chemically driven responsive valve system. Several microvalve designs have been researched in the literature using conducting polymers as electrochemically-driven active material.

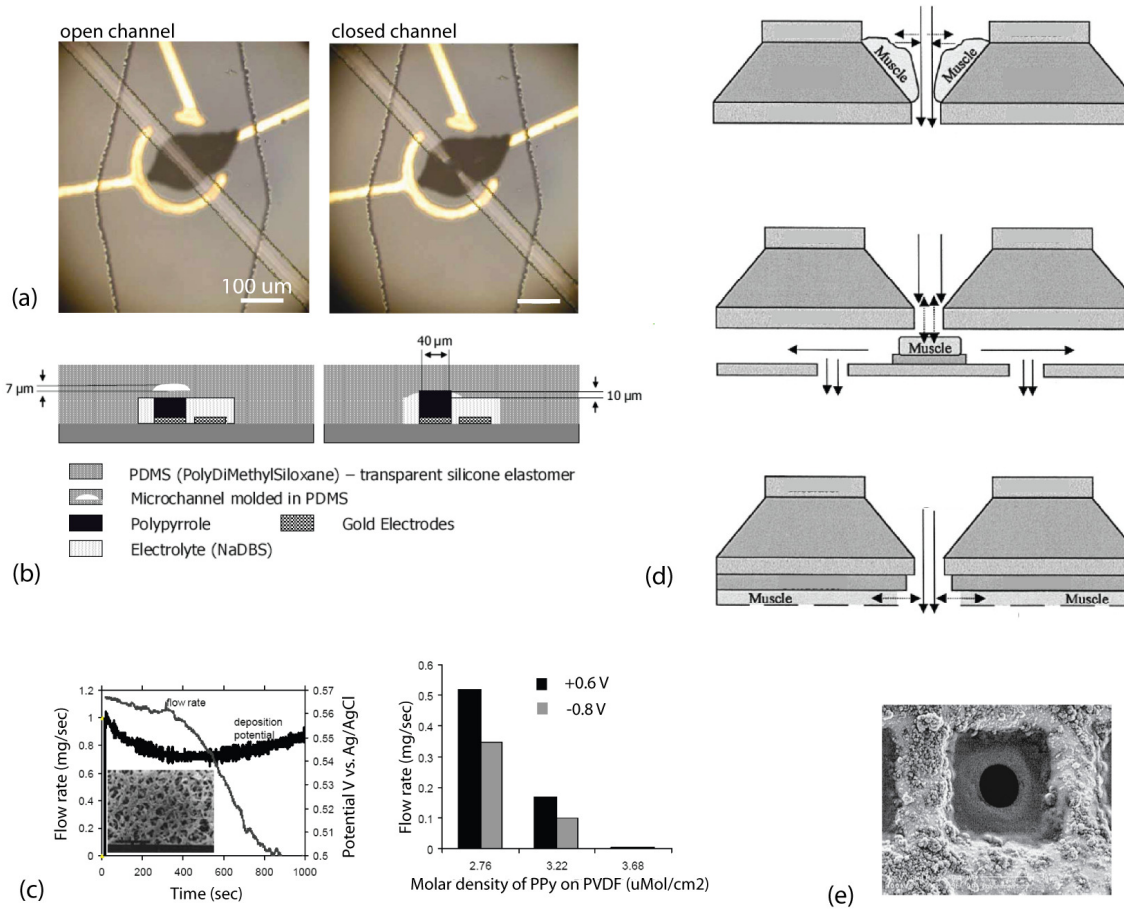

Fig. B.1 Various implementations of microvalves where (a) a liquid channel is opened and closed by the out-of-plane volume change of PPy in a second channel below, (b) schematic illustration [236], (c) the pore sizes in a Pt/PPy coated polyvinylidenefluoride (PVDF) membrane can be switched [237], and (d) in microfabricated structures, the volume of polyaniline influences the sizes of orifices (e) [238].

The out-of-plane volumetric expansion was applied to close and open a channel, which is separated from the channel containing the PPy actuator by an elastomer membrane [236] (Fig. B.1a-b). In another work, instead of opening and closing one channel, a filter membrane was employed [237]. The PPy on the surface of the membrane can be switched between swollen and contracted forms, which closes and opens the pores (Fig. B.1c).
Another approach was implemented with a PANI/hydrogel blend (Fig. B.1d-e). The conducting polymer was polymerised onto orifices to modify the orifice diameter [238]. In-plane strain was used to actuate flaps, which released drugs contained in drug reservoirs [150]. The drawback of this implementation was however that once opened, the drug was released and could not be reversibly controlled. A pulsed release with several reservoirs might be achieved with this mechanism.
We chose a simple but promising fabrication method for our PPy microfluidic valve. A filter membrane was used as a substrate for deposition of PPy, which changes its volume when different potentials are applied. In this way, the pores surrounded by PPy are opened and closed and control the flow through the filter membrane. Instead of sputter-coating the membrane with a metal before electrochemically polymerising PPy, we chose to directly coat the filter structure with PPy by chemical polymerisation. This polymerisation method improves the surface coverage since chemical polymerisation can take place throughout the whole filter and not only on the surface where the metal was deposited. This work was carried out together with Lukas Schlagenhauf in the scope of a student project.

B.1 Fabrication process

Different filter membranes were analysed to be used as substrate for the chemical polymerisation of PPy. A cellulose filter with a pore size of about 8 μm (average retention capacity 4 – 12 μm particle size) and a thickness of 160 μm (Macherey-Nagel, MN 615) did not show substantial reduction of the flow after coating with PPy. This is why we focused on filter membranes with smaller pores. For the fabrication of the PPy membrane valves we used two different kinds of substrates, a mixed cellulose esters filter (MCE) with a pore size of 0.8 μm and 180 μm thickness (AAWP, Millipore) and a polycarbonate track-etch membrane (PCTE) with a pore size of 0.2 μm and 10 μm thickness (Sartorius Type 230). The filters have different pore sizes as well as different structures, as can be seen in Fig. B.2.
The PPy was polymerised chemically onto the membranes instead of electrochemically as it was done for the bending-beam actuators. Chemical

polymerisation requires an oxidant inside the solution, which oxidises the pyrrole monomer similar to the positive potential applied at an electrode. $FeCl_3$ is an oxidant used very often during chemical synthesis [239-242]. Besides the oxidant also a dopant is needed during synthesis, just as in electrochemical polymerisation. We employed ClO_4^- as small dopant and PSS^- as large dopant ion. Two different fabrication processes, which are explained below, were chosen to be compared for their polymerisation behaviour. For both methods the pyrrole monomer was first passed over neutral alumina until colourless before use and stored under 4°C.

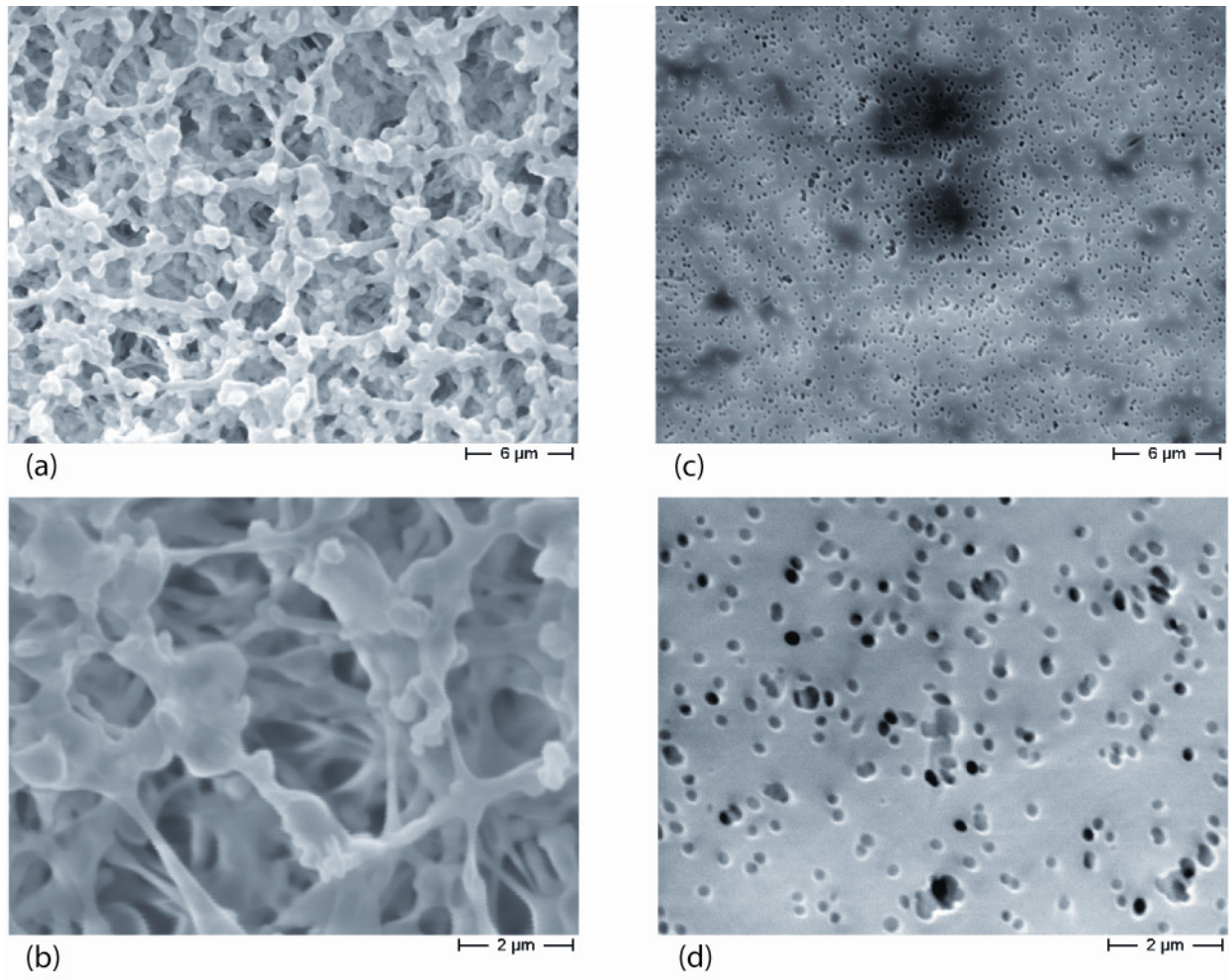

Fig. B.2 SEM images of the two different filter membranes, mixed cellulose esters (MCE) (a), (b), and polycarbonate track-etch membrane (PCTE) (c), (d). Images are taken with two different magnifications, 3100x (a), (c) and 10000x (b), (d). The filters were sputter-coated with an Au layer of 10 nm before imaging. Images were taken at 11 kV and 2 kV, respectively, for MCE and PCTE membranes.

B.1.1 One-step process with pyrrole in solution

The PPy in this process is synthesized directly in the polymerisation solution, which consists of pyrrole, the dopant ions as well as the oxidant $FeCl_3$ in water [240]. Since best conductivities were obtained at low temperatures [239], the synthesis was done at approx. 4°C. High conductivities are required such that the films can be electrically connected on the outside and the whole volume is actuated. The molarities were 0.043 M for pyrrole, 0.013 M for the dopant (either $NaClO_4$ or NaPSS), and 0.1 M for $FeCl_3$. The filter paper was immersed into the solution with pyrrole and dopant, before the oxidant solution was added to start the reaction (Fig. B.3a). After the synthesis, the membrane was cleaned by ethanol and deionized water, and then kept in a 0.1 M $NaClO_4$ solution.

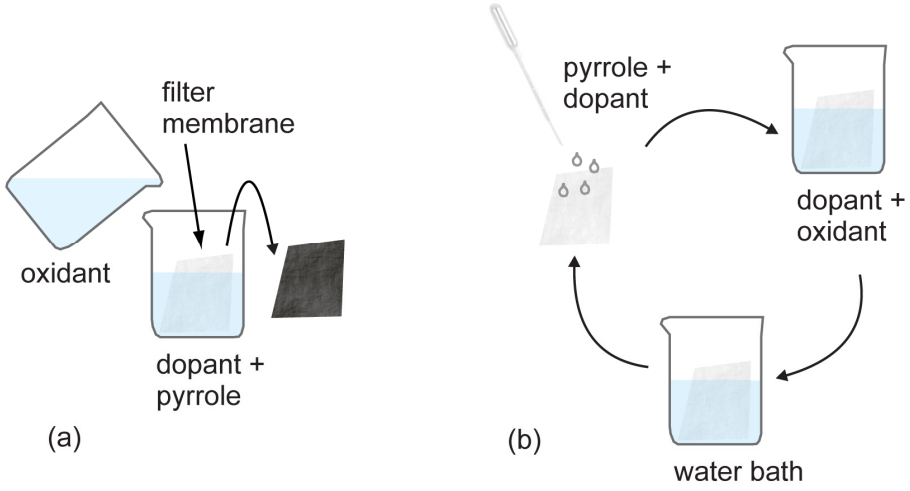

Fig. B.3 Schematic illustrations of the two different processes for fabrication of the PPy filter membranes. (a) One-step process where the filter is immersed into the solution with dopant and pyrrole before the oxidant solution is added to initiate the polymerisation. (b) Two-step process where the filter is impregnated with a solution containing the dopant and pyrrole and in a second step, the impregnated film is immersed into a solution with dopant and oxidant.

B.1.2 Two-step process

This method, which is similar to that reported by Thiéblemont et al. [240], was employed since the PPy film produced during the one-step processes was rather thin, such that the flow through the MCE filters was not largely reduced (Table B.1). The first step included impregnation of the sample with 0.6 M pyrrole and 0.18 M dopant

in ethanol or in water (NaPSS could harly be dissolved in ethanol and therefore water was used instead). Alcohols are usually added to the polymerisation solution to slow down the process because alcohols are reported to partly deactivate the oxidant $FeCl_3$. Secondly, the sample was dipped into the aqueous solution with 0.18 M dopant and 2.4 M $FeCl_3$ for 15 minutes without agitation. After a rinsing step in a water bath and letting the sample dry for a short time, the steps are performed again and repeated several times. The different steps are illustrated in Fig. B.3b. The two-step process was only applied for MCE filters, since the PCTE filter coated with the one-step method already yielded very low flow rates (Table B.2).

B.2 Experimental results

B.2.1 Visual inspection

In a first step, the fabricated filter membranes were analysed in a scanning electron microscope (SEM) to see the surface coverage and structure. The samples were not coated with gold because they were already inherently conducting. In Fig. B.4 an MCE filter coated with PPy after one-step synthesis for 360 minutes with $NaClO_4$ is shown.

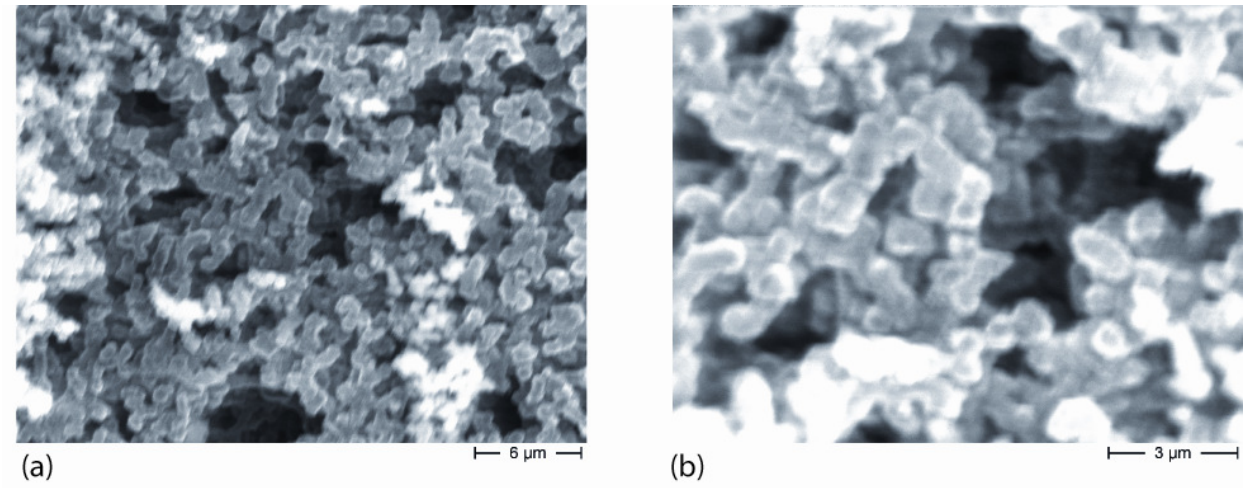

Fig. B.4 SEM pictures of MCE filters after coating with PPy using the one-step method, with $NaClO_4$ as dopant. Different magnifications of the film surface: (a) 3100x and (b) 7500x. Images were taken at 25 kV.

When comparing to the untreated filter in Fig. B.2, no remarkable changes are visible. We however still expect an increase in thickness of the branches, since the

flow rate decreased after this treatment, as we can see in the next section (Table B.1).

Fig. B.5 shows the SEM images of a filter fabricated with 10 cycles of the two-step method and $NaClO_4$ as dopant. Here a substantial difference to the untreated membrane is visible at all magnifications. The branches increased in thickness and the appearance of the surface resembles a filtrate of nanoparticles, just as it would be obtained through chemical polymerisation [242]. Either nanoparticles have formed directly at the surface of the MCE branches or the nanoparticles have developed inside the solution and subsequently attached to the filter surface, building their own mesh.

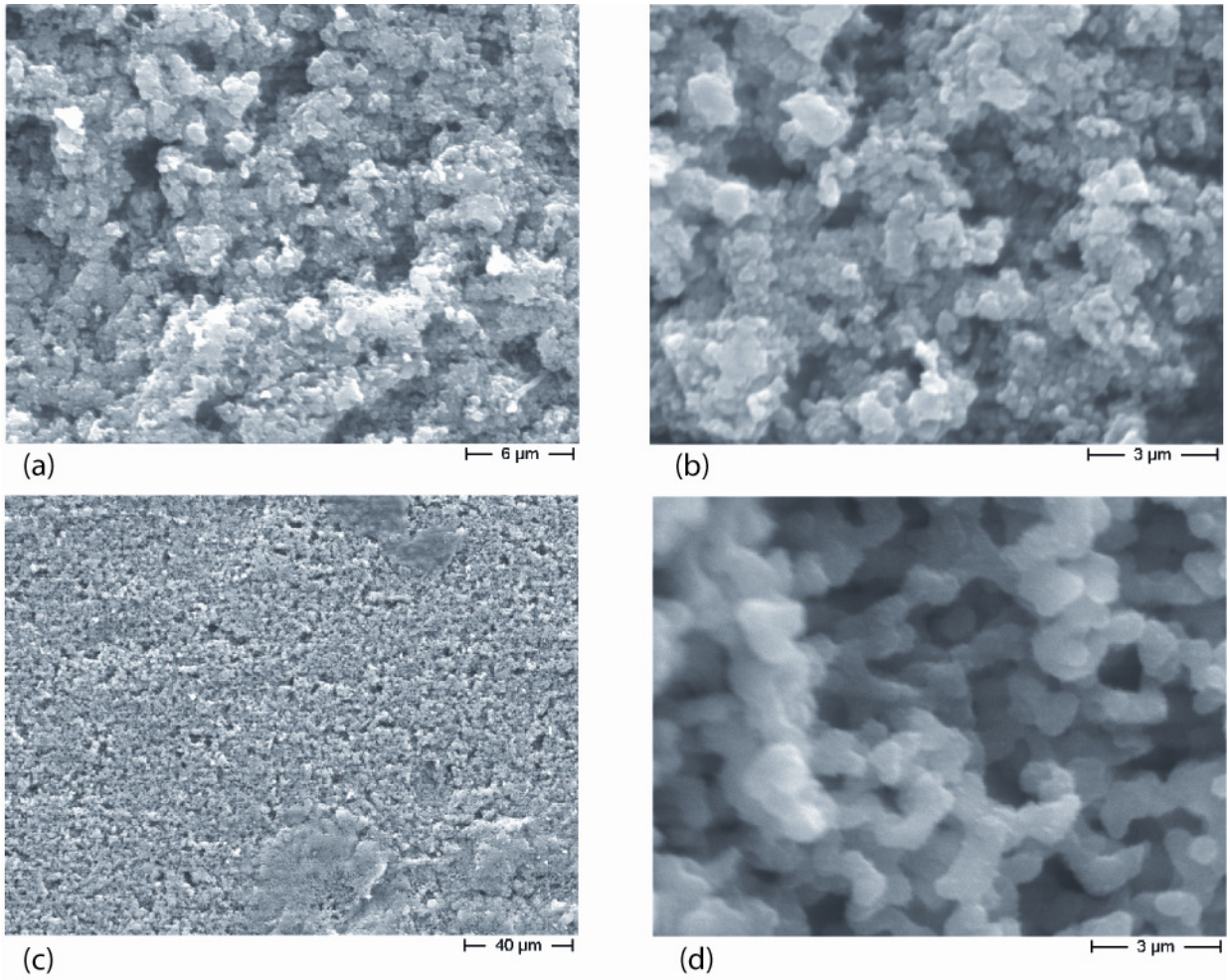

Fig. B.5 SEM pictures of MCE filters after coating with PPy using the two-step method, 10 cycles, with $NaClO_4$ as dopant. Different magnifications of the film surface: (a) 3100x, (b) 7500x, and (c) 470x. (d) shows the structure in the center of the film at a cross-section at a magnification of 7500x. Images were taken at 11 kV.

Fig. B.5d displays the structures in the center of the film by imaging a cross-section. The PPy coverage seems much lower than on the surface. We however checked the

colour of the cross-section under the microscope and could not detect brighter regions in the center of the film (MCE filters are white while PPy tends to black). The small dots which are discernible could indicate, that PPy nanoparticles are developing on the surface, instead of adsorbing onto the filter branches after formation in the solution.
The surface of the coated membranes is not totally homogeneous, as can be seen in Fig. B.5c. Still, the flow rate measurements are taken over an area of 1.3 cm^2 and thus we expect that these variations do not influence the flow rate to a large extent.

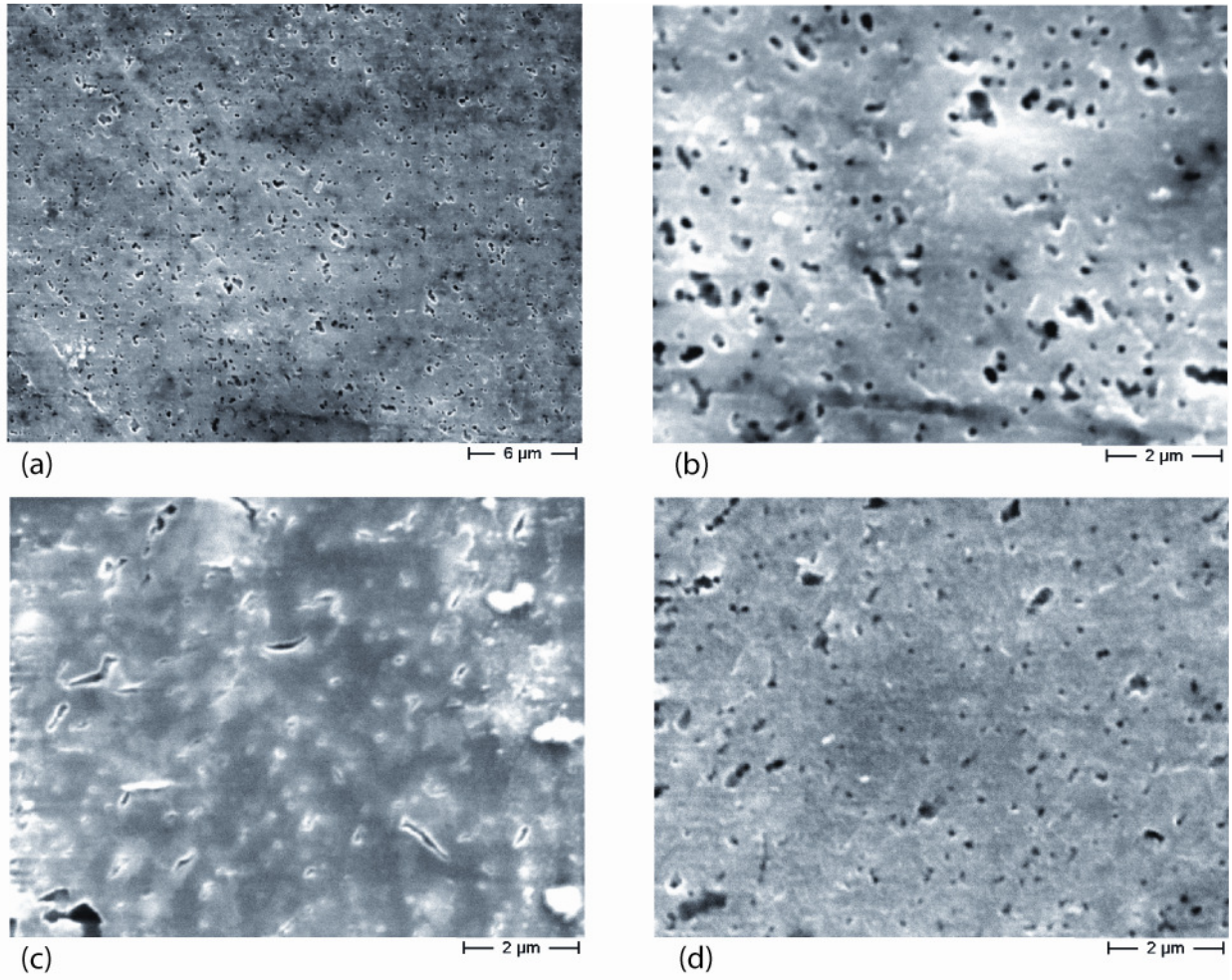

Fig. B.6 SEM pictures of PCTE filters after coating with PPy using the one-step method, with $NaClO_4$ as dopant for sample 1 (a-b) and sample 2 (c) and NaPSS as dopant for sample 3 (d). Sample 1 and 3 are fabricated with 15 minutes polymerisation time while sample 2 was left in solution for 120 minutes. Different magnifications of the films : (a) 3100x, (b-d)10000x. Images were taken at 11 kV.

For the PCTE filter, three different samples are shown in Fig. B.6. Sample 1 (Fig. B.6a and b) was fabricated with $NaClO_4$ in solution for 15 minutes. We assume that a thin layer of PPy has been formed on the surface of the PCTE membrane, slightly

reducing the pore size. In sample 2 (Fig. B.6c) this reduction in pore size is even more distinct due to the longer polymerisation time of 120 minutes. These assumptions are also supported by the flow rate measurements mentioned in the next paragraph. In the third sample polymerised with NaPSS as dopant during 15 minutes, the pore size lies approximately between the sizes of sample one and two.

B.2.2 Flow rate measurements

The flow rates through the filter valves were measured in the setup illustrated in Fig. B.7. A liquid column exerts constant pressure maintained by gravity which leads to a liquid flux through the filter membrane. For the assembly, the sample is placed between two rubber sealings, with an extra o-ring on top to avoid leakage, and between two PMMA-plates, which are attached to the liquid column and output tubing, respectively (Fig. B.7a). The o-ring inner-diameter of 0.65 cm defines the flow rate. Efflux is collected in a beaker on a scale (Delta Range AG204) to detect the amount of collected liquid. To quantify the flow rate, the change of weight of the beaker content is measured over time, taking into account the evaporation of liquid (about 0.1 μL/sec).
For the electrochemical measurements where a potential is applied to the PPy, the filter is electrically connected with adhesive copper-tape attached to the borders on both surfaces. To actuate the PPy in the valve, a three-electrode configuration is used, where the filter functions as working-electrode (WE). An Ag/AgCl reference-electrode (RE, World Precision Instruments, Flexref) and a platinum counter-electrode (CE) are placed into the liquid column. The potentials are applied by a Model 283 Princeton Applied Research (EG&G) potentiostat/galvanostat. For reduction and oxidation of the PPy valves, potentials of -0.8 V and +0.6 V vs. Ag/AgCl were applied to properly oxidise and reduce the PPy coating.
The height of the liquid column on top of the filter was constantly re-adjusted to 3.2 cm to have a constant cross-membrane pressure. Slight variations in the height can be neglected. The outlet tubing had an overall length of 10.2 cm, while the tubing outlet was positioned to touch the liquid surface inside the beaker. A free-hanging tubing outlet led to drop formation and thus irregular flow rates.

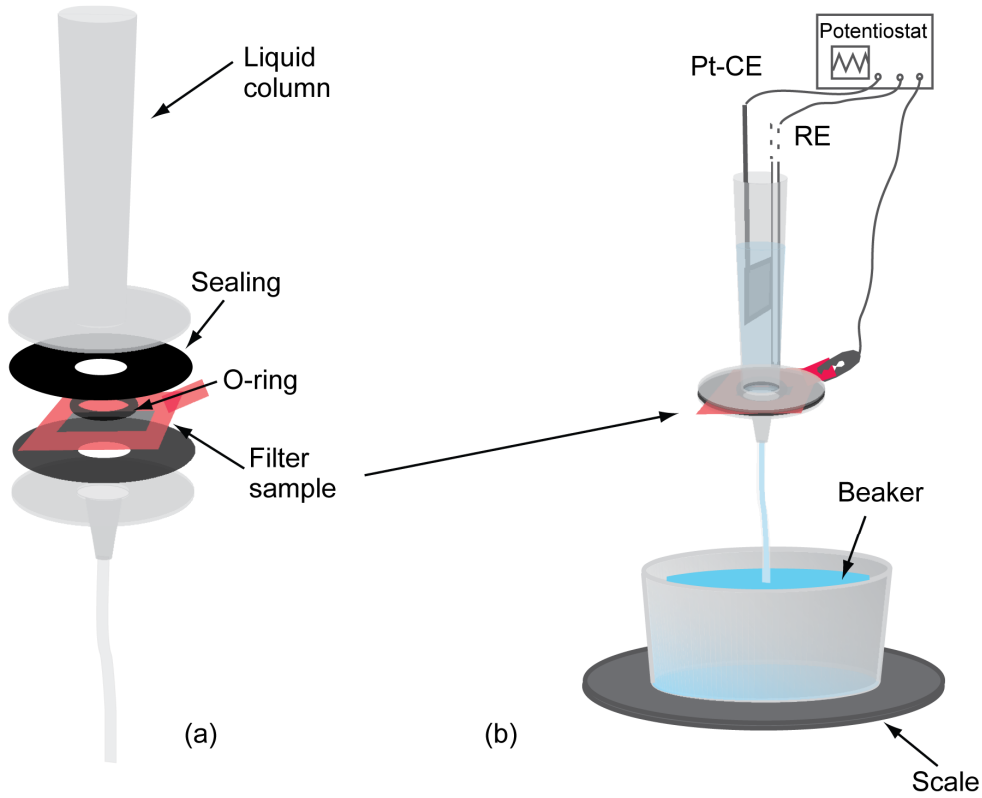

Fig. B.7 Illustrations of (a) the measurement assembly and (b) the setup for flow rate measurements with or without electrochemical potential applied. For electrochemical actuation, a potential between sample (WE) and RE can be applied by a potentiostat.

The pressure onto the filter can thus be calculated through the hydrostatic pressure equation

$$P_h = hg\rho + P_a \tag{4.20}$$

with P_h the pressure inside the column at depth h from the top surface, g the gravitational constant (9.81 m/s^2), ρ the density of the liquid, in this case 0.998 kg/m^3 for water, and P_a the atmospheric pressure. On top and below the filter the established pressure is

$$P_{top} = h_{top}g\rho + P_a \tag{4.21}$$

$$P_{bottom} = P_a - h_{bottom}g\rho \tag{4.22}$$

which yields a pressure difference over the filter of

$$P = P_{top} - P_{bottom} = h_{top}g\rho + h_{bottom}g\rho = h_{tot}g\rho \tag{4.23}$$

This pressure is not dependent on the volume of the column or the area of the filter and results with the mentioned constants to 1312 Pa ($190 \cdot 10^{-3}$ psi).

Table B.1 lists the flow rates of MCE membrane filters. A general decrease in flow rate can be observed with either longer deposition time in the one-step method or more deposition cycles in the two-step method. For the electrochemical measurements we applied the filters coated with the two-step method due to the thicker PPy coatings.

Table B.1 Flow rate measurements of coated MCE filter membranes using the one- or two-step method with either $NaClO_4$ or NaPSS as electrolyte.

Fabrication	Flow rate (μL/sec)
MCE uncoated	9.68±0.2
$NaClO_4$, 60 minutes (1-step)	8.14±0.11
$NaClO_4$ 360 minutes (1-step)	6.85±0.06
$NaClO_4$ 5x 2-step	4.66±0.14
$NaClO_4$ 10x 2-step	3.22±0.15
NaPSS 4x 2-step	1.0±0.03

Measurements with a 4x two-step method PPy(PSS) MCE filter in 0.1 M NaPSS are shown in Fig. B.8a. By application of a positive potential to the coated membrane filter, the flow rate is increased and vice versa. We have made the assumption, that these changes in flow rate are caused by the PPy bulk volume changes due to ion-exchange. When a positive potential is applied, cations leave the polymer, which leads to a decrease in thickness and to an opening of the pores and therefore an increased flow rate. The opposite happens at negative potentials. The same effects were measured to be evoked with an electrolyte of 0.1 M $NaClO_4$ instead of NaPSS. The difference of mean values at positive and negative potentials is 0.11 μL/sec. At the beginning of the measurements in Fig. B.8a, when a negative potential is applied, an increase in flow rate can be observed, which indicates shrinking of the PPy volume instead of expansion. This effect was reported several times for cation-exchanging PPy actuators [77, 93] and is therefore not considered irregular behaviour. Control measurements in water (Fig. B.8b) did not show a general tendency for applied potentials, which means that ions are needed to effect a response. To investigate the effect of large cations on the valve behaviour, the 0.1 M NaPSS

solution was replaced by a 0.1 M Tris base solution. With large cations in solution, the cation-exchanging PPy should not be able to change its volume. Tris is an abbreviation for tris(hydroxymethyl)aminomethane with the formula $(HOCH_2)_3CNH_2$, a molecule with a large cation and a hydroxide ion OH^-. As indicated in Fig. B.8b, no effects were observed on the flow rate with Tris as electrolyte when positive and negative potentials were applied to the PPy film.

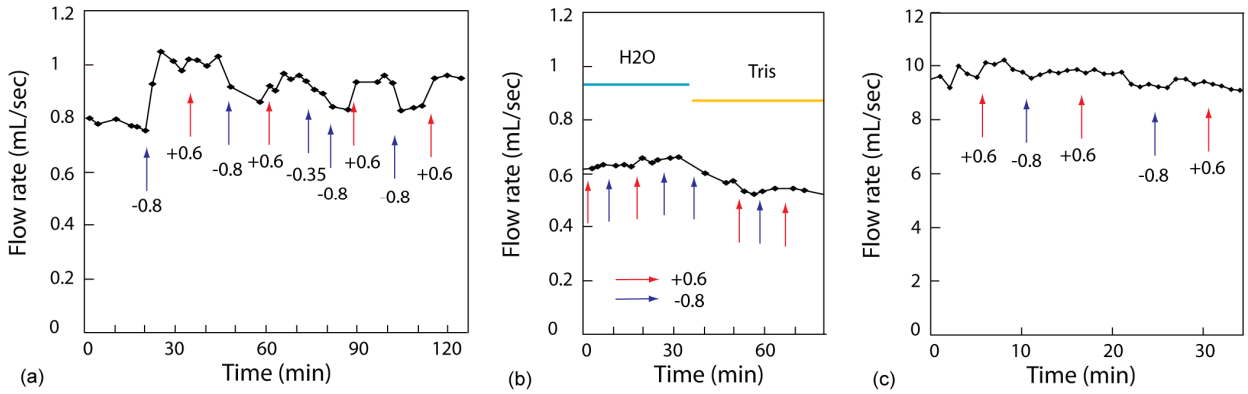

Fig. B.8 Flow rate measurements of a 4x two-step method PPy(PSS) MCE filter with alternating potentials of +0.6 V and -0.8 V applied (a) in 0.1 M NaPSS and (b) in pure water and 0.1 M Tris buffer. (c) Flow rate through an uncoated MCE filter membrane in 0.1 M $NaClO_4$ solution with alternating potentials applied.

A 5x two-step $NaClO_4$ MCE filter was also analysed under alternating potentials. The average flow rate at a potential of +0.6 V was 4.71 μL/sec, while at -0.8 V it was 4.41 μL/sec. It is obvious that the behaviour is not as expected from an anion exchanging PPy film because the polarity of pore opening and closing is the same as in the NaPSS valve. To make sure that the influence on the flow rate for either $NaClO_4$ as well as NaPSS does not originate from the MCE membrane itself, we analysed the uncoated membrane in a 0.1 M $NaClO_4$ solution (Fig. B.8c), which did not show these tendencies. It was reported by Inzelt et al. [186] that PPy(Cl) and PPy(ClO_4) films can exhibit cation transport, if the films are very thin, i.e. < 0.5 μm. Such a small film thickness can indeed be assumed for our PPy films, due to the small pore size of the membrane (0.8 μm). Considering the above mentioned results and control measurements, we conclude that the flow rate is influenced by the PPy coating, most likely due to ion in- and efflux and with this PPy volume and pore size change.

SEM images (Fig. B.6) as well as flow rate measurements without applied potential (Table B.2) of coated PCTE membranes showed the successful formation of PPy in both dopant solutions. Polymerisation times of 15 or 30 minutes for either $NaClO_4$ or

NaPSS on the PCTE filter membranes however resulted in too low conductivities of the PPy films (Table B.2), especially for the PPy(PSS) films [241] (2-step MCE filters showed resistances of around 100-500 Ω / □). Thicker films posed problems on the exact flow rate measurement in our setup. Using membranes with pore sizes as small as 0.2 μm and as flat as PCTE we therefore expect that a thin metallic layer is beneficial for the fabrication of filter valves or the fabrication parameters have to be further optimised, to achieve a high conductivity while maintaining the volume change characteristics of the PPy.

Table B.2 Flow rate measurements as well as sheet resistances of coated PCTE filter membranes using the one-step method with either $NaClO_4$ or NaPSS as electrolyte.

Fabrication	Flow rate (μL/sec)	R_s (Ω / □)
PCTE uncoated	1.24±0.016	-
$NaClO_4$, 15 minutes (1-step)	0.36±0.012	3.3 ± 0.3 kΩ
$NaClO_4$ 30 minutes (1-step)	0.23±0.005	930 ± 40 Ω
$NaClO_4$ 120 minutes (1-step)	n.a.	470 ± 40 Ω
NaPSS 15 minutes (1-step)	0.31±0.012	14.8 ± 0.5 kΩ
NaPSS 30 minutes (1-step)	0.23±0.007	12.4 ± 0.7 kΩ
NaPSS 120 minutes (1-step)	n.a.	8.1 ± 1.7 kΩ

B.3 Conclusion and Discussion

In this chapter we demonstrated a simple and low-cost fabrication method of PPy valves with membrane filters by chemical polymerisation, without additional metal coating. Coating of PCTE membranes lead to either low conductivities if the PPy films were very thin or to hardly measurable flow for PPy films nearly closing the 0.2 μm pores. With MCE membranes we demonstrated that it is indeed possible to influence the flow rate through the valve by an applied potential. 4x two-step PSS valves yielded a mean flow rate difference during electrochemical switching of 0.11 μL/sec (a 12 % reduction of the 0.94 μL/sec flow rate), while with 5x two-step ClO_4 valves a mean difference of 0.3 μL/sec was achieved, which is a 6.5 % reduction of 4.71 μL/sec. A flow rate modulation of around 10%, as it was gained with the PPy

filter valves, is rather low for direct use in an application, where for instance a certain drug efflux should be controlled. A full on-off response would be desirable [24]. Due to the quadratic dependence of flow rate to volume change, better flow rate modulations might be achieved. A valve made of a polyvinylidenefluoride (PVDF) membrane coated with platinum and electrochemically synthesised PPy for instance showed a 32 % reduction of 0.52 mg/sec flow rate [237]. Out-of-plane volume change of PPy films was reported to achieve several tens of percent [82]. Improvements in PPy thickness to pore size ratios can help addressing a larger range of flow rate values. Thereby, on-off reponses might be approached with flow rates in the on-state around 0.1 - 1 μL, depending on the active surface area. We suggest that the use of a branched membrane matrix like PCTE or PVDF helps to improve the flow rate modulation.

Despite the unexpected polarity of the PPy(ClO_4) valve, we understand the change in flow rate in response to applied potentials as the alteration of pore diameter due to ion-transport induced PPy volume change. Analysis of the flow rate dependency on a potential scan and measurements with different dopants and electrolytes [243] can yield further insight into the working principles of such valves and confirm that the flow rate is not controlled through surface energy changes or electrohydrodynamic effects [244-246].

References

[1] J.T. Kraska, J. Burke. Battery technology for implants is overcoming technological hurdles, December 2008. visited in june 2009.

[2] Calabrese, Josh Gallaway, and Plamen Atanassov. Enzymatic biofuel cells for implantable and microscale devices. *Chemical Reviews*, 104(10):4867–4886, October 2004.

[3] Ray H. Baughman. Materials science: Playing nature's game with artificial muscles. *Science*, 308(5718):63–65, April 2005.

[4] S. Chaterji, I. Kwon, and K. Park. Smart polymeric gels: Redefining the limits of biomedical devices. *Progress in Polymer Science*, 32(8-9):1083–1122, August 2007.

[5] J.F. Mano. Stimuli-responsive polymeric systems for biomedical applications. *Advanced Engineering Materials*, 10(6):515–527, 2008.

[6] Paul Calvert. Hydrogels for soft machines. *Advanced Materials*, 21(7):743–756, 2009.

[7] Rustem F. Ismagilov, Alexander Schwartz, Ned Bowden, and George M. Whitesides. Autonomous movement and self-assembly13. *Angewandte Chemie International Edition*, 41(4):652–654, 2002.

[8] Walter F. Paxton, Kevin C. Kistler, Christine C. Olmeda, Ayusman Sen, Sarah K. St. Angelo, Yanyan Cao, Thomas E. Mallouk, Paul E. Lammert, and Vincent H. Crespi. Catalytic nanomotors: Autonomous movement of striped nanorods. *Journal of the American Chemical Society*, 126(41):13424–13431, October 2004.

[9] Sebastien Fournier-Bidoz, Andre C. Arsenault, Ian Manners, and Geoffrey A. Ozin. Synthetic self-propelled nanorotors. *Chem. Commun.*, (4):441–443, 2005.

[10] Christoph Stock, Nicolas Heureux, Wesley r, and Ben l. Autonomous movement of silica and glass micro-objects based on a catalytic molecular propulsion system. *Chemistry - A European Journal*, 14(10):3146–3153, 2008.

[11] Nicolas Mano and Adam Heller. Bioelectrochemical propulsion. *Journal of the American Chemical Society*, 127(33):11574–11575, August 2005.

[12] Von H. Ebron, Zhiwei Yang, Daniel J. Seyer, Mikhail E. Kozlov, Jiyoung Oh, Hui Xie, Joselito Razal, Lee J. Hall, John P. Ferraris, Alan G. Macdiarmid, and Ray H. Baughman. Fuel-powered artificial muscles. *Science*, 311(5767):1580–1583, March 2006.

[13] John D. Madden. Materials science: Artificial muscle begins to breathe. *Science*, 311(5767):1559–1560, March 2006.

[14] J. Biener, A. Wittstock, L. A. Zepeda-Ruiz, M. M. Biener, V. Zielasek, D. Kramer, R. N. Viswanath, J. Weissmuller, M. Baumer, and A. V. Hamza. Surface-chemistry-driven actuation in nanoporous gold. *Nat Mater*, 8(1):47–51, January 2009.

[15] Y. Bar-Cohen, editor. *Electroactive polymer (EAP) actuators as artificial muscles, Reality, Potential, and Challenges Ionomeric Polymer-Metal Composites*. SPIE, 2004.

[16] P. G. A. Madden, J. D. W. Madden, P. A. Anquetil, N. A. Vandesteeg, and I. W. Hunter. The relation of conducting polymer actuator material properties to performance. *Ieee Journal of Oceanic Engineering*, 29(3):696–705, Jul 2004.

[17] Timothy E. Herod and Joseph B. Schlenoff. Doping-induced strain in polyaniline: stretchoelectrochemistry. *Chemistry of Materials*, 5(7):951–955, July 1993.

[18] J. D. W. Madden, N. A. Vandesteeg, P. A. Anquetil, P. G. A. Madden, A. Takshi, R. Z. Pytel, S. R. Lafontaine, P. A. Wieringa, and I. W. Hunter. Artificial muscle technology: Physical principles and naval prospects. *Ieee Journal of Oceanic Engineering*, 29(3):706–728, Jul 2004.

[19] Christine E. Schmidt, Venkatram R. Shastri, Joseph P. Vacanti, and Robert Langer. Stimulation of neurite outgrowth using an electrically conducting polymer. *Proceedings of the National Academy of Sciences of the United States of America*, 94(17):8948–8953, August 1997.

[20] Ze Zhang, Raynald Roy, Francine J. Dugré, Dominic Tessier, and Lê H. Dao. *in vitro* biocompatibility study of electrically conductive polypyrrole-coated polyester fabrics. *Journal of Biomedical Materials Research*, 57(1):63–71, 2001.

[21] Xioadong Wang, Xioasong Gu, Chunwai Yuan, Shujian Chen, Peiyun Zhang, Tianyi Zhang, Jian Yao, Fen Chen, and Gang Chen. Evaluation of biocompatibility of polypyrrole *in vitro* and *in vivo*. *Journal of Biomedical Materials Research Part A*, 68A(3):411–422, 2004.

[22] C. Immerstrand, K. Holmgren-Peterson, K. E. Magnusson, E. Jager, M. Krogh, M. Skoglund, A. Selbing, and O. Inganas. Conjugated-polymer micro- and milliactuators for biological applications. *Mrs Bulletin*, 27(6):461–464, Jun 2002.

[23] Lawrence Kulinsky, Han Xu, Han, and Marc Madou. System-based approach for an advanced drug delivery platform. *Smart Structures and Materials 2006: Smart Structures and Integrated Systems*, 6173(1):61730M+, 2006.

[24] A. Baldi, Y. D. Gu, P. E. Loftness, R. A. Siegel, and B. Ziaie. A hydrogel-actuated environmentally sensitive microvalve for active flow control. *Journal of Microelectromechanical Systems*, 12(5):613–621, Oct 2003.

[25] E. Smela. Conjugated polymer actuators for biomedical applications. *Advanced Materials*, 15(6):481–494, Mar 17 2003.

[26] H. S. Tzou, Lee, and S. M. Arnold. Smart materials, precision sensors/actuators, smart structures, and structronic systems. *Mechanics of Advanced Materials and Structures*, 11(4):367–393, 2004.

[27] Yasuhiro Mizutani, Yukitoshi Otani, and Norihiro Umeda. Optically driven actuators using poly(vinylidene difluoride). *Optical Review*, 15(3):162–165, May 2008.

[28] C. Mavroidis. Development of advanced actuators using shape memory alloys and electrorheological fluids. *Research in Nondestructive Evaluation*, 14(1):1–32, September 2002.

[29] L. H. Yahia, A. Manceur, and P. Chaffraix. Bioperformance of shape memory alloy single crystals. *Bio-medical materials and engineering*, 16(2), 2006.

[30] J. Weissmuller, R. N. Viswanath, D. Kramer, P. Zimmer, R. Wurschum, and H. Gleiter. Charge-induced reversible strain in a metal. *Science*, 300(5617):312–315, April 2003.

[31] Wesley R. Browne and Ben L. Feringa. Making molecular machines work. *Nat Nano*, 1(1):25–35, October 2006.

[32] I. Willner, B. Basnar, and B. Willner. From molecular machines to microscale motility of objects: Application as "smart materials", sensors, and nanodevices. *Advanced Functional Materials*, 17(5):702–717, Mar 23 2007.

[33] Jan O. Jeppesen, Kent A. Nielsen, Julie Perkins, Scott A. Vignon, Alberto Di Fabio, Roberto Ballardini, Teresa M. Gandolfi, Margherita Venturi, Vincenzo Balzani, Jan Becher, and Fraser J. Stoddart. Amphiphilic bistable rotaxanes. *Chemistry - A European Journal*, 9(13):2982–3007, 2003.

[34] T. Mirfakhrai, J. D. W. Madden, and R. H. Baughman. Polymer artificial muscles. *Materials Today*, 10(4):30–38, Apr 2007.

[35] Graham. Towards the integration of carbon nanotubes in microelectronics. *Diamond and related materials*, 13(4-8):1296–1300, 2004.

[36] B.L. Allen, P.D. Kichambare, and A. Star. Carbon nanotube field-effect-transistor-based biosensors. *Advanced Materials*, 19(11):1439–1451, 2007.

[37] T.A. Skotheim et al. *Handbook of conducting polymers*. Marcel Dekker, New York, 1998.

[38] Keisuke Oguro, Naoko Fujiwara, Kinji Asaka, Kazuo Onishi, and Shingo Sewa. Polymer electrolyte actuator with gold electrodes. *Smart Structures and Materials 1999: Electroactive Polymer Actuators and Devices*, 3669(1):64–71, 1999.

[39] Sia N. Nasser. Micromechanics of actuation of ionic polymer-metal composites. *Journal of Applied Physics*, 92(5):2899–2915, 2002.

[40] Kwang J. Kim and Mohsen Shahinpoor. Ionic polymer/metal composites: Ii. manufacturing techniques. *Smart Materials and Structures*, 12(1):65–79, 2003.

[41] S. Nemat-Nasser C.W. Thomas. *Electroactive polymer (EAP) actuators as artificial muscles, Reality, Potential, and Challenges*, chapter Ionomeric Polymer-Metal Composites, pages 171–230. SPIE, 2004.

[42] Mohsen Shahinpoor and Kwang J. Kim. Ionic polymer-metal composites: Iv. industrial and medical applications. *Smart Materials and Structures*, 14(1):197+.

[43] M. Shahinpoor. Ionic polymer-conductor composites as biomimetic sensors, robotic actuators and artificial muscles-a review. *Electrochimica Acta*, 48(14-16):2343–2353, June 2003.

[44] M.S. Dresselhaus P. Avouris, editor. *Carbon Nanotubes - Synthesis, Structure, Properties, and Applications*. Springer Berlin / Heidelberg, 2001.

[45] Ray H. Baughman, Anvar A. Zakhidov, and Walt A. de Heer. Carbon nanotubes–the route toward applications. *Science*, 297(5582):787–792, August 2002.

[46] Min-Feng Yu, Bradley S. Files, Sivaram Arepalli, and Rodney S. Ruoff. Tensile loading of ropes of single wall carbon nanotubes and their mechanical properties. *Physical Review Letters*, 84(24):5552+, June 2000.

[47] Ray H. Baughman, Changxing Cui, Anvar A. Zakhidov, Zafar Iqbal, Joseph N. Barisci, Geoff M. Spinks, Gordon G. Wallace, Alberto Mazzoldi, Danilo De Rossi, Andrew G. Rinzler, Oliver Jaschinski, Siegmar Roth, and Miklos Kertesz. Carbon nanotube actuators. *Science*, 284(5418):1340–1344, May 1999.

[48] D. Suppiger. *Carbon nanotube actuators based on solid electrolytes - Diss. ETH No. 18264*. PhD thesis, ETH Zurich, 2008.

[49] C. Li, E. Thostenson, and T. Chou. Sensors and actuators based on carbon nanotubes and their composites: A review. *Composites Science and Technology*, 68(6):1227–1249, May 2008.

[50] L. Qu, Q. Peng, P. Dai, G. M. Spinks, G. G. Wallace, and R. H. Baughman. Carbon nanotube electroactive polymer materials: Opportunities and challenges. *MRS Bulletin*, 33, March 2008.

[51] D. Suppiger, S. Busato, and P. Ermanni. Characterization of single-walled carbon nanotube mats and their performance as electromechanical actuators. *Carbon*, 46(7):1085–1090, June 2008.

[52] Tissaphern Mirfakhrai, Jiyoung Oh, Mikhail Kozlov, Eddie C. Fok, Mei Zhang, Shaoli Fang, Ray H. Baughman, and John D. Madden. Electrochemical actuation of carbon nanotube yarns. *Smart Materials and Structures*, 16(2):S243–S249, 2007.

[53] J. Barisci. Investigation of ionic liquids as electrolytes for carbon nanotube electrodes. *Electrochemistry Communications*, 6(1):22–27, January 2004.

[54] M. Hughes and G. . M. Spinks. Multiwalled carbon nanotube actuators. *Advanced Materials*, 17(4):443–446, 2005.

[55] S. Iijima. Helical microtubules of graphitic carbon. *Nature*, 354, November 1991.

[56] Mei Zhang, Ken R. Atkinson, and Ray H. Baughman. Multifunctional carbon nanotube yarns by downsizing an ancient technology. *Science*, 306(5700):1358–1361, November 2004.

[57] J. Fraysse. Carbon nanotubes acting like actuators. *Carbon*, 40(10):1735–1739, August 2002.

[58] G. M. Spinks, G. G. Wallace, L. S. Fifield, L. R. Dalton, A. Mazzoldi, D. De Rossi, I. I. Khayrullin, and R. H. Baughman. Pneumatic carbon nanotube actuators. *Advanced Materials*, 14(23):1728–1732, 2002.

[59] Joseph N. Barisci, Geoffrey M. Spinks, Gordon G. Wallace, John D. Madden, and Ray H. Baughman. Increased actuation rate of electromechanical carbon

nanotube actuators using potential pulses with resistance compensation. *Smart Materials and Structures*, 12(4):549–555, 2003.

[60] J.D.W. Madden, J.N. Barisci, P.A. Anquetil, G.M. Spinks, G.G. Wallace, R.H. Baughman, and I.W. Hunter. Fast carbon nanotube charging and actuation. *Advanced Materials*, 18(7):870–873, 2006.

[61] Shaoxin Lu and Balaji Panchapakesan. Photomechanical responses of carbon nanotube/polymer actuators. *Nanotechnology*, 18(30):305502+, 2007.

[62] Y. Zhang and S. Iijima. Elastic response of carbon nanotube bundles to visible light. *Physical Review Letters*, 82(17):3472–3475, Apr 1999.

[63] John Cumings and A. Zettl. Low-friction nanoscale linear bearing realized from multiwall carbon nanotubes. *Science*, 289(5479):602–604, July 2000.

[64] A. F. Diaz and J. I. Castillo. A polymer electrode with variable conductivity - polypyrrole. *Journal of the Chemical Society-Chemical Communications*, (9):397–398, 1980.

[65] R. H. Baughman. Conducting polymer artificial muscles. *Synthetic Metals*, 78(3):339–353, Apr 15 1996.

[66] M. Levi and E. Pisarevskaya. Recent developments in the electrode kinetics of solute redox couple reactions during electrochemical doping of electron-conducting polymers. *Synthetic Metals*, 45(3):309–322, December 1991.

[67] Xuezheng Wang and Elisabeth Smela. Understanding ion transport in conjugated polymers. *Smart Structures and Materials 2005: Electroactive Polymer Actuators and Devices (EAPAD)*, 5759(1):414–422, 2005.

[68] J. D. W. Madden, P. G. A. Madden, and I. W. Hunter. Polypyrrole actuators: modeling and performance. *Smart Structures and Materials 2001: Electroactive Polymer Actuators and Devices*, 4329:72–83 524, 2001.

[69] T. F. Otero, H. Grande, and J. Rodriguez. Role of conformational relaxation on the voltammetric behavior of polypyrrole. experiments and mathematical model. *Journal of Physical Chemistry B*, 101(42):8525–8533, Oct 16 1997.

[70] A. Lewenstam, J. Bobacka, and A. Ivaska. Mechanism of ionic and redox sensitivity of p-type conducting polymers .1. theory. *Journal of Electroanalytical Chemistry*, 368(1-2):23–31, Apr 25 1994.

[71] T. F. Otero, H. J. Grande, and J. Rodriguez. Reinterpretation of polypyrrole electrochemistry after consideration of conformational relaxation processes. *Journal of Physical Chemistry B*, 101(19):3688–3697, May 8 1997.

[72] E. Smela. Conjugated polymer actuators. *Mrs Bulletin*, 33(3):197–204, Mar 2008.

[73] Edwin W. Jager, Elisabeth Smela, and Olle Inganas. Microfabricating conjugated polymer actuators. *Science*, 290(5496):1540–1545, November 2000.

[74] G.B. Street. *Polypyrrole, from powders to plastics Handbook of Conducting Polymers vol 1.* New York: Dekker, 1986.

[75] A. Alumaa, A. Hallik, V. Sammelselg, and J. Tamm. On the improvement of stability of polypyrrole films in aqueous solutions. *Synthetic Metals*, 157(10-12):485–491, Jun 2007.

[76] E. Smela, W. Lu, and B. Mattes. Polyaniline actuatorspart 1. pani(amps) in hcl. *Synthetic Metals*, 151(1):25–42, May 2005.

[77] S. Shimoda and E. Smela. The effect of ph on polymerization and volume change in ppy(dbs). *Electrochimica Acta*, 44(2-3):219–238, 1998.

[78] C. Weidlich, K. M. Mangold, and K. Juttner. EQCM study of the ion exchange behaviour of polypyrrole with different counterions in different electrolytes. *Electrochimica Acta*, 50(7-8):1547–1552, Feb 15 2005.

[79] T. Zama, S. Hara, W. Takashima, and K. Kaneto. Comparison of conducting polymer actuators based on polypyrrole doped with bf4(-), pf6(-), cf3so3-, and clo4-. *Bulletin of the Chemical Society of Japan*, 78(3):506–511, Mar 15 2005.

[80] S. Hara, T. Zama, W. Takashima, and K. Kaneto. Artificial muscles based on polypyrrole actuators with large strain and stress induced electrically. *Polymer Journal*, 36(2):151–161, 2004.

[81] K. Yamato and K. Kaneto. Tubular linear actuators using conducting polymer, polypyrrole. *Analytica Chimica Acta*, 568(1-2):133–137, May 24 2006.

[82] E. Smela and N. Gadegaard. Volume change in polypyrrole studied by atomic force microscopy. *Journal of Physical Chemistry B*, 105(39):9395–9405, Oct 4 2001.

[83] L. Bay, K. West, P. Sommer-Larsen, S. Skaarup, and M. Benslimane. A conducting polymer artificial muscle with 12% linear strain. *Advanced Materials*, 15(4):310–313, Feb 17 2003.

[84] L. Bay, K. West, and S. Skaarup. Pentanol as co-surfactant in polypyrrole actuators. *Polymer*, 43(12):3527–3532, June 2002.

[85] G.M. Spinks, V. Mottaghitalab, M. Bahrami-Samani, P.G. Whitten, and G.G. Wallace. Carbon-nanotube-reinforced polyaniline fibers for high-strength artificial muscles. *Advanced Materials*, 18(5):637–640, 2006.

[86] J. D. Madden, R. A. Cush, T. S. Kanigan, and I. W. Hunter. Fast contracting polypyrrole actuators. *Synthetic Metals*, 113(1-2):185–192, Jun 15 2000.

[87] J. Ding. High performance conducting polymer actuators utilising a tubular geometry and helical wire interconnects. *Synthetic Metals*, 138(3):391–398, July 2003.

[88] S. Hara, T. Zama, W. Takashima, and K. Kaneto. Free-standing polypyrrole actuators with response rate of 10.8%s. *Synthetic Metals*, 149(2-3):199–201, March 2005.

[89] Xuezheng Wang and Elisabeth Smela. Cycling conjugated polymers with different cations. *Smart Structures and Materials 2006: Electroactive Polymer Actuators and Devices (EAPAD)*, 6168(1):61680T+, 2006.

[90] S. Skaarup, L. Bay, and K. West. Polypyrrole actuators working at 2–30hz. *Synthetic Metals*, 157(6-7):323–326, April 2007.

[91] E. Smela. Microfabrication of ppy microactuators and other conjugated polymer devices. *Journal of Micromechanics and Microengineering*, 9(1):1–18, Mar 1999.

[92] Gordon G. Wallace and Peter C. Innis. Inherently conducting polymer nanostructures. *Journal of Nanoscience and Nanotechnology*, pages 441–451, October 2002.

[93] Han Xu, Chunlei Wang, Lawrence Kulinsky, Jim Zoval, and Marc Madou. Sensor-integrated polymer actuators for closed-loop drug delivery system. *Smart Structures and Materials 2006: Smart Electronics, MEMS, BioMEMS, and Nanotechnology*, 6172(1):61720R+, 2006.

[94] Alexander S. Lee, Serban F. Peteu, James V. Ly, Aristides A. Requicha, Mark E. Thompson, and Chongwu Zhou. Actuation of polypyrrole nanowires. *Nanotechnology*, 19(16):165501+, 2008.

[95] Benjamin L. Fletcher, Scott T. Retterer, Timothy E. Mcknight, Anatoli V. Melechko, Jason D. Fowlkes, Michael L. Simpson, and Mitchel J. Doktycz. Actuatable membranes based on polypyrrole-coated vertically aligned carbon nanofibers. *ACS Nano*, 2(2):247–254, February 2008.

[96] J. D. Madden, R. A. Cush, T. S. Kanigan, C. J. Brenan, and I. W. Hunter. Encapsulated polypyrrole actuators. *Synthetic Metals*, 105(1):61–64, Aug 16 1999.

[97] J. M. Sansinena, V. Olazabal, T. F. Otero, Fonseca, and Marco-A Paoli. A solid state artificial muscle based on polypyrrole and a solid polymeric electrolyte working in air. *Chem. Commun.*, (22):2217–2218, 1997.

[98] Manuel Aschwanden. *Tunable Optical Elements based on Dielectric Elastomer Actuators*. PhD thesis, ETH Zurich, 2007.

[99] Joo-Woon Lee, Francisco Serna, and Christine E. Schmidt. Carboxy-endcapped conductive polypyrrole: Biomimetic conducting polymer for cell scaffolds and electrodes. *Langmuir*, 22(24):9816–9819, November 2006.

[100] T. J. Rivers, T. W. Hudson, and C. E. Schmidt. Synthesis of a novel, biodegradable electrically conducting polymer for biomedical applications. *Advanced Functional Materials*, 12(1):33–37, 2002.

[101] Alexander N. Zelikin, David M. Lynn, Jian Farhadi, Ivan Martin, Venkatram Shastri, and Robert Langer. Erodible conducting polymers for potential biomedical applications. *Angewandte Chemie International Edition*, 41(1):141–144, 2002.

[102] Vincent Tabard-Cossa, Michel Godin, Peter Grutter, Ian Burgess, and R. B. Lennox. Redox-induced surface stress of polypyrrole-based actuators. *The Journal of Physical Chemistry B*, 109(37):17531–17537, September 2005.

[103] M. Christophersen, B. Shapiro, and E. Smela. Characterization and modeling of ppy bilayer microactuators - part 1. curvature. *Sensors and Actuators B-Chemical*, 115(2):596–609, Jun 26 2006.

[104] S. Maw, E. Smela, K. Yoshida, P. Sommer-Larsen, and R. B. Stein. The effects of varying deposition current density on bending behaviour in ppy(dbs)-

actuated bending beams. *Sensors and Actuators a-Physical*, 89(3):175–184, Apr 15 2001.

[105] S. Maw, E. Smela, K. Yoshida, and R. B. Stein. Effects of monomer and electrolyte concentrations on actuation of ppy(dbs) bilayers. *Synthetic Metals*, 155(1):18–26, Oct 15 2005.

[106] K. Kaneto, H. Fujisue, M. Kunifusa, and W. Takashima. Conducting polymer soft actuators based on polypyrrole films - energy conversion efficiency. *Smart Materials & Structures*, 16(2):S250–S255, Apr 2007.

[107] T. Otero and J.M. Sansinena. Bilayer dimensions and movement in artificial muscles. *Bioelectrochemistry and Bioenergetics*, 42(2):117–122, May 1997.

[108] Hisashi Fujisue, Tomokazu Sendai, Kentaro Yamato, Wataru Takashima, and Keiichi Kaneto. Work behaviors of artificial muscle based on cation driven polypyrrole. *Bioinspiration & Biomimetics*, 2(2):S1–S5, 2007.

[109] T. F. Otero, J. J. L. Cascales, and G. V. Arenas. Mechanical characterization of free-standing polypyrrole film. *Materials Science & Engineering C-Biomimetic and Supramolecular Systems*, 27(1):18–22, Jan 2007.

[110] G. Y. Han and G. Q. Shi. Electrochemical actuator based on single-layer polypyrrole film. *Sensors and Actuators B-Chemical*, 113(1):259–264, Jan 17 2006.

[111] Rajesh, S. S. Pandey, D. Kumar, W. Takashima, and K. Kaneto. Electrochemomechanical deformation studies of [fe(cn)(6)](3-) ion doped conducting polypyrrole film. *Thin Solid Films*, 467(1-2):227–230, Nov 22 2004.

[112] D. Kaneko, J. P. Gong, and Y. Osada. Polymer gels as soft and wet chemomechanical systems - an approach to artificial muscles. *Journal of Materials Chemistry*, 12(8):2169–+, Aug 2002.

[113] I. Z. Steinberg, A. Oplatka, and A. Katchalsky. Mechanochemical engines. *Nature*, 210:568–571, 1966.

[114] Aharon Katchalsky. Rapid swelling and deswelling of reversible gels of polymeric acids by ionization. *Cellular and Molecular Life Sciences (CMLS)*, 5(8):319–320, August 1949.

[115] Masao Doi, Mitsuhiro Matsumoto, and Yoshiharu Hirose. Deformation of ionic polymer gels by electric fields. *Macromolecules*, 25(20):5504–5511, September 1992.

[116] Tomohiro Shibuya, Hidekazu Yasunaga, Hiromichi Kurosu, and Isao Ando. Spatial information on a polymer gel as studied by 1h nmr imaging. 2. shrinkage by the application of an electric field to a polymer gel. *Macromolecules*, 28(13):4377–4382, June 1995.

[117] Tohru Shiga and Toshio Kurauchi. Deformation of polyelectrolyte gels under the influence of electric field. *Journal of Applied Polymer Science*, 39(11-12):2305–2320, 1990.

[118] Y. Osada, H. Okuzaki, and H. Hori. A polymer gel with electrically driven motility. *Nature*, 355, January 1992.

[119] Brett H. Schreyer, Nouvelle Gebhart, Kwang J. Kim, and Mohsen Shahinpoor. Electrical activation of artificial muscles containing polyacrylonitrile gel fibers. *Biomacromolecules*, 1(4):642–647, December 2000.

[120] A. Sahoo, K. Ramasubramani, M. Jassal, and A. Agrawal. Effect of copolymer architecture on the response of ph sensitive fibers based on acrylonitrile and acrylic acid. *European Polymer Journal*, 43(3):1065–1076, March 2007.

[121] Xian-Zheng Zhang, Fang-Jing Wang, and Chih-Chang Chu. Thermoresponsive hydrogel with rapid response dynamics. *Journal of Materials Science: Materials in Medicine*, 14(5):451–455, May 2003.

[122] R. Yoshida, K. Uchida, Y. Kaneko, K. Sakai, A. Kikuchi, Y. Sakurai, and T. Okano. Comb-type grafted hydrogels with rapid deswelling response to temperature changes. *Nature*, 374:240–242, 1995.

[123] J. Heijl and F. Duprez. Fast, multi-responsive microgels based on photo-crosslinkable poly(2-(dimethylamino)ethyl methacrylate). *Polymer*, 45(20):6771–6778, September 2004.

[124] J. Kopecek. Hydrogel biomaterials: A smart future?? *Biomaterials*, 28(34):5185–5192, December 2007.

[125] J. P. Gong, Y. Katsuyama, T. Kurokawa, and Y. Osada. Double-network hydrogels with extremely high mechanical strength. *Advanced Materials*, 15(14):1155–1158, 2003.

[126] Y. Okumura and K. Ito. The polyrotaxane gel: A topological gel by figure-of-eight cross-links. *Advanced Materials*, 13(7):485–487, 2001.

[127] K. Haraguchi and T. Takehisa. Nanocomposite hydrogels: A unique organic-inorganic network structure with extraordinary mechanical, optical, and swelling/de-swelling properties. *Advanced Materials*, 14(16):1120–1124, 2002.

[128] Siddharthya K. Mujumdar and Ronald A. Siegel. Introduction of ph-sensitivity into mechanically strong nanoclay composite hydrogels based on *n*-isopropylacrylamide. *Journal of Polymer Science Part A: Polymer Chemistry*, 46(19):6630–6640, 2008.

[129] N.A. Peppas, J.Z. Hilt, A. Khademhosseini, and R. Langer. Hydrogels in biology and medicine: From molecular principles to bionanotechnology. *Advanced Materials*, 18(11):1345–1360, 2006.

[130] J. D. Ehrick, S. K. Deo, T. W. Browning, L. G. Bachas, M. J. Madou, and S. Daunert. Genetically engineered protein in hydrogels tailors stimuli-responsive characteristics. *Nature Materials*, 4(4):298–302, Apr 2005.

[131] Zhijie Sui, William J. King, and William L. Murphy. Protein-based hydrogels with tunable dynamic responses. *Advanced Functional Materials*, 18(12):1824–1831, 2008.

[132] Weiwei Yuan, Jiyuan Yang, Pavla Kopeckova, and Jindrich Kopecek. Smart hydrogels containing adenylate kinase: Translating substrate recognition into

macroscopic motion. *Journal of the American Chemical Society*, 130(47):15760–15761, November 2008.
[133] C. Huang, R. Klein, F. Xia, H. Li, Q. M. Zhang, F. Bauer, and Z. Y. Cheng. Poly(vinylidene fluoride-trifluoroethylene) based high performance electroactive polymers. *Dielectrics and Electrical Insulation, IEEE Transactions on*, 11(2):299–311, 2004.
[134] R. Kornbluh et al. *Electro Active Polymers (EAP) as Artificial Muscles: Reality, Potential and Challenges*, chapter Application of dielectric EAP actuators, pages 530–577. SPIE Press, 2004.
[135] Ron Pelrine, Roy D. Kornbluh, Qibing Pei, Scott Stanford, Seajin Oh, Joseph Eckerle, Robert J. Full, Marcus A. Rosenthal, and Kenneth Meijer. Dielectric elastomer artificial muscle actuators: toward biomimetic motion. *Smart Structures and Materials 2002: Electroactive Polymer Actuators and Devices (EAPAD)*, 4695(1):126–137, 2002.
[136] Roy D. Kornbluh, Ron Pelrine, Qibing Pei, Seajin Oh, and Jose Joseph. Ultrahigh strain response of field-actuated elastomeric polymers. *Smart Structures and Materials 2000: Electroactive Polymer Actuators and Devices (EAPAD)*, 3987(1):51–64, 2000.
[137] Helmut F. Schlaak, Markus Jungmann, Marc Matysek, and Peter Lotz. Novel multilayer electrostatic solid state actuators with elastic dielectric (invited paper). *Smart Structures and Materials 2005: Electroactive Polymer Actuators and Devices (EAPAD)*, 5759(1):121–133, 2005.
[138] C. Löwe, X. Zhang, and G. Kovacs. Dielectric elastomers in actuator technology. *Advanced Engineering Materials*, 7(5):361–367, 2005.
[139] Ravi Shankar, Tushar K. Ghosh, and Richard J. Spontak. Dielectric elastomers as next-generation polymeric actuators. *Soft Matter*, 3(9):1116–1129, 2007.
[140] M. Warner E.M. Terentjev. *Liquid crystal elastomers*. Oxford University Press, 2003.
[141] Min-Hui Li and Patrick Keller. Artificial muscles based on liquid crystal elastomers. *Philosophical Transactions of the Royal Society A: Mathematical, Physical and Engineering Sciences*, 364(1847):2763–2777, October 2006.
[142] W. Lehmann, H. Skupin, C. Tolksdorf, E. Gebhard, R. Zentel, P. Kruger, M. Losche, and F. Kremer. Giant lateral electrostriction in ferroelectric liquid-crystalline elastomers. *Nature*, 410(6827):447–450, March 2001.
[143] Measurement of the pyroelectric response and of the thermal diffusivity of microtomized sections of 'single crystalline' ferroelectric liquid crystalline elastomers. *Liquid Crystals*, 27(2):289–297, 2000.
[144] H. Skupin, F. Kremer, S. V. Shilov, P. Stein, and H. Finkelmann. Time-resolved ftir spectroscopy on structure and mobility of single crystal ferroelectric liquid crystalline elastomers. *Macromolecules*, 32(11):3746–3752, June 1999.

[145] Mark Staples, Karen Daniel, Michael Cima, and Robert Langer. Application of micro- and nano-electromechanical devices to drug delivery. *Pharmaceutical Research*, 23(5):847–863, May 2006.
[146] M.J. Rathbone M.S. Roberts. *Modified-release drug delivery technology*. Marcel Dekker, New York, 2003.
[147] J. Hilt and N. Peppas. Microfabricated drug delivery devices. *International Journal of Pharmaceutics*, 306(1-2):15–23, December 2005.
[148] Adam Heller. Integrated medical feedback systems for drug delivery. *AIChE Journal*, 51(4):1054–1066, 2005.
[149] Marc Madou and John Florkey. From batch to continuous manufacturing of microbiomedical devices. *Chemical Reviews*, 100(7):2679–2692, July 2000.
[150] H. Xu, C. Wang, C. Wang, J. Zoval, and M. Madou. Polymer actuator valves toward controlled drug delivery application. *Biosensors and Bioelectronics*, February 2006.
[151] James H. Prescott, Sara Lipka, Samuel Baldwin, Norman F. Sheppard, John M. Maloney, Jonathan Coppeta, Barry Yomtov, Mark A. Staples, and John T. Santini. Chronic, programmed polypeptide delivery from an implanted, multireservoir microchip device. *Nature Biotechnology*, 24(4):437–438, March 2006.
[152] Y. Li, B. Tyler, T. Williams, M. Tupper, R. Langer, H. Brem, and M. Cima. In vivo delivery of bcnu from a mems device to a tumor model. *Journal of Controlled Release*, 106(1-2):138–145, August 2005.
[153] H. Huang. Probe beam deflection study on electrochemically controlled release of 5-fluorouracil. *Electrochimica Acta*, 43(9):999–1004, April 1998.
[154] Amy C. Grayson, Insung S. Choi, Betty M. Tyler, Paul P. Wang, Henry Brem, Michael J. Cima, and Robert Langer. Multi-pulse drug delivery from a resorbable polymeric microchip device. *Nat Mater*, 2(11):767–772, November 2003.
[155] Shashishekar Adiga, Larry Curtiss, Jeffrey Elam, Michael Pellin, Chun-Che Shih, Chun-Ming Shih, Shing-Jong Lin, Yea-Yang Su, Shaun Gittard, Junping Zhang, and Roger Narayan. Nanoporous materials for biomedical devices. *JOM Journal of the Minerals, Metals and Materials Society*, 60(3):26–32, March 2008.
[156] Debiostari: an innovative solution for sustained drug delivery, 05 2009.
[157] Hisako Ohgawara, Sachiko Hirotani, Jun-Ichi Miyazaki, and Satoshi Teraoka. Membrane immunoisolation of a diffusion chamber for a bioartificial pancreas. *Artificial Organs*, 22(9):788–794, 1998.
[158] J.C. Wright A.E. Chester R. Skowronski C. Lucas. *Modified Release Drug Delivery Technology*, chapter Longterm controlled delivery of therapeutic agents via an implantable osmotically driven system: The DUROS implant, pages 657–669. Marcel Dekker, New York, 2003.
[159] Duros system, 05 2009.
[160] Martin Malmsten. Soft drug delivery systems. *Soft Matter*, 2(9):760–769, 2006.

[161] Pich, Z. Andrij, Adler, and P. Hans-Juergen. Composite aqueous microgels: an overview of recent advances in synthesis, characterization and application. *Polymer International*, 56(3):291–307, March 2007.

[162] B. Ziaie. Hard and soft micromachining for biomems: review of techniques and examples of applications in microfluidics and drug delivery. *Advanced Drug Delivery Reviews*, 56(2):145–172, February 2004.

[163] C. Küttel A. Stemmer X. Wei. Strain response of polypyrrole actuators induced by redox agents in solution. submitted April 2009.

[164] Guillaume Sabouraud, Said Sadki, and Nancy Brodie. The mechanisms of pyrrole electropolymerization. *Chem. Soc. Rev.*, 29(5):283–293, 2000.

[165] Q. Pei and O. Inganas. Electrochemical applications of the bending beam method; a novel way to study ion transport in electroactive polymers. *Solid State Ionics*, 60(1-3):161–166, March 1993.

[166] K. Maksymiuk, A. S. Nyback, J. Bobacka, A. Ivaska, and A. Lewenstam. Metallic and non-metallic redox response of conducting polymers. *Journal of Electroanalytical Chemistry*, 430(1-2):243–252, Jun 30 1997.

[167] S. Timoshenko. Analysis of bi-metal thermostats. *Journal of the Optical Society of America and Review of Scientific Instruments*, 11(3):233–255, Sep 1925.

[168] Q. B. Pei and O. Inganas. Electrochemical applications of the bending beam method .1. mass-transport and volume changes in polypyrrole during redox. *Journal of Physical Chemistry*, 96(25):10507–10514, Dec 10 1992.

[169] Q. B. Pei and O. Inganas. Electrochemical applications of the bending beam method .2. electroshrinking and slow relaxation in polypyrrole. *Journal of Physical Chemistry*, 97(22):6034–6041, Jun 3 1993.

[170] G. Han. Conducting polymer electrochemical actuator made of high-strength three-layered composite films of polythiophene and polypyrrole. *Sensors and Actuators B: Chemical*, 99(2-3):525–531, May 2004.

[171] T. Otero. Artificial muscles based on conducting polymers. *Bioelectrochemistry and Bioenergetics*, 38(2):411–414, October 1995.

[172] Q. B. Pei and O. Inganas. Conjugated polymers and the bending cantilever method - electrical muscles and smart devices. *Advanced Materials*, 4(4):277–278, Apr 1992.

[173] Q. B. Pei and O. Inganas. Conjugated polymers as smart materials, gas sensors and actuators using bending beams. *Synthetic Metals*, 57(1):3730–3735, Apr 12 1993.

[174] J. Joo and M. Pyo. Effects of cationic species on strain changes of polypyrrole doped with perchlorate anions. *Electrochemical and Solid State Letters*, 6(10):E27–E29, Oct 2003.

[175] Clay Bohn, Said Sadki, Anthony B. Brennan, and John R. Reynolds. In situ electrochemical strain gage monitoring of actuation in conducting polymers. *Journal of The Electrochemical Society*, 149(8):E281–E285, 2002.

[176] M. Pyo, C. C. Bohn, E. Smela, J. R. Reynolds, and A. B. Brennan. Direct strain measurement of polypyrrole actuators controlled by the polymer/gold interface. *Chemistry of Materials*, 15(4):916–922, Feb 25 2003.
[177] V. Tabardcossa, M. Godin, L. Beaulieu, and P. Grutter. A differential microcantilever-based system for measuring surface stress changes induced by electrochemical reactions. *Sensors and Actuators B: Chemical*, 107(1):233–241, May 2005.
[178] S. T. Mcgovern, G. M. Spinks, B. Xi, G. Alici, V. Truong, and G. G. Wallace. Fast bender actuators for fish-like aquatic robots. *Electroactive Polymer Actuators and Devices (EAPAD) 2008*, 6927(1):69271L+, 2008.
[179] T. Otero and E. Delarreta. Electrochemical control of the morphology, adherence, appearance and growth of polypyrrole films? *Synthetic Metals*, 26(1):79–88, October 1988.
[180] Allen J. Bard Larry R. Faulkner. *Electrochemical Methods, Fundamentals and Applications*. John Wiley and Sons, Inc., 2001.
[181] V. Krishna, Y. H. Ho, S. Basak, and K. Rajeshwar. Luminescence probe and voltammetry study of ion transport during redox switching of poly(pyrrole) thin films. *Journal of the American Chemical Society*, 113(9):3325–3333, April 1991.
[182] S. Chu, H. Peng, P. Kilmartin, G. Bowmaker, R. Cooney, and J. Travassejdic. Effect of deposition current density on the linear actuation behaviour of ppy(cf3so3) films. *Current Applied Physics*, 8(3-4):324–327, May 2008.
[183] S. Chu, P. Kilmartin, S. Jing, G. Bowmaker, R. Cooney, and J. Travassejdic. The effect of monomer and electrolyte concentrations during synthesis on the actuation of ppy(cf3so3) films in aqueous electrolytes. *Synthetic Metals*, 158(1-2):38–44, January 2008.
[184] G. Wallace. Conducting electroactive polymer-based biosensors. *TrAC Trends in Analytical Chemistry*, 18(4):245–251, April 1999.
[185] H. Varela, M. Malta, and R. M. Torresi. Microgravimetric study of the influence of the solvent on the redox properties of polypyrrol modified electrodes. *Journal of Power Sources*, 92(1-2):50–55, Jan 2001.
[186] G. Inzelt, V. Kertesz, and A. S. Nyback. Electrochemical quartz crystal microbalance study of ion transport accompanying charging-discharging of poly(pyrrole) films. *Journal of Solid State Electrochemistry*, 3(5):251–257, Jul 1999.
[187] C. S. C. Bose, S. Basak, and K. Rajeshwar. Electrochemistry of poly(pyrrole chloride) films - a study of polymerization efficiency, ion-transport during redox and doping level assay by electrochemical quartz crystal microgravimetry, ph, and ion-selective electrode measurements. *Journal of Physical Chemistry*, 96(24):9899–9906, Nov 26 1992.
[188] T. Lewis, G. Wallace, C. Kim, and D. Kim. Studies of the overoxidation of polypyrrole. *Synthetic Metals*, 84(1-3):403–404, January 1997.

[189] Y. J. Yuan, S. B. Adeloju, and G. G. Wallace. In-situ electrochemical studies on the redox properties of polypyrrole in aqueous solutions. *European Polymer Journal*, 35(10):1761–1772, Oct 1999.

[190] T. F. Otero, M. Marquez, and I. J. Suarez. Polypyrrole: Diffusion coefficients and degradation by overoxidation. *Journal of Physical Chemistry B*, 108(39):15429–15433, Sep 30 2004.

[191] T. Otero and I. Boyano. Characterization of polypyrrole degradation by the conformational relaxation model. *Electrochimica Acta*, 51(28):6238–6242, September 2006.

[192] R. Mazeikiene. Kinetics of the electrochemical degradation of polypyrrole. *Polymer Degradation and Stability*, 75(2):255–258, 2002.

[193] Arzu Ersöz, Vasilis G. Gavalas, and Leonidas G. Bachas. Potentiometric behavior of electrodes based on overoxidized polypyrrole films. *Analytical and Bioanalytical Chemistry*, 372(7):786–790, April 2002.

[194] C. K. Baker, Y. J. Qiu, and J. R. Reynolds. Electrochemically induced charge and mass-transport in polypyrrole/poly(styrenesulfonate) molecular composites. *Journal of Physical Chemistry*, 95(11):4446–4452, May 30 1991.

[195] G. Vázquez, T. F. Otero, and J. J. L. Cascales. Electro-chemo-mechanical response of a free-standing polypyrrole strip. *J. Phys.: Conf. Ser.*, 127(1):012005+, 2008.

[196] J. O. Bockris and F. B. Diniz. Aspects of electron-transfer at a conducting membrane solution interface. *Electrochimica Acta*, 34(4):567–575, Apr 1989.

[197] A. Michalska, U. Nadrzycka, and K. Maksymiuk. The modelled and observed transition from redox to ionic potentiometric sensitivity of poly(pyrrole). *Electrochimica Acta*, 46(26-27):4113–4123, Aug 24 2001.

[198] M. Cappadonia, K. Doblhofer, and D. Woermann. Study of the electrical state of the phase boundary between polyelectrolyte gel and electrolyte solution by measurements of membrane potential and volta potential. *Journal of Colloid and Interface Science*, 143(1):222–231, April 1991.

[199] Karl Doblhofer. The non-metallic character of solvated conducting polymers. *Journal of Electroanalytical Chemistry*, 331:1015–1027, 1992.

[200] A. Alumaa. Potentiometric properties of polypyrrole bilayers. *Electrochimica Acta*, 49(11):1767–1774, April 2004.

[201] J. Bobacka, Z. Q. Gao, A. Ivaska, and A. Lewenstam. Mechanism of ionic and redox sensitivity of p-type conducting polymers .2. experimental-study of polypyrrole. *Journal of Electroanalytical Chemistry*, 368(1-2):33–41, Apr 25.

[202] M. Nishizawa, T. Sawaguchi, T. Matsue, and I. Uchida. Insitu characterization of copolymers of pyrrole and n-methylpyrrole at microarray electrodes. *Synthetic Metals*, 45(2):241–248, Nov 1991.

[203] A. Michalska, A. Lewenstam, A. Ivaska, and A. Hulanicki. Study of polypyrrole film as redox electrode. *Electroanalysis*, 5(3):261–263, Apr 1993.

[204] K. Maksymiuk and K. Doblhofer. Kinetics and mechanism of charge-transfer reactions between conducting polymers and redox ions in electrolytes. *Electrochimica Acta*, 39(2):217–227, Feb 1994.

[205] L. S. Curtin, G. C. Komplin, and W. J. Pietro. Diffusive anion-exchange in polypyrrole films. *Journal of Physical Chemistry*, 92(1):12–13, Jan 14 1988.

[206] Karl Doblhofer and Chuanjian Zhong. The mechanism of electrochemical charge-transfer reactions on conducting polymer films. *Synthhetic Metals*, 41-43:2865–2870, 1991.

[207] A. Michalska, U. Nadrzycka, and K. Maksymiuk. Interference of sulfate(vi) with poly(pyrrole) electrochemistry. *Fresenius Journal of Analytical Chemistry*, 371(1):35–38, Sep 2001.

[208] A. Ambrosi, A. Morrin, M. R. Smyth, and A. J. Killard. The application of conducting polymer nanoparticle electrodes to the sensing of ascorbic acid. *Analytica Chimica Acta*, 609(1):37–43, Feb 18 2008.

[209] Y. F. Li and R. Y. Qian. On the nature of redox processes in the cyclic voltammetry of polypyrrole nitrate in aqueous-solutions. *Journal of Electroanalytical Chemistry*, 362(1-2):267–272, Dec 30 1993.

[210] K. K. Shiu, F. Y. Song, and K. W. Lau. Effects of polymer thickness on the potentiometric ph responses of polypyrrole modified glassy carbon electrodes. *Journal of Electroanalytical Chemistry*, 476(2):109–117, Nov 1 1999.

[211] T. Silk. Afm studies of polypyrrole film surface morphology i. the influence of film thickness and dopant nature. *Synthetic Metals*, 93(1):59–64, February 1998.

[212] M. E. G. Lyons, W. Breen, and J. Cassidy. Ascorbic-acid oxidation at polypyrrole-coated electrodes. *Journal of the Chemical Society-Faraday Transactions*, 87(1):115–123, Jan 7 1991.

[213] J. H. Hwang and M. Pyo. ph-induced mass and volume changes of perchlorate-doped polypyrrole. *Synthetic Metals*, 157(2-3):155–159, Feb 15 2007.

[214] O. Inganas, R. Erlandsson, C. Nylander, and I. Lundstrom. Proton modification of conducting polypyrrole. *Journal of Physics and Chemistry of Solids*, 45(4):427–432, 1984.

[215] Q. Pei and R. Qian. Protonation and deprotonation of polypyrrole chain in aqueous-solutions. *Synthetic Metals*, 45(1):35–48, Oct 1991.

[216] X. Zhang and Bai. Surface electric properties of polypyrrole in aqueous solutions. *Langmuir*, 19(26):10703–10709, December 2003.

[217] M. Yamaura, T. Hagiwara, and K. Iwata. Enhancement of electrical conductivity of polypyrrole film by stretching: Counter ion effect. *Synthetic Metals*, 26(3):209–224, November 1988.

[218] P. George, A. Lyckman, D. Lavan, A. Hegde, Y. Leung, R. Avasare, C. Testa, P. Alexander, R. Langer, and M. Sur. Fabrication and biocompatibility of polypyrrole implants suitable for neural prosthetics. *Biomaterials*, 26(17):3511–3519, June 2005.

[219] L. Bay, N. Mogensen, S. Skaarup, P. Sommer-Larsen, M. Jorgensen, and K. West. Polypyrrole doped with alkyl benzenesulfonates. *Macromolecules*, 35(25):9345–9351, Dec 3 2002.

[220] U. L. Zainudeen, M. A. Careem, and S. Skaarup. Pedot and ppy conducting polymer bilayer and trilayer actuators. *Sensors and Actuators B: Chemical*, 134(2):467–470, September 2008.

[221] Jing Sui, Jadranka Travas-Sejdic, Shu Y. Chu, Kwong C. Li, and Paul A. Kilmartin. The actuation behavior and stability of *p*-toluene sulfonate doped polypyrrole films formed at different deposition current densities. *Journal of Applied Polymer Science*, 111(2):876–882, 2009.

[222] M. A. Careem, Y. Velmurugu, S. Skaarup, and K. West. A voltammetry study on the diffusion of counter ions in polypyrrole films. *Journal of Power Sources*, 159(1):210–214, Sep 13 2006.

[223] T. Matencio. Ionic exchanges in dodecylbenzenesulfonate doped polypyrrole part 1. optical beam deflection studies. *Synthetic Metals*, 72(1):59–64, April 1995.

[224] R. M. Torresi, S. I. C. Detorresi, T. Matencio, and M. A. Depaoli. Ionic exchanges in dodecylbenzenesulfonate-doped polypyrrole .2. electrochemical quartz-crystal microbalance study. *Synthetic Metals*, 72(3):283–287, Jun 1995.

[225] Ming Zhou, Markus Pagels, Beate Geschke, and Jurgen Heinze. Electropolymerization of pyrrole and electrochemical study of polypyrrole. 5. controlled electrochemical synthesis and solid-state transition of well-defined polypyrrole variants. *The Journal of Physical Chemistry B*, 106(39):10065–10073, October 2002.

[226] I. Willner, Y. M. Yan, B. Willner, and R. Tel-Vered. Integrated enzyme-based biofuel cells-a review. *Fuel Cells*, 9(1):7–24, 2009.

[227] A. Macdiarmid. Electrostatically-generated nanofibers of electronic polymers. *Synthetic Metals*, 119(1-3):27–30, March 2001.

[228] L. Brunel, J. Denele, K. Servat, K. Kokoh, C. Jolivalt, C. Innocent, M. Cretin, M. Rolland, and S. Tingry. Oxygen transport through laccase biocathodes for a membrane-less glucose/o2 biofuel cell. *Electrochemistry Communications*, 9(2):331–336, February 2007.

[229] Marek Trojanowicz and Michael L. Hitchman. A potentiometric polypyrrole-based glucose biosensor. *Electroanalysis*, 8(3):263–266, 1996.

[230] S. Adeloju. Fabrication of ultra-thin polypyrrole–glucose oxidase film from supporting electrolyte-free monomer solution for potentiometric biosensing of glucose. *Biosensors and Bioelectronics*, 16(3):133–139, May 2001.

[231] V. Ravaine, C. Ancla, and B. Catargi. Chemically controlled closed-loop insulin delivery. *Journal of Controlled Release*, 132(1):2–11, November 2008.

[232] R. A. Siegel, Y. D. Gu, A. Baldi, and B. Ziaie. Novel swelling/shrinking behaviors of glucose-binding hydrogels and their potential use in a microfluidic insulin delivery system. *Macromolecular Symposia*, 207:249–256, Feb 2004.

[233] Y. Imanishi and Y. Ito. Glucose-sensitive insulin-releasing molecular systems. *Pure and Applied Chemistry*, 67(12):2015–2021, 1995.

[234] E. Pestel J. Wittenburg. *Technische Mechanik, Band 2: Festigkeitslehre*. B.I.-Wissenschaftsverlag, 1981.

[235] H. D. Espinosa and B. C. Prorok. Size effects on the mechanical behavior of gold thin films. *Journal of Materials Science*, 38(20):4125–4128, October 2003.

[236] Yevgeny Berdichevsky and Y. H. Lo. Polymer microvalve based on anisotropic expansion of polypyrrole. volume 782, 2004.

[237] Yanzhe Wu, L. Nolan, S. Coyle, King T. Lau, G. G. Wallace, and D. Diamond. Polypyrrole based switchable filter system. In *Engineering in Medicine and Biology Society, 2007. EMBS 2007. 29th Annual International Conference of the IEEE*, pages 4090–4091, 2007.

[238] L. Low. Microactuators toward microvalves for responsive controlled drug delivery. *Sensors and Actuators B: Chemical*, 67(1-2):149–160, August 2000.

[239] S. Rapi. Conducting polypyrrole by chemical synthesis in water. *Synthetic Metals*, 24(3):217–221, May 1988.

[240] J. Thieblemont, M. Planche, C. Petrescu, J. Bouvier, and G. Bidan. Stability of chemically synthesized polypyrrole films. *Synthetic Metals*, 59(1):81–96, June 1993.

[241] C. Arribas and D. Rueda. Preparation of conductive polypyrrole-polystyrene sulfonate by chemical polymerization. *Synthetic Metals*, 79(1):23–26, April 1996.

[242] Zhigang Qi and Peter G. Pickup. Size control of polypyrrole particles. *Chemistry of Materials*, 9(12):2934–2939, December 1997.

[243] Wataru Takashima, Shyam S. Pandey, Masaki Fuchiwaki, and Keiichi Kaneto. Cyclic step-voltammetric analysis of cation-driven and anion-driven actuation in polypyrrole films. *Japanese Journal of Applied Physics*, 41(12):7532–7536, 2002.

[244] R. Hernandez, A. F. Diaz, R. Waltman, and J. Bargon. Surface characteristics of thin films prepared by plasma and electrochemical polymerizations. *The Journal of Physical Chemistry*, 88(15):3333–3337, July 1984.

[245] J. Isaksson, C. Tengstedt, M. Fahlman, N. Robinson, and M. Berggren. A solid-state organic electronic wettability switch. *Advanced Materials*, 16(4):316–320, 2004.

[246] Kwok S. Teh and Yen-Wen Lu. Topography and wettability control in biocompatible polymer for biomems applications. In *Nano/Micro Engineered and Molecular Systems, 2008. NEMS 2008. 3rd IEEE International Conference on*, pages 1100–1103, 2008.